

Doctoral theses at NTNU, 2022:38

Elisabeth Leite Skare

Prediction of rheological properties of filler modified cement paste from constituent properties, flow measurements and modelling

ISBN 978-82-326-5753-7 (printed ver.)  
ISBN 978-82-326-6958-5 (electronic ver.)  
ISSN 1503-8181 (printed ver.)  
ISSN 2703-8084 (electronic ver.)

Doctoral theses at NTNU, 2022:38

**NTNU**  
Norwegian University of  
Science and Technology  
Thesis for the degree of  
Philosophiae Doctor  
Faculty of Engineering  
Department of Structural Engineering

Elisabeth Leite Skare

# Prediction of rheological properties of filler modified cement paste from constituent properties, flow measurements and modelling

Thesis for the degree of Philosophiae Doctor

Trondheim, February 2022

Norwegian University of Science and Technology  
Faculty of Engineering  
Department of Structural Engineering



**NTNU**

Norwegian University of Science and Technology

Thesis for the degree of Philosophiae Doctor

Faculty of Engineering  
Department of Structural Engineering

© Elisabeth Leite Skare

ISBN 978-82-326-5753-7 (printed ver.)

ISBN 978-82-326-6958-5 (electronic ver.)

ISSN 1503-8181 (printed ver.)

ISSN 2703-8084 (electronic ver.)

Doctoral theses at NTNU, 2022:38



Printed by Skipnes Kommunikasjon AS

## Preface

This thesis is submitted in partial fulfilment of the requirements for the degree of Philosophiae Doctor (PhD) at the Norwegian University of Science and Technology (NTNU) and the Technical University of Denmark (DTU). The thesis is a double degree with NTNU as home university and DTU as host university. The work has been carried out in guidance of main supervisor Stefan Jacobsen (NTNU) as well as co-supervisors Jon Spangenberg (DTU), Ernst Mørtzell (NTNU/Norbetong AS) and Rolands Cepuritis (NTNU/Norcem AS). The thesis is written as a collection of articles and was carried out during the period 01.03.2017 – 27.11.2021, which included a ten-month maternity leave. The work has mainly been conducted at the Department of Structural Engineering, Faculty of Engineering, NTNU, as well as a total of 1 year at the Department of Mechanical Engineering, DTU. The laboratory work has been performed at the NTNU concrete laboratory at Materialteknisk (MTI), as well as the paste- and instrument laboratories at SINTEF Grønnygget. The PhD-position is a four-year contract, whereof required duties make up 25 % of the workload.

The thesis is a part of the MiKS-project, which is a Competence Project for the Industry. Funding was provided by the Research Council of Norway, contract No. 247619, as well as the industrial partners Norcem AS, Skanska Norge AS and Feiring Bruk AS. MiKS is short for *Mikroproporsjonering med Knust Sand* (Norwegian for *Microproportioning with Crushed Sand*). The MiKS-project started in 2016, and Evgeny Ramenskiy was the PhD-candidate within the project at that time. However, Ramenskiy quit his position after one year of employment, hence a planned outline for the thesis work was already established from start in March 2017. Laboratory experiments were also already conducted during the first year of the project, and the presented results from 51 of the 141 filler modified cement pastes (matrices) were obtained by Ramenskiy. The remaining 90 matrices were tested during the employment of the current PhD candidate, whereof 11 matrices were tested by Malin Sletnes and Roger Leistad at SINTEF. The rest of the matrices have been mixed and tested by the PhD-candidate, together with master students Patricia Y. Sosa, Juni C. M. Foslie and Andreas Erlien Grefstad. Viscosity and packing measurements on smaller replica mixes have been performed by master student Metathip Sihaklang and internship student David Nicolas. The artificial neural network modelling presented in Publication III and VI is performed by research assistant Shohreh Sheiat. The presented numerical model in Publication IV, which is later used in Publication V, VII, VIII and IX, is developed by the authors in [1]. Other than this, the candidate is responsible for the performed work, unless else is stated.



## **Abstract**

The world is facing a sand crisis due to depletion of natural deposits of good quality construction sand. Replacement of natural sand is crucial to curb the impact of the crisis. Though several alternatives exist, this thesis solely focus on crushed sand as replacement for natural sand. However, unless the crushed sand is properly processed, it is more angular and contains more fines than natural sand, which have a negative impact on concrete rheology. Measuring concrete rheology requires a lot of materials and labour, however, small scale rheology testing on equivalent cement pastes is found to correlate to concrete rheology. The thesis investigates the rheology of cement pastes with fillers from crushed sand, denoted matrices. The scope of the thesis is to investigate methods for quantification of matrix rheology, with emphasis on characteristics of the ingoing materials. Special focus is on the possibilities of establishing a one-point measurement of matrix rheology, i.e., a method describing the rheological behaviour of matrix by only one parameter. Limitations of and possibilities for further developing the flow viscometer FlowCyl are studied. Additionally, the accuracy and efficiency of artificial neural network predictions of the cement paste rheology are investigated and compared to semi-empirical suspension models. The rheological properties of the matrices have been quantified experimentally by four parameters; the flow resistance ratio (obtained from the FlowCyl), the mini slump flow, the Bingham yield stress and the Bingham plastic viscosity. From the work of the thesis it is found that it is possible to predict rheology of matrices based on constituent materials when all dry materials (except silica fume) are characterized by the volumetric specific surface area per volume of matrix, as well as their mix proportions. An empirical equation is developed, which correlates especially good to the plastic viscosity of the matrices. The main limitation of the FlowCyl is its weak correlation to yield stress, however, it is found that this correlation can be increased by changing the geometry of the FlowCyl. Based on numerical simulations a prototype of a modified geometry of the FlowCyl has been produced, called the FlowFunnel, which provides better correlations to the yield stress than the FlowCyl. Lastly, artificial neural network predictions are found to be an efficient and accurate prediction tool for matrix rheology.



## Acknowledgements

Besides the generous funding received from the Research Council of Norway and the industrial partners Norcem AS, Skanska Norge AS and Feiring Bruk AS, there are many people I would like to thank for making this accomplishment a reality. First of all, I want to express my gratitude to my main supervisor Professor Stefan Jacobsen and co-supervisor Associate Professor Jon Spangenberg. Thank you both so much for always supporting, encouraging and guiding me through the years of my PhD. You have provided me with academic guidance, and you are impressively deep in knowledge within your fields. Your doors are always open, and you always find time to answer my many questions. Even since the corona virus broke out and home offices became the “new normal”, you have always been easily available either by phone, video-meetings or e-mail. In this regard, I have to give Stefan a special attention, as it to me seems like his e-mail is a 24-hour service with 15 minutes response time. I must also point out that I really have appreciated our many informal and casual talks about everything from family, holidays, dogs, sheep farming to politics etc. You both show interest in my personal life, as well as sharing from your everyday lives, which has contributed to make my work experience even better with respect to the personal and social aspects. I truly appreciate our many laughs during our meetings, and that you always find time to share some funny stories from outside the “concrete sphere”.

I also would like to thank my co-supervisors Professor Ernst Mørtzell and Adjunct Associate Professor Rolands Cepuritis. You both always reply quickly on my requests, providing me with relevant information and nice explanations, and you always eager to share your expertise within the field of microproportioning with crushed sand. Thank you for our many constructional and useful discussions throughout the years, and for always demonstrating that most aspects in life can be met with a laidback attitude and a minimum level of stress. In some way or another, you make everything seem easy and straightforward, and you have truly impressed me with your wide knowledge within all the work groups in the project.

Special thanks go to all my colleagues in the Concrete Group at NTNU. You are talented, knowledgeable and truly inspiring colleagues, which through the years have become my friends. The social environment is just as important as the scientific, and you guys have truly contributed to a social and fun working environment which has made me look forward to every day at work. I really appreciate our informal talks in the lunch room as well as social happenings outside working hours, such as cross-country skiing and board game nights. I would especially like to express my gratitude to my office mates when I first started my PhD, Jelena Zivkovic and Andrei Shpak, for welcoming me in such a wonderful way! Jelena even baked a cake on my first day at work! You have included me in the group and treated me like your friend from the first moment. You have been so hospitable and welcoming, and early introduced me and my family to your wonderful families. You have really made a warm and fun environment in our office, which has been a place where we have shared both ups and downs in life. Thank you for that! I would also thank my office mates at a later stage in the PhD; Kathrine M. Stemland and Pamela Zuschlag. Thank you so much for our many laughs, casual talks and rememberable moments! I am truly thankful for the many friendships I have made, and I know these friendships will last also in the future.



A part of the work was carried out at the department of Mechanical Engineering at DTU. Thank you, Jon, for welcoming me and introducing me to my Danish colleagues! Even though you continuously pinpoint that you don't understand my Norwegian dialect, as I have "lived too long in the mountains", and that Rolands' Norwegian pronunciation with Baltic accent is much easier to understand, I have truly enjoyed our many conversations in our Scandinavian languages. I want to thank everyone at DTU Mechanical Engineering for setting a fantastic social and professional environment, and for answering my many questions regarding (to me) the unknown field of computational fluid dynamics. Special thanks go to my office mates for our many conversations, laughs and not least funny misunderstandings due to the differences between the Scandinavian languages. Also, I would like to say sorry for my noisy crispbread- and carrot eating in the office. In my defence, I was pregnant.

Last, but not least, I would like to thank all my family and friends, for always supporting me and believing in me throughout the years of the study. I am especially thankful for the extra support from my mum and dad in the last leg of the PhD, including making dinners, picking up our son from kindergarten and always asking whether they can help in any way. I would also give special thanks to my brother, Thomas, who thought me how to use Solidworks (over and over again as I seem to forget it between each time I use it). I am also so very grateful for the period we shared office, which was a time filled with interesting discussions, laughter and lots of coffee and candy. The support from my friends has also been endless, and I want to give special thanks to my two close friends Susanne Thomesen and Helle Ulvestad, for help with practical questions regarding everything from the hand-in process and format styles to English grammar. It has been a joy to be colleague with you, Susanne, and I can for sure say that the working day would not have been the same without you. Thanks for our many (always a bit too long) lunch breaks, coffee breaks and cake breaks, as well as our compensation for the latter; our many hours at the gym in the basement of Materialteknisk, NTNU. Thank you, Helle, for the short period we were sharing home office, which for me was the best part of the "corona time". But most of all, thank you so much for all your help and support regarding English grammar and sentence structure!

Heartfelt thanks go to my husband and our son for your endless love, support and encouragement. You are truly the best! It is hard to fully express my gratitude, as your support is so overwhelming. Thank you so much, Ivar André, for putting an extra effort in the housework, grocery shopping, the dogs, the farm, looking after our little Isak and so on. Your support has really been priceless. And to my precious Isak: Thank you so much for always being so patient while waiting for mummy to finish up her work, and for never complaining even if you would love to start playing straight away. Parts of the thesis have been written to the tunes of "Peppa Pig" and "Thomas the Tank Engine" from the extra monitor on my desk, while you've been waiting patiently next to me. And of course, a small thank you should also be given to our three beautiful dogs (and 30 sheep) that have made sure I have gotten enough fresh air and exercise through the years of study.

20.11.21

Elisabeth Leite Skare

## Contents

Preface	i
Abstract	iii
Acknowledgements	v
Contents	vii
List of publications	ix
Contribution to publications	x
1. Introduction	1
1.1 Background	1
1.2 A short overview of related research	2
1.3 Challenges and research needs	3
1.4 Objectives	4
2. Theoretical Background	5
2.1 Characterization of the rheology of cementitious suspensions	5
2.2 Proportioning of concrete	6
2.3 Particle characterization	7
2.4 Suspension rheology models	8
2.5 Numerical simulations	9
3. Summary of appended publications	11
4. Conclusions	15
5. Further research work	17
References	19



## List of publications

This thesis includes the following appended publications, referred to by their Roman letters in the thesis.

- I      Microproportioning paste with crushed aggregate filler by use of specific surface area**  
Skare EL, Cepuritis R, Spangenberg J, Ramenskiy E, Mørtzell E, Smepllass S, Jacobsen S. *15th International Congress on the Chemistry of Cement* (2019).
- II     Application of an Improved Empirical Model for Rheology Prediction of Cement Pastes Modified with Filler from Manufactured Sand**  
Skare EL, Cepuritis R, Mørtzell E, Smepllass S, Spangenberg J, Jacobsen S. *Nordic Concrete Research* 65 (2021) pp. 1-18.
- III    Rheology Modelling of Cement Paste with Manufactured Sand and Silica Fume: Comparing Suspension Models with Artificial Neural Network Predictions**  
Skare EL, Sheiati S, Cepuritis R, Mørtzell E, Smepllass S, Spangenberg J, Jacobsen S. *Construction and Building Materials* 317 (2022) 126114.
- IV    FlowCyl: one-parameter cement paste rheology test developed at NTNU, Norway**  
Cepuritis R, Skare EL, Jacobsen S, Spangenberg J, Smepllass S, Mørtzell E. *Rhéologie* 35 (2019) pp. 20-24.
- V     Analysing limitations of the FlowCyl as a one-point viscometer test for cement paste**  
Cepuritis R, Skare EL, Ramenskiy E, Mørtzell E, Smepllass S, Li S, Jacobsen S, Spangenberg J. *Construction and Building Materials* 218 (2019) pp. 333-340.
- VI    Neural network predictions of the simulated rheological response of cement paste in the FlowCyl**  
Sheiati S, Ranjbar N, Frellsen J, Skare EL, Cepuritis R, Jacobsen S, Spangenberg J. *Neural Computing and Applications* 33 (2021) pp. 13027-13037.
- VII   Decreasing the Magnitude of Shear Rates in the FlowCyl**  
Skare EL, Jacobsen S, Cepuritis R, Smepllass S, Spangenberg J. *Proceedings for the International Federation for Structural Concrete 5th International FIB Congress* (2018).
- VIII Investigating the flow curve of the FlowCyl test as a measure of yield stress**  
Skare EL, Jacobsen S, Spangenberg J. Manuscript submitted to *The International Federation for Structural Concrete 6th International FIB Congress 2022*.
- IX    FlowFunnel for measuring yield stress and plastic viscosity of cement paste**  
Skare EL, Jacobsen S, Spangenberg J.  
Manuscript submitted to *Cement and Concrete Research*.

### **Contribution to publications**

Elisabeth L. Skare wrote Publications I, II, III, VII, VIII and IX, planned and conducted the major part of the experiments, as well as analysing the results. The candidate also conducted the numerical simulations in Publications VII, VIII and IX, while the artificial neural network modelling in Publication III was performed by Shohreh Sheiati. In publications IV, V and VI the candidate's main contribution has been proof reading and constructive criticism to the content.

# 1. Introduction

## 1.1 Background

In most of the world, sand is a common-pool resource, meaning it is a resource that is open to all because access can be limited only at high costs [2]. Such resources are prone to overexploitation or degradation, as they often are extracted without regard to long-term consequences [2]. The global volume of natural resources used in buildings and transport infrastructure has increased 23-fold over the 20<sup>th</sup> century [3], where sand and gravel are the major portion of these resources [2]. Sand and gravel are estimated to be the fastest-growing material groups extracted over the 20<sup>th</sup> and 21<sup>st</sup> centuries [4]. However, the industry overall is affected by illegality, violence and a strong black market [4]. Precise quantitative data on sand extraction are therefore unavailable. The world is facing a global sand crisis with multi-dimensional negative ecological, economic and social consequences, and the sand scarcities are especially prominent in South-east and South Asia [4].

Even though deserts cover approximately one third of the Earth's land surface area [5], the depletion of natural sand has been a subject for several years. This is mainly because the chemical constituents and particle distributions of desert sand differ widely from ordinary sand [6], hence desert sand is not suitable for construction purposes unless it is improved by proper technology and used in combination with sand with larger grain size. Al-Harthy *et al.* [7] showed experimentally that the slump and mechanical properties of concrete decreased with increasing desert sand replacement ratio. The fineness modulus and particle size of desert sand are smaller than that of normal construction sand, and concrete produced with desert sand is shown to obtain lower strength, poorer cohesiveness and poorer workability [6]. Powers [8] stated that no clear definition of the term workability exists, however, when used in this thesis the term could be understood as the flowability of the concrete. It should be noted that the fineness modulus is an ambiguous parameter, as the same value can be obtained from different particle size distributions. However, the use of desert sand for constructional purpose is an expensive and intricate process. Clearly, good alternatives to natural sand are necessary to limit the global depletion of natural construction sand deposits. One such alternative is to replace natural sand with crushed sand, which is investigated in this thesis.

In Norway, the consequences of the sand crisis are mainly the unwanted extraction of unique glaciofluvial deposits. Such aggregates are often naturally graded with excellent petrography, particle size distribution and particle shape, and can be used directly in concrete. Many of these deposits are now protected and it is expected that such protections will increase in the near future [9]. As Norway is a relatively large net aggregate exporter, the main concern is to replace natural deposits with crushed sand. Norway is probably the most important hard-rock country in the northern Europe, being composed almost entirely of Precambrian and Palaeozoic igneous and metamorphic crystalline bedrock [10]. The Norwegian production of primary aggregates in 2014 was approximately 144 million tonnes, whereof approximately 19 million tonnes were exported [11]. Therefore, the development of manufactured aggregate will contribute to preservation of nature as well as developing export potentials.

## 1.2 Short overview of related research

The properties of crushed sand differ from natural sand and replacing natural sand with crushed sand will hence affect concrete rheology [12]. The rheological behaviour of concrete is of major importance both with respect to concrete placement and finishing, as well as for its hardened state properties [13]. The most accepted tool for fresh concrete testing at construction site is the truncated Abrams cone or slump cone [14]. The test procedure consists of filling the metal cone in three layers with tamping in between each layer. The cone is then lifted, and the concrete sample will deform due to gravity. The height difference between the concrete and the cone is called the slump, while the diameter of base of the slumped material is called the slump flow [15]. Another cheap and simple concrete rheology test is the LCPC box, which was introduced by Roussel [16]. Self-consolidating concrete is filled into the LCPC box, and the length,  $L$ , and largest thickness of the sample,  $h_0$ , is measured at stoppage, and used to calculate the yield stress. Several other test methods for concrete rheology exist, however, full scale testing of concrete is a cumbersome task, which requires a lot of materials and labour. Contrary, testing on smaller cement paste samples is more economical and efficient, and such small-scale testing has shown to be promising for rheology prediction of equivalent concrete mixes [17]. Several rheology methods are developed for cement pastes and grouts, such as the Marsh cone. The Marsh cone obtains a relative measure of the fluidity as the inverse of the flow time by measuring the time taken for a certain volume of material to flow through the Marsh cone [18-19]. Other examples of rheology test on cement pastes and mortars are the mini slump cone and FlowCyl. The latter two methods are investigated in this thesis, and the test principles are described in detail in Section 2.1.

To limit full scale testing, Schwartzentruber and Catherine [20] proposed concrete equivalent mortar to predict the rheological behaviour of corresponding concrete mixes. The approach consists in replacing the coarse aggregates by fine aggregates to provide an equivalent specific surface area at mortar scale [21]. The method predicted the slump, slump variations, water reduction, air content, setting time and compressive strength of equivalent concrete mixes with coefficients of correlation,  $R^2$ , greater than 0.86 between the measured values on the concrete and on the concrete equivalent mortar [22]. However, the approach is less successful in rheology prediction of self-consolidating concretes, which is mainly because the specific surface area of the aggregate is the only criterion used to design the mortars [21]. Kabagire *et al.* [21] showed that when both the excess paste thickness and the coarse aggregate content were considered, good correlations were observed between the slump flow and V-funnel flow time of the concrete equivalent mortar and self-consolidating concrete. Similarly, Lee *et al.* [23] derived a multi-scale approach yield stress model for self-consolidating concrete and concrete equivalent mortar, which adopts the excess paste theory for both concrete and mortar. The model variables were the volume fraction and the paste layer thickness of aggregates in mortar or concrete. The model could predict the yield stress of mortars and concretes under the assumption of a constant layer thickness. Hence, small scale testing has shown to be a promising, efficient and economical approach, achieving rheological parameters that correlates well to fresh concrete properties.

The aggregate properties have an important influence on the quality of fresh and hardening concrete [24]. Crushed aggregate properties such as chemical and mineralogical composition

depend on the properties of the parent rock, while other properties, such as absorption, surface texture, shape and size, are affected by the crushing process [24]. Several studies focus on the influence of crushed aggregate properties on hardened concrete and mortars [25-31]. However, the literature on the effect of crushed aggregate properties on fresh cementitious materials is sparse [24]. Safiddine *et al.* [24] studied the effect of limestone crushed sand dust (LCSD) on rheological properties of mortars based on crushed sand and found that an increase in LCSD increased the yield stress and plastic viscosity, and accordingly decreased the slump of the mortars. The study showed that the mortar rheology was strongly affected by the increasing volume concentration of crushed sand, and that mortars based on crushed sand obtained high viscosities and yield stresses, compared to mortars based on natural sand. Similar results were found by Bouziani [32], which investigated the effect of river sand, crushed sand and dune sand on rheological and mechanical properties of self-compacting concrete. An increase in the crushed sand/river sand-ratio was found to decrease the slump flow and increase the V-funnel time. Cepuritis *et al.* [33] investigated the effect of crushed aggregates fines ( $\leq 0.250$  mm) on cement paste rheology and found that the rheology mainly is governed by the specific surface area of the fines (defined as surface area per volume of material [ $\text{mm}^2/\text{mm}^3$ ]), as well as the interaction between fines and superplasticizer (SP). The effect of the specific surface area of the fines was found to be general, as the rheology could be controlled either by altering the particle size distribution of the fines or their total volume. Also, the effect of fines mineralogy was highlighted, as cement pastes with different fillers but similar specific surface areas obtained different rheological properties. The observed differences were assigned to different SP adsorption due to different mineralogy.

### 1.3 Challenges and research needs

Replacing natural sand with crushed sand in concrete is not a straightforward task as their properties in general differ quite a lot from each other. In [12], the differences between natural and crushed sand were highlighted as the following: Natural sand has weathered particles with sub-angular to rounded shape, and their surface is often smooth. Contrary, sand from traditional crushing techniques has angular particles with a rough surface. However, by optimal crushing it is possible to obtain cubical particles, but still with a rough surface. Also, their particle size distributions (PSDs) differ from each other. In contrast to natural sand, crushed sand that is not processed adequately for optimization of particle shape and particle size distribution, normally has a PSD that is hanging or dense with high content of fines. Such PSDs could reduce the water demand of the concrete and improve the workability if the fines content is not too high. However, crushed sand often contains a high content of flaky and elongated particles, and for such particles a dense grading could cause a harsh mix. Harsh mixes require a high content of fines to compensate for the voids content, meaning that the water demand increases [12]. The PSDs of crushed sand in a log (size) vs. linear (volume passed) graph are generally parabolic, while PSDs of natural sand generally are “S-shaped” or sometimes linear [34].

Unless the crushed sand is properly processed for particle shape and particle size distribution, poorer workability is observed in concrete with crushed sand than with natural sand [34]. In mortars with such crushed sand, the high amount of fines is found to increase the yield stress,



whereas the combined effect of the fines content and particle shape of the crushed sand is found to increase the plastic viscosity [35]. Cortes *et al.* [36] showed that the loosest packing density of the fines is dependent on the particle shape. Hence, an increased paste volume is required to obtain adequate flowability and strength when natural round fines are replaced by angular crushed fines of the same grain size distribution.

Mørtzell [37] investigated the rheology of matrices with crushed sand and concluded that the matrix phase of the concrete could be fully described by the flow resistance ratio,  $\lambda_q$ , which is a unitless measure of the internal resistance of the matrix, further described in Section 2.1. However, later studies highlight that  $\lambda_q$  shows limitations in prediction of the rheology of self-compacting concrete [38]. This is mainly because concretes and other cementitious suspensions are two-parameter fluids, described by the plastic viscosity and the yield stress of the suspension [39], while  $\lambda_q$  only shows good correlations to the plastic viscosity [1, 40]. Cepuritis *et al.* [1, 40] have analysed the limitations of the FlowCyl and state that the reason why  $\lambda_q$  is dominated by the plastic viscosity is that the tested material undergoes very high shear rates at the outlet of the FlowCyl.

Even though several suspension models exist in literature, and many of them have been verified on cement pastes, there is a lack of good rheology models for cement pastes with crushed sand that predicts rheology based on constituent properties. As most rheology suspension models correlate to either the yield stress or the plastic viscosity of the cement pastes, there is a need for a one-parameter characterization or test method for cement paste rheology, that yields high correlations to both parameters.

#### 1.4 Objectives

This thesis investigates the rheology of cement pastes with filler from crushed sand, i.e., matrices. The objective is to investigate methods for quantification of matrix rheology as follows:

- Investigate to what extent the specific surface area per volume of matrix (including water and all particles less than 125  $\mu\text{m}$ ) correlates to rheological properties of a matrix (Publication I)
- Investigate the possibilities of establishing a proportioning tool for the ready-mix concrete industry based on the composition of the constituent materials, that accounts for the rheological effect from crushed sand (Publication II)
- Compare the predictive capabilities of traditional semi-empirical suspension models with artificial neural network predictions with respect to matrix rheology (Publication III)
- Investigate the limitations of the FlowCyl test method as a one-point viscometer test (Publication IV and V)
- Investigate the accuracy and efficiency of neural network predictions of the rheological behaviour of cement pastes in the FlowCyl (Publication VI)
- Investigate whether a modification of the FlowCyl geometry could make the flow resistance ratio more dependent on the yield stress of the tested matrices (Publication VII)
- Investigate the possibility of establishing a simple yet reliable method for determining the rheology of matrix with a so called one-point measurement of flow (Publication VIII and IX).

## 2 Theoretical Background

### 2.1 Characterization of the rheology of cementitious suspensions

The flow behaviour of concrete can be modelled as a Bingham fluid. Therefore, the rheological behaviour of cement pastes, mortars and concretes is usually characterized by at least two parameters; the yield stress,  $\tau_0$ , and the plastic viscosity,  $\mu$  [41]. These parameters are referred to as the Bingham parameters, and the Bingham material model is given by:

$$\tau = \tau_0 + \mu\dot{\gamma} \quad (1)$$

where  $\tau$  [Pa] is the shear stress,  $\tau_0$  [Pa] is the yield stress,  $\mu$  [Pa×s] is the plastic viscosity and  $\dot{\gamma}$  [ $s^{-1}$ ] is the shear strain rate. To assess the rheology of concentrated suspensions based on the Bingham parameters, traditional rheometers with different geometries are used. Concentric cylinders, cone-plate and parallel-plate geometries are normally used in rotational flow modes [42]. The former type of rheometer is used for suspensions with relatively low viscosity such as cement slurries, while the parallel plate geometries often are used for assessing the rheological behaviour of pastes [42]. Rheometer tests provide a more accurate evaluation of the rheological behaviour of suspensions than for instance the slump cone test. However, as such test are more expensive, time consuming and might even provide more information than what is required, simpler and cheaper tests are often preferred [43]. Rheometers have never been particularly popular outside the laboratory due to their cost, immobility and complicity [14]. For the rheometer tests performed in this thesis, an Anton Paar Physica MCR 300 rheometer equipped with a Couette (bob and cup) geometry was used. The applied test procedure is described in Publication III, but a brief description is given in the following. The cup is filled with cement paste, and the bob is lowered into the cup. First, the paste is homogenized at a constant shear rate, and thereafter left at rest. Then, it is subjected to linearly increasing shear rates, followed by linearly decreasing shear rates. The slope of the down-curve (decreasing shear rates) is used to calculate the plastic viscosity,  $\mu$ , while the intercept at zero shear rate is used to calculate the yield stress,  $\tau_0$  [44].

In addition to rheometer testing, the mini slump flow and flow resistance ratio have been measured on the matrices investigated in this thesis. The mini slump cone is a similar but smaller test apparatus than the Abrams cone, developed for cement pastes and grouts. Different geometries of the mini slump cone are reported in the literature [33, 43, 45], however, in this thesis a cone with top diameter of 39 mm, bottom diameter of 89 mm and height of 70 mm was used. A smooth plexiglass plate was used as the base for the measurements. During a measurement, the mini-cone was filled with matrix to the top of the cone. The cone was gently lifted and the diameter of the matrix at stoppage was measured in two orthogonal directions. The mini-slump flow value was then calculated as the average of the two measured diameters.

The flow resistance ratio is a unitless measure of the internal resistance of the matrix obtained from the simple FlowCyl test. The FlowCyl is a modification of the Marsh cone, being a cylindrical container ending in a V-funnel with a narrow nozzle outlet [1]. A full description of the test procedure is presented in Publication IV, as well as a description of how  $\lambda_q$  is deduced. Hence, the principles are only given in brief here. The weight loss through the FlowCyl as function of time is recorded, and from this data  $\lambda_q$  is deduced, defined as the difference in flow rate between the test



modulus is based on the particle void content of the fine and coarse portions of the particle system, where the rheological effect is more expressed for the fine portion ( $< 4\text{mm}$ ). The fineness modulus ( $F_M$ ) was therefore introduced as a correction factor for the air voids modulus.

Additionally, a workability function was developed for mortars and concrete, where mortar was defined as matrix and particles  $< 4\text{ mm}$ . The mortar workability is controlled by the properties of the particles and the properties of the matrix, as well as the volumetric ratio between particles and matrix. The particle properties are expressed by grading and the matrix properties are expressed by the flow resistance ratio. The workability function,  $K_p$ , is a hyperbolic S-shaped function. The work concluded that there was a strong correlation between the shape of the workability function and the properties of the particles and the matrix. The particle grading correlated to the amount of matrix at the turning point of the  $K_p$ -function, while the rheological mortar properties were concluded to be fully described by  $\lambda_q$ . This thesis focuses on the matrix-phase of the concrete, while further details about the particle-phase can be found in [47].

### 2.3 Particle characterization

The characteristics of particles in a suspension have major impact on its rheological behaviour. The rheological effect from crushed aggregate fines has mainly been attributed to the specific surface area [37, 49] and particle shape of the fines [50]. However, Cepuritis *et al.* [51] studied the rheology of cement pastes with crushed fines of different mineralogical composition, shape and grading, and found that the rheology could be controlled either by grading (specific surface area), shape or mineralogy. A later study concluded that the rheological effect on cement pastes mainly was governed by the specific surface area of the fines and their interaction with the SP molecules [33].

Regarding particle characterization, the focus of the thesis has been on how the volumetric specific surface area (VSSA) of dry materials per volume of matrix impacts rheology. There is no standard procedure for determining the VSSA of crushed aggregate fines, and several different methods are presented in the literature [35, 37, 52, 53]. Cepuritis [48] found that for crushed aggregate fines ( $< 125\ \mu\text{m}$ ) approximately 50 % of the specific surface area is concentrated below  $5\ \mu\text{m}$ . Precise measurements of particles below  $5\ \mu\text{m}$  are therefore necessary, and it was concluded that X-ray sedimentation was a suitable method. Hence, in this work the VSSA has been calculated from the PSD obtained from the Sedigraph, under the assumption of spherical particles. The SediGraph III Plus measures mass of particles through X-ray absorption and calculates the equivalent particle diameter [54]. The PSD is divided into a finite number of bins, and all particles within a bin are assigned a diameter equal to the mean diameter of the bin [48]. The VSSA is calculated as the general surface area of each bin, i.e.,  $6/d$ , where  $d$  is the particle diameter, multiplied by the differentiated bin volume passing percent. The method is more thoroughly described in Publication I. Note that VSSA is denoted SSA in Publication I.

## 2.4 Suspension rheology models

Numerous of different suspension models exist in literature, and a narrow selection is presented here. The excess paste theory that was shortly introduced in Section 1.2, or lubricating liquid thickness around all particles, was first proposed by Powers [8]. The liquid thickness is inversely proportional to VSSA and is found to be strongly linked to the rheological properties of cement pastes [55]. Also, the relative concentration of solids ( $\frac{\phi}{\phi_m}$ ), i.e., the ratio between the volume fraction of solids and the maximum packing fraction, correlates well to concrete rheology [56]. Krieger and Dougherty [57], Mooney [58], Quemada [59], Chong *et al.* [60], Eilers [61] and Robinson [62] did all propose suspension models for the relative viscosity, that are directly correlated to the relative concentration of solids. Spangenberg *et al.* [63] investigated the suspension models by Krieger and Dougherty [57] and Chong *et al.* [60] and illustrated that both models provided good approximations to experimental data on viscosity of bimodal suspensions with hard spherical particles.

Contrary to traditional suspension models, artificial intelligence is an evolving technology with respect to prediction of material properties, which potentially can reduce the need for laboratory testing [64]. Artificial neural network (ANN) is one example of such technique, which has shown to provide high prediction accuracies of experimental rheological results in fields such as viscosity prediction of nanofluids [65-67]. In Publication III, the relative viscosity models are elaborated and further investigated, as well as the correlation of both the lubricating liquid thickness and VSSA to cement paste rheology. The models are then compared with ANN predictions.

A more practical approach to cement paste prediction, tailor made for the ready-mix concrete industry, was presented in [37]. An empirical equation was developed for matrices with crushed aggregate fines, with emphasis on simplicity and applicability. The equation was a fitting model based on the particle matrix method, where matrix rheology was predicted based on mix composition. This equation has been further developed to account for larger parameter variations in Publication II.

## 2.5 Numerical simulations

In addition to experimental testing and rheology prediction with empirical models and traditional suspension models, several numerical simulations have been performed during the thesis work. A computational fluid dynamics (CFD) model that simulates the flow of cement pastes as Bingham materials has been developed in the commercial software Flow3D<sup>®</sup>. CFD has successfully been applied to model the flow behaviour of cementitious materials by several authors in the literature [68-76].

In CFD, the physical characteristics of fluids in motion are described by governing equations, named the Navier-Stokes equations [77]. When simulating concrete flow, concrete is often assumed to be incompressible [78], and this assumption is made in the simulations of the matrices in this thesis as well. For incompressible flows, the density is assumed to be constant within the considered volume [79], and the Navier-Stokes equations are given by eqn. 2 and 3.

$$\nabla \cdot \mathbf{u} = 0 \quad (2)$$

$$\rho \left( \frac{\delta \mathbf{u}}{\delta t} + \mathbf{u} \cdot \nabla \mathbf{u} \right) = -\nabla p + \eta \nabla^2 \mathbf{u} + \rho \mathbf{g} \quad (3)$$

where  $\mathbf{u}$  is the velocity vector field,  $p$  is the pressure,  $\rho$  is the material density,  $\eta$  is the dynamic viscosity,  $\mathbf{g}$  is the gravity acceleration vector, and  $t$  is the time [80].



### **3 Summary of appended publications**

#### **I Microproportioning paste with crushed aggregate filler by use of specific surface area**

Skare EL, Cepuritis R, Spangenberg J, Ramenskiy E, Mørtzell E, Smepllass S, Jacobsen S.  
*15th International Congress on the Chemistry of Cement* (2019).

Publication I presents an experimental rheology study of 114 matrices, consisting of two types of cement, three different crushed aggregate fines, SP, fly ash and silica fume. The study investigates how the volumetric specific surface area of all dry materials except silica fume correlates to the rheological behaviour of the matrices. The rheology was quantified in terms of the mini slump flow, the flow resistance ratio, as well as the Bingham yield stress and plastic viscosity. The specific surface area of each material was multiplied by the volumetric fraction of that material, and the contributions from each material were summarized. The surface area was presented as volumetric surface area of all dry materials per matrix volume [ $\text{mm}^2/\text{mm}^3$ ], which is also the case in the following. No correlation was found between the surface area and the rheology of matrices with silica fume. For matrices without silica fume, the surface area was found to be strongly dependent on the two cement types used, as matrices with each cement type fell on separate regression lines. The strongest correlations were found for the plastic viscosity, yielding  $R^2 = 0.85$  for both group of matrices (matrices with Industry cement or Standard FA cement). Hence, the study highlighted that the specific surface area could be a promising input parameter in the development of a microproportioning tool for concrete with crushed aggregates.

#### **II Application of an Improved Empirical Model for Rheology Prediction of Cement Pastes Modified with Filler from Manufactured Sand**

Skare EL, Cepuritis R, Mørtzell E, Smepllass S, Spangenberg J, Jacobsen S.  
*Nordic Concrete Research* 65 (2021) pp. 1-18.

In Publication II, the empirical model by Mørtzell [37] is further developed. The developed model, being an empirical equation, predicts the rheology of matrices based on the composition of the constituent materials. The volumetric specific surface area of all dry materials (except silica fume) per matrix volume [ $\text{mm}^2/\text{mm}^3$ ], that were found to correlate well to matrix rheology in Publication I, is one of the terms in the equations. Note that the specific surface area (SSA) in Publication I is equal to the volumetric specific surface area (VSSA) in Publication II, as the authors renamed the term after feedback from one reviewer. The empirical equation was developed based on experimental testing of 117 matrices, consisting of four different crushed fillers, two different cement types, biotite, fly ash, silica fume and SP. The mini slump flow, flow resistance ratio, Bingham yield stress and Bingham plastic viscosity were measured, and the predictive ability of the empirical equation for these four parameters was investigated. The study concluded that the empirical equation is a promising tool for the concrete industry. The best correlation was seen between the measured and estimated plastic viscosity, yielding an  $R^2 = 0.98$ , which is a surprisingly good result considering the large variety in mix design and materials. Furthermore,



the correlation coefficients between predicted and measured values for mini slump flow, flow resistance ratio and yield stress equalled  $R^2 = 0.95$ ,  $R^2 = 0.91$  and  $R^2 = 0.80$ , respectively.

### **III Rheology Modelling of Cement Paste with Manufactured Sand and Silica Fume: Comparing Suspension Models with Artificial Neural Network Predictions**

Skare EL, Sheiati S, Cepuritis R, Mørtzell E, Smepllass S, Spangenberg J, Jacobsen S.  
*Construction and Building Materials* 317 (2022) 126114.

Publication III compares traditional suspension models with artificial neural network predictions. The mini slump flow, flow resistance ratio, Bingham yield stress and Bingham plastic viscosity were measured on 107 matrices with crushed aggregate fines. The correlation to the four rheology parameters were investigated for nine suspensions models: two liquid thickness models, the relative concentration of solids and six relative viscosity models that are strongly correlated to the relative concentration of solids. None of these models provided good correlations to all matrices, obtaining an  $R^2 = 0.60$  at best. However, an increase in prediction accuracy was seen for subset of matrices. When only considering matrices without Industry cement and silica fume (= 55 matrices), one of the liquid thickness models provided an  $R^2 = 0.94$ . The chosen artificial neural network, namely multilayer perceptron, clearly outperformed the investigated suspension models, providing correlation coefficients between 0.84 and 0.91 for all 107 matrices, indicating that artificial neural networks predictions of matrix rheology are a promising avenue to follow.

### **IV FlowCyl: one-parameter cement paste rheology test developed at NTNU, Norway**

Cepuritis R, Skare EL, Jacobsen S, Spangenberg J, Smepllass S, Mørtzell E.  
*Rhéologie* 35 (2019) pp. 20-24.

In Publication IV, the main principles behind the FlowCyl test method is thoroughly described, as well as the definition of the flow resistance ratio. The paper highlights that the FlowCyl struggles to predict the flow of self-compacting concretes and mixes with high amounts of crushed sand. Further, the paper states that the major limitation of the FlowCyl is that it only correlates to the plastic viscosity and not the yield stress of the matrix. The study suggests two approaches to accommodate this limitation; Either by supplementing the FlowCyl with a mini-cone measurement or modifying the FlowCyl geometry to reduce the shear rates at the outlet.

### **V Analysing limitations of the FlowCyl as a one-point viscometer test for cement paste**

Cepuritis R, Skare EL, Ramenskiy E, Mørtzell E, Smepllass S, Li S, Jacobsen S, Spangenberg J.  
*Construction and Building Materials* 218 (2019) pp. 333-340.

Publication V investigates the limitations of using the flow resistance ratio as a one-point parameter to describe the flow of matrix. The investigation was performed both experimentally and numerically. The numerical model was used to quantify the error that is introduced by going

from simulating the rheological response by a three-parameter model, i.e., the Herschel-Bulkley model, to a two-parameter model, i.e., the Bingham model. The study showed that an additional error of approximately 2% could be expected when assuming that the matrix could be described by the two-parameter model. As this error is relatively sparse, the rest of the paper focused on going from a two-point parameter to a one-point parameter, i.e., the flow resistance ratio. The study concluded that the flow resistance ratio is clearly dominated by the plastic viscosity, a finding supported by the very high shear rates at the outlet revealed by the numerical simulations. Therefore, it was argued that the flow resistance ratio could be used as one-point characterization for matrices undergoing high shear rates. Another finding from the study was that the linear correlation between the Bingham parameters are affected by the SP dosage, and that the flow resistance ratio hence could predict the yield stress of matrices with constant SP dosages.

## **VI Neural network predictions of the simulated rheological response of cement paste in the FlowCyl**

Sheiati S, Ranjbar N, Frellsen J, Skare EL, Cepuritis R, Jacobsen S, Spangenberg J. *Neural Computing and Applications* 33 (2021) pp. 13027-13037.

Publication VI presents a numerical study of the rheological response of cement pastes in the FlowCyl. Two artificial neural networks (ANNs), multi-layer perceptron and radial basis function, were trained by a CFD model that simulated the FlowCyl test. The accuracies of the predictions from the two ANNs were compared, and it was also studied how few CFD simulations the ANNs require for training without reducing the predictive capabilities. The results showed that both ANNs could predict the simulated rheological behaviour of the cement pastes very well if the majority of the dataset was used for training. The radial basis function quickly lost its accuracy when considering a reduced training data, while the multi-layer perceptron model provided an  $R^2$ -value above 0.95 even when reducing the training data to 70%. Hence, it was concluded that a coupling between CFD and ANN could reduce the number of simulations and decrease the calculation time significantly.

## **VII Decreasing the Magnitude of Shear Rates in the FlowCyl**

Skare EL, Jacobsen S, Cepuritis R, Smeplass S, Spangenberg J. *Proceedings for the International Federation for Structural Concrete 5th International FIB Congress* (2018).

In Publication VII, numerical simulations are performed to investigate whether the magnitude of shear rates at the outlet of the FlowCyl may be reduced by change of geometry of the FlowCyl. The investigation was motivated by finding a geometry with higher correlation to the yield stress than the FlowCyl test. The study showed that the magnitude of shear rates decreased with decreasing hydrostatic head, cylinder diameter and outlet diameter. The simulated Bingham material obtained a maximum shear rate of 366 /s in the FlowCyl at the start of the experiment, while a reduction of approximately 60% were observed 35 seconds after the start of the experiment. Note that the appertaining hydrostatic head at 35 seconds was not calculated in the paper, but the

presented screenshot of the simulation after 35 seconds illustrates that the hydrostatic head, i.e., height, is approximately  $\frac{1}{4}$  of the original FlowCyl. By increasing the cylinder diameter from 80 mm to 160 mm, the occurring maximum shear rates increased with approximately 60 %. Lastly, an increase in outlet diameter from 8 mm to 12 mm increased the maximum shear rates with almost 30 %.

### **VIII Investigating the flow curve of the FlowCyl test as a measure of yield stress**

Skare EL, Jacobsen S, Spangenberg J.

Manuscript submitted to *The International Federation for Structural Concrete 6th International FIB Congress (2022)*.

Publication VIII analyses whether different parts of the flow curve (volume vs time) of the FlowCyl could show better correlations to the yield stress than the flow resistance ratio. Numerical simulations reveal that the correlation to the yield stress can be significantly improved by either considering the volume loss through the FlowCyl for a given time span, or the time it takes for a given volume of matrix to leave the FlowCyl. The numerical results are investigated on experimental data of 49 matrices, and an  $R^2 = 0.81$  is obtained between the yield stress and the time it takes for a volume change from  $V = 1.1$  litres to  $V = 1.0$  litres. This is a significant improvement compared to the correlation to the originally calculated flow resistance ratio ( $R^2 = 0.60$ ) for the same matrices.

### **IX FlowFunnel for measuring yield stress and plastic viscosity of cement paste**

Skare EL, Jacobsen S, Spangenberg J.

Manuscript submitted to *Cement and Concrete Research*.

In Publication IX, the geometry of the FlowCyl is modified by CFD modelling to increase its correlation to the yield stress. A prototype of the modified geometry was made, referred to as the FlowFunnel, and experimental results from 13 matrices were reported. The matrices represent the span in Bingham parameters of which most cement pastes are found, with yield stresses between 1.90 Pa and 29.99 Pa and plastic viscosities between 0.11 Pas and 1.22 Pas. The correlation to the mini slump flow were  $R^2 = 0.86$  and  $R^2 = 0.82$  for the yield stress and plastic viscosity, respectively. For the FlowFunnel experiments, the volume loss through the FlowFunnel the first 10-14 seconds were found to provide good correlations to the Bingham parameters, resulting in  $R^2 = 0.88$  and  $R^2 = 0.94$  for the yield stress and plastic viscosity, respectively. Hence, the modification of the geometry of the FlowCyl provides promising results with respect to establishing a simple and reliable method for determining the rheology of matrix with a one-point measurement of flow.

## 4 Conclusions

The following main conclusions can be drawn from the studies within this thesis:

- For matrices without silica fume, the volumetric specific surface area of dry materials per volume of matrix [ $\text{mm}^2/\text{mm}^3$  matrix] is strongly correlated to matrix rheology. This correlation is dependent on the cement type, and for the two investigated cement types in this study, the correlation is stronger for matrices with Standard FA cement than with Industry cement. No correlation is found between the specific surface area and the rheology of matrices with silica fume.
- It is possible to predict the rheology of matrices with crushed sand based on constituent materials. The empirical model by Mørtzell [37] has been further developed by including the volumetric specific surface area, as well as several other terms reflecting the matrix composition; solid content, SP-dosage, biotite/filler-ratio, fly ash/binder-ratio and water/powder-ratio. Despite a large variety in mix design and materials, the improved empirical equation provided a coefficient of determination,  $R^2$ , equal to 0.98, 0.95, 0.91 and 0.80 between estimated and measured values for 117 matrices for plastic viscosity, mini slump flow, flow resistance ratio and yield stress, respectively. This empirical equation is a promising tool for the concrete industry.
- Artificial neural network predictions are found to be a promising prediction tool for matrix rheology. When comparing the predictive capabilities of the investigated suspension models and artificial neural networks predictions, the chosen artificial neural network, multilayer perceptron, clearly outperformed the other models. Also, a coupling between CFD and ANN for flow simulations of matrix rheology is found to possibly reduce the number of simulations and calculation time significantly.
- The main limitation of the FlowCyl is its weak correlation to yield stress. The weak correlation is assigned to the high shear rates occurring at the outlet nozzle, which were detected by numerical simulations. Therefore, the original FlowCyl test can only be used as one-point characterization for matrices undergoing high shear rates. It is also argued that the flow resistance ratio could predict the yield stress of matrices with constant SP, as the linear correlation between the Bingham parameters are affected by the SP dosage.
- It is found that by changing the geometry of the FlowCyl, the correlation to the yield stress could be increased. Numerical simulations revealed that the magnitude of shear rates at the outlet nozzle decreased with decreasing hydrostatic head, cylinder diameter and outlet diameter.
- Numerical simulations show that different parts of the flow curve of the FlowCyl could show better correlations to the yield stress than the flow resistance ratio. The numerical results are investigated on experimental data of 49 matrices, and an  $R^2 = 0.81$  is obtained between the yield stress and the time it takes for a volume change from  $V = 1.1$  litres to  $V = 1.0$  litres. The correlation is substantially improved compared to the flow resistance ratio, which yielded an  $R^2 = 0.60$  for the same set of matrices.
- Optimization of the FlowCyl geometry has shown to be a promising avenue to follow with respect to establishing a simple and reliable method for determining matrix rheology with

a one-point measurement of flow. Based on numerical simulations a prototype of a modified geometry of the FlowCyl has been produced, called the FlowFunnel. The volume loss through the FlowFunnel the first 10-14 seconds provide good correlations to the Bingham parameters, resulting in  $R^2 = 0.88$  and  $R^2 = 0.94$  for the yield stress and plastic viscosity, respectively, for 13 investigated matrices.

## 5. Further research work

To narrow the scope of this thesis, only a few suspension models have been investigated, as presented in Section 2.4. However, there are several other interesting and promising suspension models in the literature that should be given attention in future research work. Flatt and Bowen [81] developed a yield stress model for concentrated suspensions, called the YODEL model. The general principle behind the model is to identify the number of particles in contact that cannot be separated by the applied shear stress, as these unbroken bonds are responsible for the yield stress of the suspension. The model accounts for the volume fraction of solids, mean particle size, particle size distribution, maximum packing, percolation threshold and interparticle forces, and shows good correlations to experimental data. Recently, the YODEL model showed to be very useful for predicting rheology of paste with filler from crushed sand [82]. The literature provides numerous other approaches to predict the yield stress of suspensions, such as the studies reported by Buscall *et al.*, Kapur *et al.*, Scales *et al.* and Zhou *et al.* [83-86]. These models have been improved from previous yield stress models, by including parameters such as particle size distributions, volume fraction of solids and inter-particle forces. Daminieli *et al.* [87] presents a viscosity model called the Particle Interference Model, which in contrast to most traditional viscosity suspension models accounts for particle interactions when predicting the cement paste viscosity.

The experimental work in this thesis has been limited to study the effect of four crushed aggregate fines, two cement types, one type of fly ash, one type of silica fume, one type of mica (biotite) and one type of superplasticizer. In the future, the validity of the numerical and empirical models resulting from this work should be investigated and possibly improved for larger material variations. This should include more types of filler, cement and superplasticizers, as well as other alternative sustainable binders, such as slag, fines from recycled aggregates, activated clay and geopolymers. Also, to deeper understand the rheological effect of part materials in matrices, future work should be focused on further material characterizations, as well as studying the interactions between the constituent materials. Topics such as adsorption of SP, surface physics and surface chemistry have not been visited in this work, though these properties are known to affect the rheology of cementitious suspensions, see for example [88-89].



## References

- [1] Cepuritis, R., Ramenskiy, E., Mørtzell, E., Smeplass, S., Kjos-Hanssen, H.S., Li, S., Jacobsen, S. and Spangenberg, J. (2017) FlowCyl: one-parameter characterisation of matrix rheology. Second Concrete Innovation Conference (2<sup>nd</sup> CIC), Tromsø, Norway.
- [2] Torres, A., Brandt, J., Lear, K. and Liu, J. (2017) A looming tragedy of the sand commons. *Science* 357(6355), pp. 970-971. <https://doi.org/10.1126/science.aa0503>.
- [3] Krausmann, F., Wiedenhofer, D., Lauk, C., Haas, W., Tanikawa, H., Fishman, T., Miatto, A., Schandl, H. and Haberl, H. (2017) Global socioeconomic material stocks rise 23-fold over the 20th century and require half of annual resource use. *Proceedings of the National Academy of Sciences of the United States of America*, 114(8), pp. 1880-1885. <https://doi.org/10.1073/pnas.1613773114>.
- [4] Bisht, A. (2021) Conceptualizing sand extractivism: Deconstructing an emerging resource frontier. *The Extractive Industries and Society*, 8(2):100904. <https://doi.org/10.1016/j.exis.2021.100904>.
- [5] 7continents (2021) *Deserts of the world*. Available at: <https://www.whatarethe7continents.com/deserts-of-the-world/> (Accessed September 2021).
- [6] Liu, H., Chen, X., Che, J., Liu, N. and Zhang, M. (2020) Mechanical Performances of Concrete Produced with Desert Sand After Elevated Temperature. *International Journal of Concrete Structures and Materials*, 14(26), 15 pages. <https://doi.org/10.1186/s40069-020-00402-3>.
- [7] Al-Harthy, A.S., Halim, M.A., Taha, R. and Al-Jabri, K.S. (2007) The properties of concrete made with fine dune sand. *Construction and Building Materials*, 21(8), pp. 1803-1808. <https://doi.org/10.1016/j.conbuildmat.2006.05.053>.
- [8] Powers, T.C. (1968) *The Properties of Fresh Concrete*. Wiley & Sons, New York, USA, 664 pp.
- [9] United Nations – Department of Economic and Social Affairs | Sustainable Development (2021) The 17 Goals. UN SDG no. 12 Responsible consumption and production. Available at <https://sdgs.un.org/goals/goal12> (Accessed September 2021).
- [10] Neeb, P.R. (2008) Norway's coastal aggregates. Export in 2007 and potential deposits. *NGU Report no. 2008.044*. ISSN 0800-3416.
- [11] Brown, T.J., Hobbs, S.F., Idoine, N.E., Mills, A.J., Wrighton, C.E. and Raycraft, E.R. (2016) European Mineral Statistics 2010-14. *British Geological Survey*. ISBN 978-0-85272.859-8.
- [12] Wigum, B.J., Danielsen, S.W., Hotvedt, O. and Pedersen, B. (2009) Production and Utilisation of Manufactured Sand. *COIN Project report 12-2009*. ISSN 1891-1978.



- [13] Ferraris, C.F., Billberg, P., Ferron, R., Feys, D., Hu, J., Kawashima, S., Koehler, E., Sonebi, M., Tanesi, J. and Tregger, N. (2017) Role of Rheology in Achieving Successful Concrete Performance. *ACI Committee 238, Workability of Fresh Concrete*, pp. 43-51.
- [14] Wallevik, J.E. (2006) Relationship between the Bingham parameters and slump. *Cement and Concrete Research*, 36(7), pp. 1214-1221. <https://doi.org/10.1016/j.cemconres.2006.03.001>.
- [15] Saak, A.W., Jennings, H.M. and Shah, S.P. (2004) A generalized approach for the determination of yield stress by slump and slump flow. *Cement and Concrete Research*, 34(3), pp. 363-371. <https://doi.org/10.1016/j.cemconres.2003.08.005>.
- [16] Roussel, N. (2007) The LCPC BOX: a cheap and simple technique for yield stress measurements of SCC. *Materials and Structures*, 40, pp. 889–896. <https://doi.org/10.1617/s11527-007-9230-4>.
- [17] Ferraris, C.F., Obla, K.H. and Hill, R. (2001) The influence of mineral admixtures on the rheology of cement paste and concrete. *Cement and Concrete Research*, 31(2), pp. 245-255. [https://doi.org/10.1016/S0008-8846\(00\)00454-3](https://doi.org/10.1016/S0008-8846(00)00454-3).
- [18] Agullo, L., Toralles-Carbonari, B., Gettu, R. and Aguado, A. (1999) Fluidity of cement pastes with mineral admixtures and superplasticizer – A study based on the Marsh cone test. *Materials and Structures*, 32, pp. 479-485. <https://doi.org/10.1007/BF02481631>.
- [19] Nicolas, R. and Le Roy, R. (2005) The Marsh cone: a test or a rheological apparatus? *Cement and Concrete Research*, 35(5), pp. 823-830. <https://doi.org/10.1016/j.cemconres.2004.08.019>.
- [20] Schwartzenruber, A. and Catherine, C. (2000) Method of the concrete equivalent mortar (CEM)—A new tool to design concrete containing admixture. *Materials and Structures*, 33, pp. 475-482. <https://doi.org/10.1007/BF02480524> (In French)
- [21] Kabagire, D., Diederich, P. and Yahia, A. (2015) New insight into the equivalent concrete mortar approach for self-consolidating concrete. *Journal of Sustainable Cement-Based Materials*, 4, pp. 215-224. <https://doi.org/10.1080/21650373.2015.1018983>.
- [22] Assaad, J.J., Harb, J. and Chakar, E.A. (2009) Relationships Between Key ASTM Test Methods Determined on Concrete and Concrete-Equivalent-Mortar Mixtures. *Journal of ASTM International*, 6(3), 13 pages. <https://doi.org/10.1520/JAI101735>.
- [23] Lee, J.H., Kim, J.H. and Yoon, J.Y. (2018) Prediction of the yield stress of concrete considering the thickness of excess paste layer. *Construction and Building Materials*, 173, pp. 411-418. <https://doi.org/10.1016/j.conbuildmat.2018.03.124>.
- [24] Safiddine, S., Debieb, F., Kadri, E.H., Menadi, B. and Soualhi, H. (2017) Effect of crushed sand and limestone crushed sand dust on the rheology of cement mortars. *Applied Rheology*, 27, 9 pages. <https://doi.org/10.3933/applrheol-27-14490>.

- [25] Benachour, Y., Davy, C.A., Skoczylas, F. and Houari, H. (2008) Effect of a high calcite filler addition upon microstructural, mechanical, shrinkage and transport properties of a mortar. *Cement and Concrete Research*, 38(6), pp. 727-736. <https://doi.org/10.1016/j.cemconres.2008.02.007>.
- [26] Çelik, T. and Marar, K. (1996) Effects of crushed stone dust on some properties of concrete. *Cement and Concrete Research*, 26(7), pp. 1121-1130. [https://doi.org/10.1016/0008-8846\(96\)00078-6](https://doi.org/10.1016/0008-8846(96)00078-6).
- [27] Donza, H., Cabrera, O. and Irassar, E.F. (2002) High-strength concrete with different fine aggregate. *Cement and Concrete Research*, 32(11), pp. 1755-1761. [https://doi.org/10.1016/S0008-8846\(02\)00860-8](https://doi.org/10.1016/S0008-8846(02)00860-8).
- [28] Kim, J.K., Lee, C.S., Park, C.K. and Eo, S.H. (1997) The fracture characteristics of crushed limestone sand concrete. *Cement and Concrete Research*, 27(11), pp. 1719-1729. [https://doi.org/10.1016/S0008-8846\(97\)00156-7](https://doi.org/10.1016/S0008-8846(97)00156-7).
- [29] Menadi, B., Kenai, S., Khatib, J. and Ait-Mokhtar, A. (2009) Strength and durability of concrete incorporating crushed limestone sand. *Construction and Building Materials*, 23(2), pp. 625-633. <https://doi.org/10.1016/j.conbuildmat.2008.02.005>.
- [30] Eren, Ö. and Marar, K. (2009) Effects of limestone crusher dust and steel fibers on concrete. *Construction and Building Materials*, 23(2), pp. 981-988. <https://doi.org/10.1016/j.conbuildmat.2008.05.014>.
- [31] Valcuende, M., Marco, E., Parra, C. and Serna, P. (2012) Influence of limestone filler and viscosity-modifying admixture on the shrinkage of self-compacting concrete. *Cement and Concrete Research*, 42(4), pp. 583-592. <https://doi.org/10.1016/j.cemconres.2012.01.001>.
- [32] Bouziani, T. (2013) Assessment of fresh properties and compressive strength of self-compacting concrete made with different sand types by mixture design modelling approach. *Construction and Building Materials*, 49, pp. 308-314. <https://doi.org/10.1016/j.conbuildmat.2013.08.039>.
- [33] Cepuritis, R., Jacobsen, S., Smeplass, S., Mørtzell, E., Wigum, B.J. and Ng, S. (2017) Influence of Crushed Aggregate Fines with Micro-Proportioned Particle Size Distributions on Rheology of Cement Paste. *Cement and Concrete Composites*, 80, pp. 64-79. <https://doi.org/10.1016/j.cemconcomp.2017.02.012>.
- [34] Cepuritis, R., Jacobsen, S., Pedersen, B. and Mørtzell, E. (2016) Crushed sand in concrete – Effect of particle shape in different fractions and filler properties on rheology. *Cement and Concrete Composites*, 71, pp. 26-41. <https://doi.org/10.1016/j.cemconcomp.2016.04.004>.
- [35] Westerholm, M., Lagerblad, B., Silfwerbrand, J. and Forssberg, E. (2008) Influence of fine aggregate characteristics on the rheological properties of mortars. *Cement and Concrete Composites*, 30(4), pp. 274-282. <https://doi.org/10.1016/j.cemconcomp.2007.08.008>.

- [36] Cortes, D.D., Kim, H.K., Palomino, A.M. and Santamarina, J.C. (2008) Rheological and mechanical properties of mortars prepared with natural and manufactured sands. *Cement and Concrete Research*, 38(10), pp. 1142-1147. <https://doi.org/10.1016/j.cemconres.2008.03.020>.
- [37] Mørtzell, E. (1996) Modelling av Delmaterialenes Betydning for Betongens Konsistens (Eng: Modelling the Effect of Concrete Part Materials on Concrete Consistency). PhD Thesis. Norwegian University of Science and Technology, Trondheim. (In Norwegian)
- [38] Smeplass, S. and Mørtzell, E. (2001) The applicability of the particle matrix model to self compacting concrete (SCC). *Nordic Concrete Research*, 26, pp. 83-95. Available at: <https://www.danskbetonforening.dk/media/ncr/publication-no-26-06.pdf>
- [39] Ferraris, C.F. (1999) Measurement of the Rheological Properties of High Performance Concrete: State of the Art Report. *Journal of Research of the National Institute of Standards and Technology*, 104(5), pp. 461-478. <https://doi.org/10.6028/jres.104.028>.
- [40] Cepuritis, R., Jacobsen, S. and Spangenberg, J. (2017) The Particle-Matrix model: limitations and further improvements needed. *Proceedings of the XXIII Nordic Concrete Research Symposium*, 4, pp. 349-352.
- [41] Ferraris, C.F. (1999) Measurement of the rheological properties of cement paste: A new approach. *PRO 5: International RILEM conference on The Role of Admixtures in High Performance Concrete (Cabrera JG)*. RILEM Publications. ISBN 13:2912143055.
- [42] Cardoso, F.A., Fujii, A.L., Pileggi, R.G. and Chaouche, M. (2015) Parallel-plate rotational rheometry of cement paste: Influence of the squeeze velocity during gap positioning. *Cement and Concrete Research*, 75, pp. 66-74. <https://doi.org/10.1016/j.cemconres.2015.04.010>.
- [43] Roussel, N., Stefani, C. and Leroy, R. (2005) From mini-cone test to Abrams cone test: measurement of cement-based materials yield stress using slump tests. *Cement and Concrete Research*, 35(5), pp. 817-822. <https://doi.org/10.1016/j.cemconres.2004.07.032>.
- [44] Mezger, T. (2006) *The Rheology Handbook: for Users of Rotational and Oscillatory Rheometers*. Vincentz Network, Hannover.
- [45] Tan, Z., Bernal, S.A., Provis, J.L. (2017) Reproducible mini-slump test procedure for measuring the yield stress of cementitious pastes. *Materials and Structures*, 50:235, 12 pages. <https://doi.org/10.1617/s11527-017-1103-x>.
- [46] Ejiogu, I.K., Mamza, P.S., Nkeonye, P.O. and Yaro, A.S. (2018) Comparative Study of Various Methods for Designing and Proportioning Normal Concrete Mixture. *The Pacific Journal of Science and Technology*, 19, pp. 22-36.
- [47] Bartos, P.J.M., Cleland, D.J., Marrs, D.L. *et al.* (2019) *Part Eight – Mix design and models. Production Methods and Workability of Concrete*. Taylor & Francis Ltd. ISBN: 9780367448493.
- [48] Cepuritis, R. (2016) Development of Crushed Sand for Concrete Production with Micro-proportioning. PhD Thesis. Norwegian University of Science and Technology, Trondheim.

- [49] Esping, O. (2008) Effect of limestone filler BET(H<sub>2</sub>O)-area on the fresh and hardened properties of self-compacting concrete. *Cement and Concrete Research*, 38, pp. 938-944. <https://doi.org/10.1016/j.cemconres.2008.03.010>.
- [50] Westerholm, M., Lagerblad, B. and Forssberg, E. (2007) Rheological properties of micromortars containing fines from manufactured aggregates. *Materials and Structures*, 40, pp. 615–625. <https://doi.org/10.1617/s11527-006-9173-1>
- [51] Cepuritis, R., Jacobsen, S. and Pedersen, B. (2013) SCC matrix rheology with crushed aggregate fillers: effect of physical and mineralogical properties, replacement, co-polymer type and w/b-ratio. *Proceedings of the 7<sup>th</sup> international RILEM symposium on Self-Compacting Concrete*.
- [52] Järvenpää, H. (2001) Quality characteristics of fine aggregate and controlling their effects on concrete. PhD thesis. Helsinki University of Technology, Helsinki.
- [53] Erdoğan, S.T., Garboczi, E.J. and Fowler, D.W. (2007) Shape and size of microfine aggregates: X-ray microcomputed tomography vs. laser diffraction. *Powder Technology*, 177(2), pp. 53-63. <https://doi.org/10.1016/j.powtec.2007.02.016>.
- [54] Micromeritics (2003) *SediGraph III 5120 Operator's Manual v1.00*. Micromeritics Instrument Corporation.
- [55] Kwan, A.K.H., Fung, W.W.S. and Wong, H.H.S. (2010) Water film thickness, flowability and rheology of cement–sand mortar. *Advances in Cement Research*, 22 (1), pp. 3-14. <https://doi.org/10.1680/adcr.2008.22.1.3>.
- [56] Ferraris, C. and de Larrard, F. (1998) Testing and modelling of fresh concrete rheology. *Journal of National Institute of Standards and Technology*, NISTIR 6094. <https://doi.org/10.6028/NIST.IR.6094>.
- [57] Krieger, I.M. and Dougherty, T.J. (1959) A Mechanism for Non-Newtonian Flow in Suspensions of Rigid Spheres. *Transaction of the Society of Rheology* III, pp. 137-152. <https://doi.org/10.1122/1.548848>.
- [58] Mooney, M. (1951) The viscosity of a concentrated suspension of spherical particles. *Journal of Colloid and Interface Science*, 6(2), pp. 162-170. [https://doi.org/10.1016/0095-8522\(51\)90036-0](https://doi.org/10.1016/0095-8522(51)90036-0).
- [59] Quemada, D. (1977) Rheology of concentrated disperse systems and minimum energy dissipation principle. *Rheologica Acta*, 16, pp. 82-94. <https://doi.org/10.1007/BF01516932>.
- [60] Chong, J.S., Christiansen, E.B. and Baer, A.D. (1971) Rheology of Concentrated Suspensions. *Journal of Applied Polymer Science*, 15, pp. 2007-2021. <https://doi.org/10.1002/app.1971.070150818>.
- [61] Eilers, H. (1941) Die Viskosität von Emulsionen hochviskoser Stoffe als Funktion der Konzentration. *Kolloid-Zeitschrift*, 97(3), pp. 313-321. <https://doi.org/10.1007/BF01503023>. (In German)

- [62] Robinson, J.V. (1949) The viscosity of suspensions of spheres. *Journal of Physical and Colloid Chemistry*, 53(7), pp. 1042-1056. <https://doi.org/10.1021/j150472a007>.
- [63] Spangenberg, J., Scherer, G.W., Hopkins, A.B. and Torquato, S. (2014) Viscosity of bimodal suspensions with hard spherical particles. *Journal of Applied Physics*, 116, 184902, pp. 1-7. <https://doi.org/10.1063/1.4901463>.
- [64] Nadooshan, A.A., Esfe, M.H. and Afrand, M. (2018) Prediction of rheological behavior of SiO<sub>2</sub>-MWCNTs/10W40 hybrid nanolubricant by designing neural network. *Journal of Thermal Analysis and Calorimetry*, 131, pp. 2741–2748. <https://doi.org/10.1007/s10973-017-6688-3>.
- [65] Esfe, M.H., Saedodin, S., Sina, N., Afrand, M. and Rostami, S. (2015) Designing an artificial neural network to predict thermal conductivity and dynamic viscosity of ferromagnetic nanofluid. *International Communications in Heat and Mass Transfer*, 68, pp. 50–57. <https://doi.org/10.1016/j.icheatmasstransfer.2015.06.013>.
- [66] Afrand, M., Najafabadi, K.N., Sina, N., Safaei, M.R., Kherbeet, A.S., Wongwises, S. and Dahari, M. (2016) Prediction of dynamic viscosity of a hybrid nano-lubricant by an optimal artificial neural network. *International Communications in Heat and Mass Transfer*, 76, pp. 209–214. <https://doi.org/10.1016/j.icheatmasstransfer.2016.05.023>.
- [67] Karimi, H., Yousefi, F. and Rahimi, M.R. (2011) Correlation of viscosity in nanofluids using genetic algorithm-neural network (GA-NN). *Heat and Mass Transfer*, 47, pp. 1417–1425. <https://doi.org/10.1007/s00231-011-0802-z>.
- [68] Ferrara, L., Cremonesi, M., Tregger, N., Frangi, A. and Shah, S.P. (2012) On the identification of rheological properties of cement suspensions: Rheometry, Computational Fluid Dynamics modeling and field test measurements. *Cement and Concrete Research*, 42(8):1134–1146. <https://doi.org/10.1016/j.cemconres.2012.05.007>.
- [69] Liu, L., Fang, Z., Wang, M., Qi, C., Zhao, Y. and Huan, C. (2020) Experimental and numerical study on rheological properties of ice-containing cement paste backfill slurry. *Powder Technology*, 370:206-214. <https://doi.org/10.1016/j.powtec.2020.05.024>.
- [70] Hosseinpour, M., Yahia, A. and Khayat, K.H. (2019) Modeling of flow performance of self-consolidating concrete using Dam Break Theory and computational fluid dynamics. *Cement and Concrete Composites*, 102, pp. 14-27. <https://doi.org/10.1016/j.cemconcomp.2019.04.018>.
- [71] Comminal, R., da Silva, W.R.L., Andersen, T.J., Stang, H. and Spangenberg, J. (2020) Modelling of 3D concrete printing based on computational fluid dynamics. *Cement and Concrete Research*, 138:106256, 12 pages. <https://doi.org/10.1016/j.cemconres.2020.106256>.
- [72] Spangenberg, J., Roussel, N., Hattel, J.H., Stang, H., Skocek, J., Geiker, M.R. (2012) Flow induced particle migration in fresh concrete: Theoretical frame, numerical simulations and experimental results on model fluids. *Cement and Concrete Research*, 42(4), pp. 633-641. <https://doi.org/10.1016/j.cemconres.2012.01.007>.

- [73] Roussel, N., Spangenberg, J., Wallevik, J., Wolfs, R. (2020) Numerical simulations of concrete processing: From standard formative casting to additive manufacturing. *Cement and Concrete Research*, 135, 106075, 10 pages. <https://doi.org/10.1016/j.cemconres.2020.106075>.
- [74] Comminal, R., da Silva, W.R.L., Andersen, T.J., Stang, H., Spangenberg, J. (2020) Modelling of 3D concrete printing based on computational fluid dynamics. *Cement and Concrete Research*, 138, 106256, 12 pages. <https://doi.org/10.1016/j.cemconres.2020.106256>.
- [75] Spangenberg, J., Roussel, N., Hattel, J.H., Thorborg, J., Geiker, M.R., Stang, H., Skocek, J. (2010) Prediction of the impact of flow-induced inhomogeneities in self-compacting concrete (SCC). In: Khayat K., Feys D. (eds) *Design, Production and Placement of Self-Consolidating Concrete*. RILEM Bookseries, 1, pp. 209-215. Springer, Dordrecht. [https://doi.org/10.1007/978-90-481-9664-7\\_18](https://doi.org/10.1007/978-90-481-9664-7_18)
- [76] Jacobsen, S., Cepuritis, R., Peng, Y., Geiker, M.R., Spangenberg, J. (2013) Visualizing and simulating flow conditions in concrete form filling using pigments. *Construction and Building Materials*, 49, pp. 328-342. <https://doi.org/10.1016/j.conbuildmat.2013.08.027>.
- [77] Tu, J., Yeoh, G.H. and Liu, C. (2008) *Chapter 1 – Introduction, Computational Fluid Dynamics*. Butterworth-Heinemann. Pages 1-28. ISBN 9780750685634. <https://doi.org/10.1016/B978-075068563-4.50003-3>.
- [78] Roussel, N., Gram, A., Cremonesi, M., Ferrara, L., Krenzer, K., Mechtcherine, V., Shyshko, S., Skocek, J., Spangenberg, J., Svec, O., Thrane, L. and Vasilic, K (2016) Numerical simulations of concrete flow: A benchmark comparison. *Cement and Concrete Research*, 79, pp. 265-271. <https://doi.org/10.1016/j.cemconres.2015.09.022>.
- [79] Bingham, H.B., Larsen, P.S. and Barker, V.A. (2015) *Computational Fluid Dynamics – Lecture Note for Course no. 41319*. Compendium, Technical University of Denmark.
- [80] Comminal, R., Jafarzadeh, S., Serdeczny, M. and Spangenberg, J. (2020) Estimations of Interlayer Contacts in Extrusion Additive Manufacturing Using a CFD Model. *Industrializing Additive Manufacturing – Proceedings of AMPA 2020*, Zürich, Switzerland, 01.09.20-03.09.20.
- [81] Flatt, R.J., Bowen, P. (2006) Yodel: A Yield Stress Model for Suspensions. *Journal of the American Ceramic Society*, 89(4), pp. 1244-1256. <https://doi.org/10.1111/j.1551-2916.2005.00888.x>
- [82] Zhu, J., Shu, X., Tang, J., Li, T., Ran, Q., Liu, J. (2021) Effect of microfines from manufactured sand on yield stress of cement paste. *Construction and Building Materials*, 267, 120987, 12 pages. <https://doi.org/10.1016/j.conbuildmat.2020.120987>.
- [83] Buscall, R., McGowan, I.J., Mills, P.D.A., Stewart, R.F., Sutton, D., White, L.R. and Yates, G.E. (1987) The rheology of strongly-flocculated suspensions. *Journal of Non-Newtonian Fluid Mechanics*, 24, pp. 183-202. [https://doi.org/10.1016/0377-0257\(87\)85009-7](https://doi.org/10.1016/0377-0257(87)85009-7).

- [84] Kapur, P.C., Scales, P.J., Boger, D.V. and Healy, T.W. (1997) Yield stress of suspensions loaded with size distributed particles. *AIChE Journal*, 43, pp. 1171-1179. <https://doi.org/10.1002/aic.690430506>.
- [85] Scales, P.J., Johnson, S.B., Healy, T.W. and Kapur, P.C. (1998) Shear yield stress of partially flocculated colloidal suspensions. *AIChE Journal*, 44, pp. 538-544. <https://doi.org/10.1002/aic.690440305>.
- [86] Zhou, Z., Solomon, M.J., Scales, P.J. and Boger, D.V. (1999) The yield stress of concentrated flocculated suspensions of size distributed particles. *Journal of Rheology*, 43, pp. 651-671. <https://doi.org/10.1122/1.551029>.
- [87] Damineli, B.L., John, V.M., Lagerblad, B. and Pileggi, R.G. (2016) Viscosity prediction of cement-filler suspensions using interference model: A route for binder efficiency enhancement. *Cement and Concrete Research*, 84, pp. 8-19. <https://doi.org/10.1016/j.cemconres.2016.02.012>.
- [88] Colombo, A., Geiker M., Justnes, H., Lauten, R.A., De Weerd, K. (2017) On the mechanisms of consumption of calcium lignosulfonate by cement paste. *Cement and Concrete Research*, 98, pp. 1-9. <https://doi.org/10.1016/j.cemconres.2017.02.026>.
- [89] Colombo, A., Geiker M., Justnes, H., Lauten, R.A., De Weerd, K. (2017) On the effect of calcium lignosulfonate on the rheology and setting time of cement paste. *Cement and Concrete Research*, 100, pp. 435-444. <https://doi.org/10.1016/j.cemconres.2017.06.009>.

**Microproportioning paste with crushed aggregate filler by use of specific surface area**  
Skare EL, Cepuritis R, Spangenberg J, Ramenskiy E, Mørtzell E, Smeplass S, Jacobsen S.  
*15th International Congress on the Chemistry of Cement (2019).*





## Microproportioning paste with crushed aggregate filler by use of specific surface area

Elisabeth Leite Skare<sup>1,2,3,a</sup>, Rolands Cepuritis<sup>4,1,b</sup>, Jon Spangenberg<sup>2,c</sup>, Evgeny Ramenskiy<sup>1,d</sup>, Ernst Mørtzell<sup>1,5,e</sup>, Sverre Smepllass<sup>1,6,f</sup>, Stefan Jacobsen<sup>1,6,g</sup>

<sup>1</sup>*Structural Engineering, NTNU, Trondheim, Norway*

<sup>2</sup>*Department of Mechanical Engineering, Technical University of Denmark, Kongens Lyngby, Denmark*

<sup>3</sup>*Betong Øst Trøndelag, Trondheim, Norway*

<sup>4</sup>*R&D Department, Norcem AS, Brevik, Norway*

<sup>5</sup>*Norbetong AS, Heimdal, Norway*

<sup>6</sup>*Skanska Norge AS, Oslo, Norway*

<sup>a</sup>elisabeth.l.skare@ntnu.no

<sup>b</sup>rolands.cepuritis@ntnu.no

<sup>c</sup>josp@mek.dtu.dk

<sup>d</sup>evgeny.ramenskiy@ntnu.no

<sup>e</sup>ernst.mortzell@norbetong.no

<sup>f</sup>sverre.smepllass@skanska.no

<sup>g</sup>stefan.jacobsen@ntnu.no

### ABSTRACT

It is necessary to understand how to combine the fines with various cementitious and pozzolanic binders and admixtures, in order to develop the use of crushed aggregate fines in concrete, obtaining target rheological properties. Following previous studies on the effect of crushed aggregate fines specific surface area (SSA) and its relation to rheology, we extended this approach to all materials and still find that SSA relates to rheology measurements on largely different powders: crushed fines, Portland cement, blended cements (fly ash ground with clinker) and also additional bulk fly ash. First, we developed a single method for powder particle size distribution (PSD) and SSA using an X-ray Sedigraph covering all powders of the filler modified paste. Then we investigated both mixes with constant and varying solid fraction and found that they correlated reasonably well to rheology at constant SP dosage, in spite of the big differences in both powder composition and higher range of SSA values compared to the early filler studies. The current study reports some additional experiments, where mixes incorporating also silica fume and variable SP-dosage have been included, with the purpose of further understanding the suitability of using the SSA of all the powders in a mix as the main parameter for developing a practical concrete micro-proportioning tool.

## 1. INTRODUCTION

Sand is a widely used material all over the world, especially in the construction industry. Hence, the deposits of natural sand of good quality are becoming depleted, and a replacement for the natural sand is needed. Crushed sand, that is rocks crushed down to smaller fractions, is a good alternative. However, the manufactured sand, unless properly processed, is more angular and contains more fines due to the crushing process, and will result in a less flowing concrete when it equally replaces natural sand.

The primary method for proportioning concrete in Norway over the last two decades is the particle-matrix method. It is a two-phase approach based on the assumption that concrete rheology is controlled by the volume fraction of coarse aggregate particles in the mix and by the flow properties of the suspending matrix (Smeplass & Mørtzell 2001). In this model all fines less than 125 microns are considered as a part of the suspending matrix – also called filler modified cement paste. However, when using crushed sand, the proportion of particles less than 125 microns have a dominating effect on the flow. Hence, a further development of the method is necessary, where the effect of the fine particles on the rheology of the matrix is taken into account. A microproportioning tool is under development, where the rheology of paste could be predicted using the proportions and some property of part materials as input. It is well known that the paste rheology is affected by factors like SP-dosage, w/c – ratio, solid content etc. However, there is a need of developing a method that also takes into account the properties of the fillers, especially with respect to the fineness. In this study we investigate to what extent the specific surface area (SSA) per volume of paste, correlates with the rheological properties of the suspending matrix. Later, the rheology of concrete could be predicted by using microproportioning together with the particle-matrix model.

## 2. EXPERIMENTS

### 2.1 Materials

The mixing and rheological measurements on the filler modified cement pastes were performed in five series, denoted the A-, B-, C-, D- and E- series, representing a wide variability and large range of part materials and proportions. The five series results in 114 different mixes. Series A and B have been performed by former Ph.D student Evgeny Ramenskiy in the MiKS-project, and a calculation of the SSA is done for these fillers, based on the latest results of the PSDs for the fillers. The cement pastes consist of different combinations of filler, cement, superplasticiser, fly ash and silica fume. Three different types of crushed aggregate fillers are used, originating from the same granitic rock type and prepared by the same production process. The rock type is mainly composed of feldspar and quartz, representing approximately 48 % each, while amphibolite, mica and chlorite represent less than 5 % in total. The crushing of the aggregates took place in 4 different steps, and the generated fillers were extracted from the rest of the aggregates by an air-classification method. The three different types of fines were extracted at different steps in the air-classification process, and differ from each other in particle size distributions (PSDs). The different fillers are denoted Velde Fine, Velde Intermediate and Velde Coarse, justified in that they are extracted at cut-size 63  $\mu\text{m}$ , 125  $\mu\text{m}$  and 500  $\mu\text{m}$ , respectively. The particle sizes for all three crushed fillers are 0-125  $\mu\text{m}$ , adjusted by mechanical sieving in our lab before mixing. The densities for the crushed fillers were measured by helium pycnometry to be the same, *i.e.* 2.65  $\text{g}/\text{cm}^3$ . The cement type used in test series A and B is the Norwegian standard fly-ash (Std FA) cement from Norcem AS with 20 % fly ash ground with the clinker, CEM II/B-M 42.5 R. For test series C and D, the Norwegian OPC “Industry” cement from Norcem AS, CEM I 52,5 R, is used in all the pastes. Both cement types are represented in the E-series. A polycarboxylate ether-based superplasticiser (SP) Dynamon SR-N from Mapei, with dry solids content of 19.5 %, is used in all the mixes. Additional fly ash from Norcem AS is introduced in some of the pastes in the C-, D- and E-series. Undensified Elkem Microsilica, 940-U, was also included in some of the pastes in the E-series. The PSD for the fillers, cements and fly ash were measured by the x-ray sedimentation machine SediGraph III Plus; the results are shown in Figure 1.

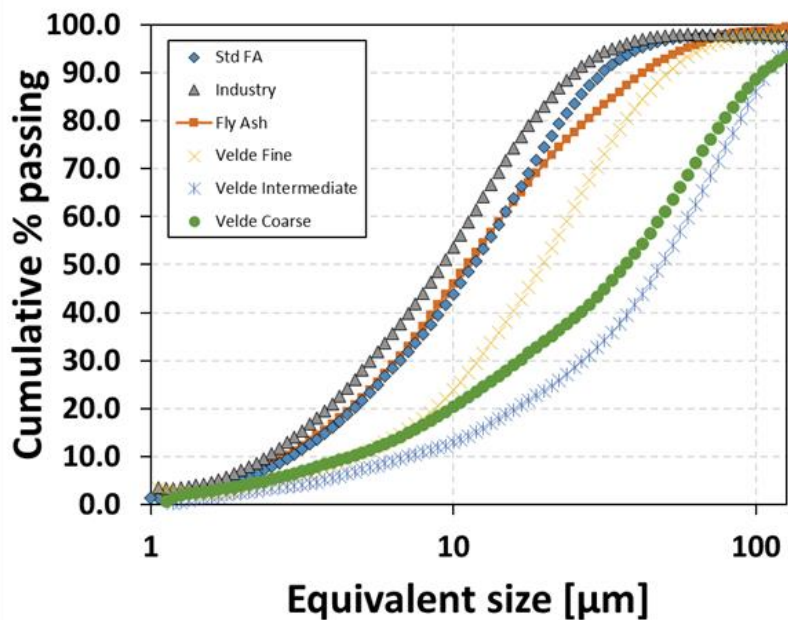


**Figure 1. PSDs of all dry materials used for the study (except silica fume) determined with the SediGraph III Plus.**

The SediGraph III Plus measures mass of particles dispersed in a fluid with known viscosity and density, through x-ray absorption. Based on the mass and the particle falling rates, the equivalent particle diameter is calculated (Micromeritics 2003). In this study, the dispersing liquid used is Micromeritics Sedisperse A-12. The A-12 fluid was selected after review and studies of reactivity and settling of fly ash, filler and cement with particle densities 2380 – 3130 kg/m<sup>3</sup>, maximum diameter 125 microns and maximum Reynolds number = 0.30 (Sosa 2017). The specific surface area (SSA) is a parameter defined as surface area per volume of a material, and may be used to characterize the properties of the dry materials (Bentz et al. 2012). Different approaches for calculating the SSA exist, but it may be calculated from the particle size distribution from the Sedigraph, under the assumption of spherical particles (Cepuritis 2016). The particle size distribution is divided into a finite number of bins, and all particles within a bin are assigned a diameter equal to the mean diameter of the bin. The general surface area is obtained by dividing the area of a sphere by the volume of a sphere, resulting in  $6/d$ , where  $d$  is the diameter of the particle. The SSA is calculated as the general surface area of each bin, multiplied by the differentiated bin volume passing percent. The SSAs for all the dry materials except silica fume, together with an overview of different ingoing part materials in the pastes are listed in Table 1 as mm<sup>2</sup>/mm<sup>3</sup> of powder volume. In the analysis of the results of rheology of the different filler modified cement pastes (Figures 2-4) the surface is expressed as surface area mm<sup>2</sup>/mm<sup>3</sup> of paste volume. This is obtained by multiplying the SSAs in Table 1 with the individual volume fractions in the mixes and summing up the total area of each paste mix. In (Cepuritis, Garboczi et al. 2017) a micro x-ray CT and numerical analysis of the resulting PSDs of 10 different rocks VSI (vertical shaft impactor)-crushed into 3 different filler fractions of 4/25, 20/60 and 40/200 microns were performed. It was found that the SSA of the 30 different powder materials had consistently 1.19 – 1.3 times larger areas than their volume equivalent spheres. Hence, this method of determining surface area is believed to be suitable for the crushed fillers. A PSD-analysis of the silica fume could not be performed in the Sedigraph, due to its small grain sizes. The mean size of silica fume is approximately 0.05 microns (Sellevold 2015), and the density 2200 kg/m<sup>3</sup> (Smeplass & Cepuritis 2015), which results in a specific surface area of 60 000 mm<sup>2</sup>/mm<sup>3</sup>.

**Table 1. Part materials in the filler modified cement pastes in the different test series.**

Material	Specific surface area [mm <sup>2</sup> /mm <sup>3</sup> ]	A	B	C	D	E
Filler type		Mix no.				
• Velde Coarse	522	1-9		x	x	
• Velde Intermediate	367	10-18	x			x
• Velde Fine	728	19-27				
Cement type						
• Std FA, CEM II/B-M 42.5 R	829	x	x			x
• Industry, CEM I 52,5 R	1302			x	x	x
Pozzolans						
• Fly Ash	970			x	x	x
• Undensified Microsilica 940-U	60 000*					x
Admixtures						
• Dynamon SR-N (superplasticizer)		x	x	x	x	x

\* Not determined from Sedigraph measurement results, but by simply assuming a mean grain size of 0.05 µm.

## 2.2 Cement paste compositions

The test series are designed with intension of exploring a micro-proportioning principle based on controlled specific surface area of all ingoing powders on a rational basis. An overview of the main proportioning parameters that have been varied or kept constant is listed in Table 2.

**Table 2. Main parameters that are varied or kept constant in the five test series.**

Series	Variables	Constants
A	<ul style="list-style-type: none"> <li>• Filler-to-binder ratio</li> <li>• Water-to-binder ratio</li> <li>• Solid volume fraction</li> </ul>	<ul style="list-style-type: none"> <li>• SP – dosage (0.75% of cement weight)</li> </ul>
B	<ul style="list-style-type: none"> <li>• Filler-to-binder ratio</li> <li>• Water-to-binder ratio</li> <li>• Solid volume fraction</li> <li>• SP – dosage</li> </ul>	
C	<ul style="list-style-type: none"> <li>• Filler-to-binder ratio</li> <li>• Fly ash-to-binder ratio</li> <li>• Solid volume fraction</li> </ul>	<ul style="list-style-type: none"> <li>• Water-to-binder ratio = 0.5 (two exceptions)</li> <li>• SP - dosage (0.60% of cement weight)</li> </ul>
D	<ul style="list-style-type: none"> <li>• Filler-to-binder ratio</li> <li>• Water-to-binder ratio</li> <li>• Fly ash-to-binder ratio</li> </ul>	<ul style="list-style-type: none"> <li>• SP - dosage (0.60% of cement weight)</li> <li>• Solid volume fraction (φ = 0.390)</li> </ul>
E	<ul style="list-style-type: none"> <li>• Filler-to-binder ratio</li> <li>• Fly ash-to-binder ratio</li> </ul>	

- Silica fume-to-binder ratio
- Water-to-binder ratio
- Solid volume fraction

The combinations of cement paste compositions are chosen both for a practical range used in ready mix concrete production with crushed sand in Norway, as well as validating the methods for mixes of extremity (very viscous or very flowable). The outline of the compositions is presented in Table 3, which together with the material data in Table 1, gives the full mix designs. Note that explanations of the abbreviations that are used in the table, are explained below the table.

**Table 3: Outline of the investigated cement paste compositions.**

Series A				Series B					Series E					
	$\frac{w}{b}$	$\frac{sp}{c}$	$\frac{fi}{c}$	$\frac{w}{b}$	$\frac{sp}{c}$	$\frac{fi}{c}$	$\frac{fa}{c}$		$\frac{w}{b}$	$\frac{sp}{c}$	$\frac{fi}{c}$	$\frac{fa}{c}$	$\frac{s}{c}$	
1	0.40	0.75	0.28	13	0.55	1.00	0.51	-	7*	0.55	0.75	0.63	-	0.06
2	0.40	0.75	0.36	14	0.55	1.00	0.59	-	8	0.55	0.75	0.60	-	0.06
3	0.40	0.75	0.44	15	0.55	1.00	0.67	-	9*	0.55	0.75	0.73	-	0.06
4	0.55	0.75	0.51	16	0.55	1.25	0.51	-	10	0.55	0.75	0.70	-	0.06
5	0.55	0.75	0.59	17	0.55	1.25	0.59	-	11*	0.55	0.75	0.79	0.35	0.07
6	0.55	0.75	0.67	18	0.55	1.25	0.67	-	12	0.55	0.75	0.76	0.33	0.07
7	0.70	0.75	0.68	19	0.55	1.50	0.51	-	13*	0.55	0.75	0.92	0.35	0.07
8	0.70	0.75	0.76	20	0.55	1.50	0.59	-	14	0.55	0.75	0.88	0.33	0.07
9	0.70	0.75	0.82	21	0.55	1.50	0.67	-	15*	0.40	0.75	0.43	-	-
10	0.40	0.75	0.28	22	0.55	1.75	0.51	-	16*	0.40	1.50	0.43	-	-
11	0.40	0.75	0.36	23	0.55	1.75	0.59	-	17*	0.55	0.75	1.06	0.81	0.20
12	0.40	0.75	0.44	24	0.55	1.75	0.67	-	18	0.55	0.75	1.01	0.77	0.19
13	0.55	0.75	0.51	<b>Series C</b>					19*	0.55	0.75	1.22	0.81	0.20
14	0.55	0.75	0.59	1*	0.50	0.60	-	-	20	0.55	0.75	1.17	0.77	0.19
15	0.55	0.75	0.67	2*	0.45	0.60	-	-	21*	0.55	0.75	0.65	-	0.12
16	0.70	0.75	0.68	3*	0.50	0.60	-	0.33	22	0.55	0.75	0.63	-	0.12
17	0.70	0.75	0.76	4*	0.50	0.60	-	0.56	23*	0.55	0.75	0.76	-	0.12
18	0.70	0.75	0.82	5*	0.50	0.60	-	0.71	24	0.55	0.75	0.73	-	0.12
19	0.40	0.75	0.28	6*	0.45	0.60	-	0.71	25*	0.55	0.75	0.84	0.37	0.16
20	0.40	0.75	0.36	7*	0.50	0.60	0.24	-	26	0.55	0.75	0.80	0.35	0.15
21	0.40	0.75	0.44	8*	0.50	0.60	0.30	0.33	27*	0.55	0.75	0.97	0.37	0.16
22	0.55	0.75	0.51	9*	0.50	0.60	0.36	0.71	28	0.55	0.75	0.93	0.35	0.15
23	0.55	0.75	0.59	<b>Series D</b>					29*	0.55	0.75	1.06	0.81	0.20
24	0.55	0.75	0.67	1*	0.50	0.60	-	-	30	0.55	0.75	1.01	0.77	0.19
25	0.70	0.75	0.68	2*	0.53	0.60	-	0.31	31*	0.55	0.75	1.22	0.81	0.20
26	0.70	0.75	0.76	3*	0.55	0.60	-	0.62	32	0.55	0.75	1.17	0.77	0.19
27	0.70	0.75	0.82	4*	0.57	0.60	-	1.08	33*	0.53	0.75	0.63	-	0.06
<b>Series B</b>				5*	0.60	0.60	0.20	-	34*	0.51	0.75	0.65	-	0.12
1	0.40	1.00	0.28	6*	0.73	0.60	0.46	-	35*	0.51	0.75	0.73	-	0.06
2	0.40	1.00	0.36	7*	0.65	0.60	0.30	0.33	36*	0.51	0.75	0.76	-	0.12
3	0.40	1.00	0.44	8*	0.81	0.60	0.66	0.15	37*	0.51	1.00	0.76	-	0.12
4	0.40	1.25	0.28	9'	0.76	0.60	0.57	0.31	38*	0.51	1.25	0.76	-	0.12

5	0.40	1.25	0.36	10*	0.80	0.60	0.76	0.74	39*	0.51	1.50	0.76	-	0.12
6	0.40	1.25	0.44	<b>Series E</b>					40*	0.42	0.75	0.44	0.35	0.07
7	0.40	1.50	0.28	1*	0.40	0.75	0.33	-	41*	0.42	1.00	0.44	0.35	0.07
8	0.40	1.50	0.36	2*	0.40	1.50	0.33	-	42*	0.42	1.25	0.44	0.35	0.07
9	0.40	1.50	0.44	3*	0.55	0.75	0.60	-	43*	0.42	1.50	0.44	0.35	0.07
10	0.40	1.75	0.28	4*	0.55	0.75	0.70	-	44*	0.44	1.50	0.41	0.33	0.00
11	0.40	1.75	0.36	5*	0.55	1.50	0.60	-						
12	0.40	1.75	0.44	6*	0.55	1.50	0.70	-						

Abbreviations used in the table:

**w/b** = water-to-binder ratio by mass.

**sp/c** = superplasticiser dosage by mass percentage of cement.

**fi/c** = crushed filler-to-cement ratio by volume.

**fa/c** = fly ash-to-cement ratio by volume

**s/c** = silica fume-to-cement ratio by volume

\* Mixes with Industry cement. All others: Standard FA

### 2.3 Methods

The mixing of the filler modified cement pastes was carried out with the procedure developed by Ng. et. al. (Ng 2014). First, all dry powders were pre-mixed in a Hobart bowl mixer, in this case model N-50, Hobart Manufacturing Company. Subsequently, the wet-mixing was performed by a handheld drill (model TCD 180-30, Tectool) and an attached steel paddle, specially designed for mixing cement suspensions in order to reduce air entrainment (Ng 2014). The wet mixing was performed in a cylindrical plastic container with inner diameter of 110 mm and inner height of 297 mm. The batch size for each paste mix was 2.05 litres. Directly after mixing, rheometer and FlowCyl measurements were performed. The Bingham parameters yield stress and plastic viscosity are obtained from the rheometer, while the flow resistance ratio is the output parameter from the FlowCyl. The mini-slump test was performed directly after the FlowCyl measurement was done, and the same paste that had been tested in the FlowCyl was reused in the mini slump cone. All three tests were performed as described in [8]. The repeatability of the measurements was determined by repeated mixing of a paste with average rheological properties in the tested range. Based on four repetitions, the coefficient of variation for the Bingham yield stress and plastic viscosity equalled 9.7% and 5.7%, respectively. The flow resistance ratio had a variation coefficient of 2.0% (Cepuritis et al. 2018).

### 3. RESULTS AND DISCUSSION

The three laboratory tests resulted in four parameters describing the rheology of the cement pastes: The flow resistance ratio  $\lambda_Q$ , the Bingham parameters yield stress  $\tau_0$  and plastic viscosity  $\mu$ , and the mini slump flow. Figure 2 shows that the four rheological parameters correlate in a similar fashion as found earlier (Cepuritis, Jacobsen et al. 2017). Figure 2a shows that the plastic viscosity correlates well with the flow resistance ratio in line with (Pedersen & Smeplass 2003), and Figure 2b shows that the yield stress and the mini slump flow are directly linked to each other in line with (Roussel 2005). The best fit is seen between the flow resistance ratio and the plastic viscosity in line with (Mørtzell 1996), with power law regression coefficient  $R^2 = 0.93$ . The linear regression coefficient equals 0.68 for the same relation. A good linear relation has also been found in previous studies on cement-fly ash pastes (Bentz et al. 2012). A previous experimental study in the MiKS project, shows a linear relation between the yield stress and the mini slump flow, with a correlation coefficient  $R^2 = 0.79$  (Cepuritis 2016), whereas these experiments result in a linear correlation coefficient  $R^2 = 0.72$ . However, the experiments discussed in this paper have a larger range of mix design variation, especially with the filler/cement ratio ranging from 0.00 to 0.82. In this experimental study, the relation between the yield stress and the mini slump flow is best described by a power function, and the correlation coefficient is 0.85. The mini slump flow also appears to correlate somewhat with the flow resistance ratio with a  $R^2 = 0.51$  by linear regression, shown

in Figure 2c. The weakest correlation is seen between the yield stress and the plastic viscosity, Figure 2d, which is discussed and investigated further elsewhere (Cepuritis et. al 2018, Cepuritis 2012).

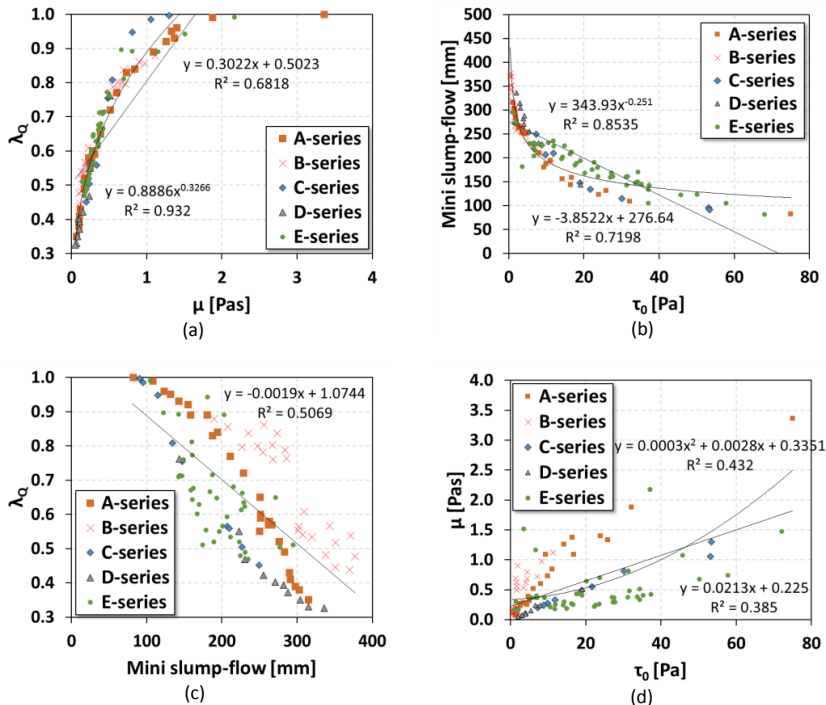


**Figure 2. Relation between the four different rheological parameters obtained from the laboratory experiments.**

Figure 3 shows the rheological parameters yield stress, plastic viscosity, mini slump flow and flow resistance for all test series in view of the scope of this work, that is in correlation with the specific surface area of the matrix. Test series B was made with intention of mapping the effect of varying filler content, filler type and SP-dosage while keeping the specific surface area fixed, and the results from this series will hence not contribute in finding a relation between SSA and the rheology parameters. Hence, the results from the B-series are not included in the graphs. Further, the size of the silica fume particles is too small to perform a PSD analysis in the Sedigraph. The mixes including silica fume in test series E are hence not included in the graphs in Figure 3. As a clear distinction between the mixes with Standard FA cement and Industry cement is observed, the mixes are grouped by the cement type. The mixes with Std FA cement represents test series A, as well as all mixes with Std FA cement and without silica fume in series E. The Industry cement mixes represents series C, D and mixes with Industry cement and without silica fume in test series E. The plots illustrate that the SSA correlates well to rheology within each group of mixes, despite large mix design variations such as SP-dosage, fi/b, w/b, filler type etc. The mixes with industry cement show better flowability than the Standard FA-mixes with similar specific surface area of the solids. The differences between these two groups of mixes at a similar SSA could be attributed to different interaction with the SP of the two cement types and/or differences in the solid concentration of the mixes, because of the high SSA of industry cement compared to the Std FA cement (see Figure 1 and Table 1). The higher SSA indicates that Industry cement pastes and Std FA cement pastes with similar SSA-values might have a different solids concentration, i.e. the pastes with the Industry cement will achieve the same SSA at a lower solids concentration and thus a higher w/c ratio. The best correlation to SSA is seen for the plastic viscosity, with an  $R^2$  value of 0.85 for both groups of mixes. In general, the flow resistance, plastic viscosity and yield stress are increasing with increasing specific surface area, while the mini slump flow is decreasing. For the Std FA mixes, one point is laying way outside the trend line. This is mix A-21, which has a flow resistance ratio of 1.00, indicating that it is too viscous for flowing through the



FlowCyl. This is not unexpected, since mix A-21 have a high  $f_i/b$ -ratio of 0.39, combined with its low  $w/b$  ratio of 0.4, and hence it is highly viscous. The different mix designs were made with the aim of obtaining a large range of flow properties of the pastes. Hence, some of the mixes are highly viscous, and not suitable for use in normal flowable concrete. For practical purposes, the flow resistance ratio should be within the range 0.25-0.80.

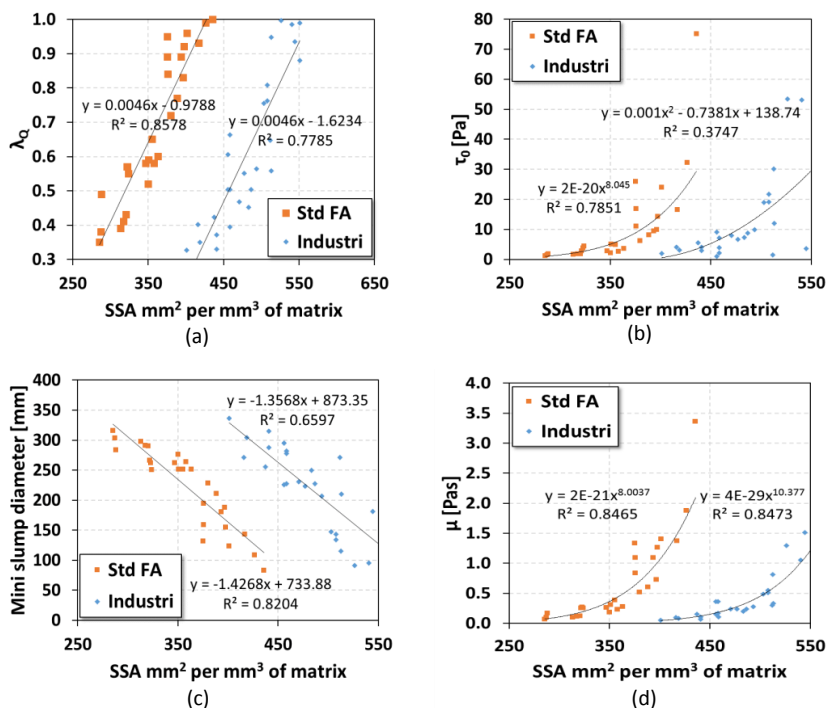


**Figure 3.** The relation between the specific surface area of the matrix [mm<sup>2</sup>/mm<sup>3</sup>] and the four parameters flow resistance, yield stress, mini slump flow and plastic viscosity.

The same relations as in Figure 3 were plotted for the mixes with silica fume, assuming the SSA value of 60 000 mm<sup>2</sup>/mm<sup>3</sup> (see Table 1), but then the correlation was very poor for all four graphs. Linear regression of  $\lambda_q$ ,  $\tau_0$ , mini-slump diameter and  $\mu$  as function of SSA, gave  $R^2 = 0.12, 0.28, 0.23$  and  $0.01$  respectively, see example plot of SSA vs  $\lambda_q$  in Figure 4a. The specific surface area of silica fume is of a much higher order of magnitude than the surface areas for the other powders. Hence, it is clear that the contribution from silica fume to the specific surface of all the powders in the matrix dominates. Figure 3 shows that the viscosity of the paste increases with increasing specific surface area. However, it is not expected that adding silica fume with such high specific surface area will increase the viscosity correspondingly. It is known that when adding silica fume in combination with water reducing admixtures, decreasing water demand and increasing workability can be expected, because the small silica fume particles can replace the water in the void space and have a “ball-bearing” effect, i.e. improve the packing of the total powder composition (Sellevold 2015). By reducing the contribution of the silica fume to the SSA of the mix by a constant factor of 0.07, the linear correlation  $R^2$  for SSA vs  $\lambda_q$  was improved from 0.12 to 0.46, see Figure 4b. Further research is needed, in order to understand how to account for the effect of the silica fume in the micro-proportioning of cement paste matrices. A possible approach that could be considered, is the approach by (Kashani et al. 2014), which shows that not only the SSA, but especially the width of the PSD, is important in determining the yield stress of cement pastes.

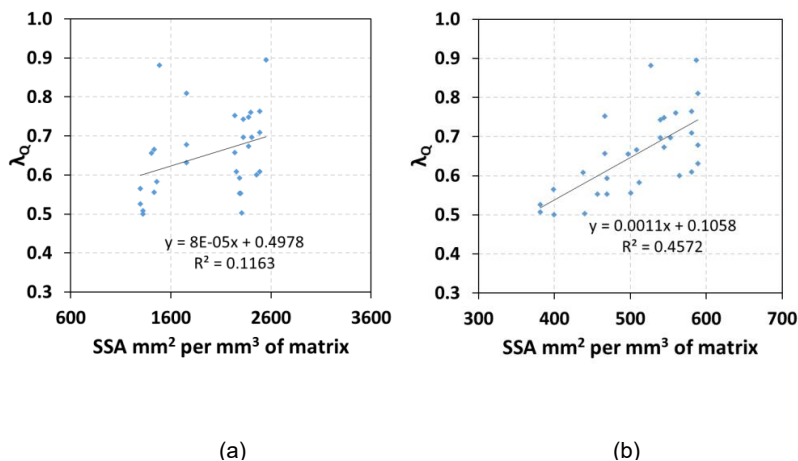


**Figure 4. Correlation between the specific surface area of the matrix [mm<sup>2</sup>/mm<sup>3</sup>] and the flow resistance ratio for all mixes including silica fume – Series E: (a) No correction factor for SSA<sub>SF</sub>, (b) Correction factor of 0.07 for SSA<sub>SF</sub>**

#### 4. CONCLUSIONS

The following main conclusions may be drawn from the presented experimental study on the rheology as function of SSA:

- For all test series, a wide range of mix design parameters is used, and the filler modified pastes consist of different combinations of cement, filler, fly ash, silica fume and SP-dosages. Regardless of these variations, the rheological parameters yield stress, plastic viscosity, mini slump flow and flow resistance are interrelated in the same way as found in the earlier studies.
- For mixes with both FA-cement and ordinary Portland cement, the specific surface area is found to correlate well to the rheological parameters. This correlation is found to be strongly dependent on cement type with the two series falling on separate regression lines. Hence, the SSA seems like a promising input parameter for developing a micro-proportioning tool.
- The mixes containing silica fume, do not show a good correlation between SSA and the rheological properties of the paste. This observation is assigned to silica fumes ability to reduce the viscosity of the paste, when used in combination with plasticizing admixtures. However, when using a correction factor of 0.07, the correlation between SSA and flow resistance ratio improves from  $R^2 = 0.12$  to 0.46.
- Further work will investigate various microproportioning approaches and materials effects including how the effect of silica fume can be included when predicting paste rheology.

#### 5. ACKNOWLEDGEMENTS

This paper is based on work performed within the MiKS project – Mikroproporsjonering med Knust Sand (Norwegian for Micro-proportioning with Crushed Sand), which is a KPN (Competence Project for the Industry) at The Norwegian University of Science and Technology, Dept. of Structural engineering, funded by the Research Council of Norway (RCN) contract No. 247619 and industrial partners. The authors would like to thank the RCN and the industrial partners (Norcem AS, Skanska Norge AS and Feiring Bruk AS) for their financial support and for facilitating the interaction between research and industry. Thanks to Master students Patricia Y. Sosa and Juni C. M. Foslie for help with Sedigraph measurements.

## 6. REFERENCES



- Bentz DP, Ferraris CF, Galler MA, Hansen AS and Guynn JM (2012). *Influence of particle size distributions on yield stress and viscosity of cement-fly ash pastes*. Cement and Concrete Research, vol. 42, pp. 404-409.
- Cepuritis, R (2016). *Development of Crushed Sand for Concrete Production with Micro-proportioning*. PhD, Norwegian University of Science and Technology, Trondheim.
- Cepuritis R, Garboczi EJ, Ferraris CF, Jacobsen S and Sørensen BE (2017). *Measurement of particle size distribution and specific surface area for crushed concrete aggregate fines*. Advanced Powder Technology, vol. 28, no. 3, pp. 706-720.
- Cepuritis R, Jacobsen S, Smeplass S, Mørtzell E, Wigum BJ and Ng S (2017). *Influence of crushed aggregate fines with micro-proportioned particle size distributions on rheology of cement paste*. Cement and Concrete Composites, vol. 80, pp. 64-79.
- Cepuritis R, Skare EL, Ramenskiy E, Mørtzell E, Smeplass S, Li S, Jacobsen S and Spangenberg J (2018). *Filler modified cement paste flow in the one-point FlowCyl test*. Submitted to Construction and Building Materials.
- Kashani A, Nicolas RS, Qiao GG and van Deventer JSJ (2014). *Modelling the yield stress of ternary cement-slag-fly ash pastes based on particle size distribution*. Powder Technology, vol 266, pp. 203-209.
- Micromeritics (2003). *SediGraph III 5120 Operator's Manual v1.00*.
- Mørtzell, E (1996). *Modelling the effect of concrete part materials on concrete consistency*. PhD, Norwegian University of Science and Technology (In Norwegian).
- Ng S, Mujica H and Smeplass S (2014). *Design of a simple and cost-efficient mixer for matrix rheology testing*. Nordic Concrete Research, vol. 51, no. 3, pp. 15-28.
- Pedersen B and Smeplass S (2003). *The relationship between the rheological properties of SCC and the corresponding matrix phase*. International RILEM Symposium on Self-Compacting Concrete.
- Roussel N, Stefani C and Leroy R (2005). *From mini-cone test to Abrams cone test: measurement of cement-based materials yield stress using slump tests*. Cement and Concrete Research, vol. 35, pp. 817-822.
- Sellevoid, E (2015). *TKT 4215 Concrete Technology 1 Chapter 7 – Pozzolana*. Norwegian University of Science and Technology.
- Smeplass S and Cepuritis R (2015). *TKT 4215 Concrete Technology 1 Chapter 4 – Fresh concrete – proportioning*. Norwegian University of Science and Technology.
- Smeplass S and Mørtzell E (2001). *The applicability of the particle matrix model to self compacting concrete*. Nordic Concrete Research, vol. 26.
- Sosa, PY (2017). *Master's thesis: Particle Size Distribution and Specific Surface Area Measurements with X-ray SediGraph on Filler, Cement and Fly Ash*. NTNU, Trondheim.

## Paper II

### **Application of an Improved Empirical Model for Rheology Prediction of Cement Pastes Modified with Filler from Manufactured Sand**

Skare EL, Cepuritis R, Mørtzell E, Smepllass S, Spangenberg J, Jacobsen S.  
*Nordic Concrete Research* 65 (2021) pp. 1-18.



	
© Article authors. This is an open access article distributed under the Creative Commons Attribution-NonCommercial-NoDerivs licens. ( <a href="http://creativecommons.org/licenses/by-nc-nd/3.0/">http://creativecommons.org/licenses/by-nc-nd/3.0/</a> ).	ISSN online 2545-2819 ISSN print 0800-6377
DOI: 10.2478/ncr-2021-0005	Received: March 26, 2021 Revision received: Nov. 29, 2021 Accepted: Nov. 29, 2021

## Application of an Improved Empirical Model for Rheology Prediction of Cement Pastes Modified with Filler from Manufactured Sand



Elisabeth Leite Skare  
M. Sc., Ph.D. candidate  
Norwegian University of Science and Technology  
Department of Structural Engineering  
Richard Birkelands vei 1a, 7491 Trondheim, Norway  
e-mail: [elisabeth.l.skare@ntnu.no](mailto:elisabeth.l.skare@ntnu.no)



Rolands Cepuritis  
M. Sc., Ph.D., Adj. Associate Professor (NTNU)  
Senior Project Manager  
Norcem AS  
Lilleakerveien 2A, 0216 Oslo, Norway  
e-mail: [rolands.cepuritis@ntnu.no](mailto:rolands.cepuritis@ntnu.no)



Ernst Mørtzell  
Ph.D., Adj. Professor (NTNU)  
R&D Manager  
Norbetong AS  
Lilleakerveien 2B, 0216 Oslo, Norway  
e-mail: [ernst.mortsell@ntnu.no](mailto:ernst.mortsell@ntnu.no)



Sverre Smepllass  
Chief Adviser  
Skanska Norge  
Lakkegata 53, 0187 Oslo, Norway  
e-mail: [Sverre.smepllass@skanska.no](mailto:Sverre.smepllass@skanska.no)



Jon Spangenberg  
Ph.D., Associate Professor  
Technical University of Denmark  
Department of Mechanical Engineering  
Building 425, room 224  
2800 Kgs. Lyngby, Denmark  
e-mail: josp@mek.dtu.dk



Stefan Jacobsen  
Ph.D., Professor  
Norwegian University of Science and Technology,  
Department of Structural Engineering  
Richard Birkelands vei 1a, 7491 Trondheim, Norway  
e-mail: stefan.jacobsen@ntnu.no

## ABSTRACT

There is a need for simple but precise prediction models for proportioning concrete with manufactured sand, for use in ready-mix concrete production. For the last two decades, the particle-matrix model has been used in Norway for proportioning and prediction of concrete flow based on the properties and proportions of two concrete phases: coarse particles and filler modified cement paste (matrix). This paper presents experimental testing of 117 cement pastes of which 107 contain filler, i.e. particles < 125 microns, from manufactured sand. Based on compositions and properties of ingoing materials in these mixes, an empirical equation is developed that predicts the rheological properties plastic viscosity, yield stress, flow resistance ratio and mini slump flow. Optimization by regression analysis provides a practical microproportioning equation that readily can be used as input in concrete proportioning with the particle-matrix model. The equation provides a coefficient of determination  $R^2 = 0.98$  for plastic viscosity,  $R^2 = 0.95$  for mini slump flow,  $R^2 = 0.91$  for flow resistance ratio and  $R^2 = 0.80$  for yield stress.

**Key words:** Rheology, empirical model, cement paste, filler, manufactured sand.

## 1. INTRODUCTION

Controlling rheological properties is of major importance for the ready-mix concrete industry, and reliable prediction models are essential for efficient optimization of mix designs. However, validation of rheological prediction models for a given set of materials requires experimental testing. It is both economical and efficient to perform testing on small cement paste samples, and such small-scale testing has shown to be promising for rheology prediction of equivalent concrete mixes [1]. The literature provides numerous approaches to predict suspension rheology. Several models are based on packing, among others the viscosity models presented in [2-7]. Spangenberg *et al.* [8] verified that the viscosity models in [2-3] provide high prediction accuracy, by investigating their applicability on bimodal suspensions with hard spherical particles. Though most traditional viscosity models are simplified packing models ignoring particles interactions, Daminieli *et al.* [9] show that the Particle Interference Model predicts viscosity of filler modified

cement paste (matrix) by correlating physical aspects of particles and fluids. Predictive yield stress models in recent literature have been improved to include aspects like particle size distributions (PSDs), volume fraction of solids and inter-particle forces, such as the work presented in [10-14]. Another approach for modelling suspension rheology is the lubricating liquid thickness around all particles, proposed by Powers [15]. The liquid thickness is inversely proportional to the volumetric specific surface area (VSSA). Matrix rheology is found to be strongly affected by the VSSA of the ingoing powder materials, defined as surface area per volume of a material [16-17].

For the prediction methods to be useful for ready mix concrete plants, the required input data must be accessible without too advanced and expensive test methods [18]. Simplicity of the models is valued, as availability is considered crucial for the implementation of the test methods at the ready mix concrete plants [18]. Even though numerous rheology models exist, the literature on their applicability on matrices with filler from manufactured sand is sparse. As global resources of natural sand are running short, use of manufactured sand in concrete is increasing [19]. Cepuritis *et al.* [16] state that a pronounced difference between natural and manufactured sand is the higher fines content of the latter, which significantly increases the VSSA. The amount of fines depends on the production process, but is especially high for manufactured sand produced by Vertical Shaft Impactor (VSI) crushing. Bengtsson and Evertsson [20] found that the amount of fines increased with increased rotor velocity of the VSI crushing, resulting in a fines content (particle diameter < 0.125 mm) of approximately 15 % for high rotor velocity. However, in order to produce sand with density similar to that of natural sand, a high rotor velocity is necessary. The increased VSSA has a major impact on paste rheology, and its effect was quantified on filler modified cement pastes in [16-17]. Linear relations between VSSA and the rheology were found in [16], and the rheological effect of different mineralogy was highlighted by experiments with controlled VSSA. Similar linear relations were found in [17] and quantified for the total volume weighted VSSA of all ingoing powders except for silica fume, where it was impossible to relate its effect on rheology linearly to surface area, presumably due to the kind of non-linear behaviour observed by Wallevik [21]. In [18], an empirical equation was developed and applied on matrices with crushed aggregate fillers, with emphasis on simplicity and applicability of the equation for the ready-mix concrete industry. The mix program consisted of two types of crushed filler, one natural filler, four different types of cement, silica fume, one superplasticiser (SP) and one plasticiser (P). The SP- and P-dosages were kept constant for all mixes, and an individual equation was developed for each filler type. The empirical equation was a fitting model based on the particle matrix method, where matrix rheology was predicted based on mix composition [18]. In a sense it may be said to be similar to neural network-based models like [22], where the behaviour of the material is learned by a new form of experience based on numerical simulation.

This paper presents an experimental study of 117 matrices, consisting of four different crushed fillers, two different cement types, biotite, fly ash, silica fume, and one type of SP with dosages between 0.6 – 1.75 % of cement weight. The scope of the paper is to further develop the empirical equation in [18] to account for large parameter variations. The overall goal is to establish a proportioning tool for the ready mix concrete industry, that is applicable also for matrices with manufactured sand. First, the original empirical equation is introduced, followed by a brief presentation of the material data and experimental test program. In the results section, a new empirical equation is presented, and the applicability of the equation is investigated on the 117 matrices.



## 2. THE EMPIRICAL EQUATION

The term microproportioning is proposed for the process of quantifying and predicting the rheology of filler-modified paste based on composition and part materials data for all fluids and particles with a diameter less than 125  $\mu\text{m}$ . So far, the term was limited to quantify the relationship between the VSSA of the filler and the rheology of the paste [17, 19]. Based on the microproportioning principle, an empirical equation was developed by Mørtzell in 1996 [18] in the form of a power law describing the flow resistance ratio,  $\lambda_q$ . The flow resistance ratio is a unitless parameter that describes the rheological properties of cementitious suspensions, described in detail in [19]. The empirical equation is given on the form:

$$\lambda_q = k \times \left( k_c \times \frac{c}{w} + k_s \times \frac{s}{c} + k_f \times \frac{f}{c} \right)^n \quad (1)$$

Where  $k_c$ ,  $k_s$  and  $k_f$  are material factors for cement, silica fume and filler, respectively, and  $k$  and  $n$  are constants obtained from optimization by curve fitting. For the materials used in [18], the factors equalled:  $k_c = 0.200$ ,  $k_s = 0.555$  and  $k_f = 0.154 - 0.311$ . Eq. (1) was optimised, via  $k$  and  $n$ , for three set of matrices with different crushed fillers, resulting in  $R^2$ -values between 0.98 and 0.99 for the three datasets. The matrices consisted of cement, crushed fillers, silica fume and plasticizer/superplasticiser. The plasticizer- and superplasticizer dosages were kept at a constant percentage of the cement weight for all matrices.

## 3. EXPERIMENTS

### 3.1 Materials data and mix compositions

Some of the matrices presented in this paper are the same as presented in [17], but in addition 11 new matrices are included here. The matrices consist of either Standard FA cement (CEM II/B-M 42.5 R) or Industry cement (CEM I 52.5 R) from Norcem AS, as well as the superplasticizer Dynamon SR-N from Mapei. Some matrices also contain Norcem Fly ash (FA) and/or Elkem Microsilica 940-U. Four crushed aggregate fillers sieved mechanically at 0.125 mm are used (Table 1). The fillers denoted Fine, Intermediate and Coarse originate from the same rock type, and is mainly composed of feldspar and quartz. They differ from each other by being extracted at cut size 63  $\mu\text{m}$ , 125  $\mu\text{m}$  and 500  $\mu\text{m}$ , respectively, in the air-classification process. The fourth filler is denoted VSI, being a Vertical Shaft Impactor (VSI) crushed 0/2 mm filler. The densities were measured by helium pycnometry. In addition, industrial biotite (mica) GW-MB-A230 with density 2.84  $\text{g/cm}^3$  from Great Wall Mineral [23] was used in some mixes.

*Table 1 - Densities, diameters, extraction cut size and producers of the four crushed aggregate fillers.*

<b>Material designation</b>	<b>Density [g/cm<sup>3</sup>]</b>	<b>Particle diameter [μm]</b>	<b>Production cut-size [μm]</b>	<b>Producer</b>
Fine	2.65	0 – 125	63 μm	Velde Pukk AS
Intermediate	2.65	0 – 125	125 μm	Velde Pukk AS
Coarse	2.65	0 – 125	500 μm	Velde Pukk AS
VSI	2.75	0 – 125	2000 μm	Feiring Bruk

Originally, 125 matrices were proportioned, but 8 of the mixes were too viscous to perform the FlowCyl test on, hence 117 matrices are presented in this paper. Appendix A supplies detailed information about the mix compositions for all matrices. The matrices were designed to cover a wide range of rheological parameters, hence mixes outside the practical range used in ready mix concrete production appear.

### 3.2 Volumetric specific surface area

The volumetric specific surface area (VSSA) is defined as surface area per volume of a powder material [19] and is calculated from the PSD obtained from the x-ray machine Sedigraph III Plus in this study. The test procedure used in the current study is described in [17]. As explained in [17], the VSSA of each material was calculated by multiplying the particle surface areas of each bin by their volume percentages within that bin. The VSSAs for all dry materials except silica fume are provided (Table 2), since Sedigraph III Plus measures particles down to 1 μm, whereas the mean diameter of silica fume is approximately 0.1 μm [24].

*Table 2 – VSSA for all dry materials, except silica fume, calculated from the PSDs obtained from the Sedigraph-analysis.*

<b>Material</b>	<b>Volumetric specific surface area [mm<sup>2</sup>/mm<sup>3</sup>]</b>
Fine filler	728
Intermediate filler	367
Coarse filler	522
VSI filler	260
Biotite	1122
Standard FA cement	829
Industry cement	1302
Fly Ash	970

In this study we define  $VSSA_{matrix}$  as the sum of volume weighted contributions from all ingoing matrix powders *except silica fume*, calculated from Eq. (2).

$$VSSA_{matrix} = \sum_i VSSA_i \times \Phi_i \quad (2)$$

Where  $\Phi_i$  is the volume fraction of powder material  $i$  in the matrix.

### 3.3 Mixing and rheology measurements

All matrices were mixed by the procedure in [25] in volumes of 2.0 litres. First, all dry materials were mixed in a Hobart mixer, model N-50, with a standard flat blade for two minutes. Subsequently, water and superplasticizer were mixed together for one minute. Subsequently, the wet-mixing of all materials was performed by a handheld drill (Tectool model TCD 180-30) with an attached steel paddle, specially designed for mixing cement suspensions. All materials were mixed at high speed for two minutes, and then left at rest for another two minutes. Lastly, the materials were mixed at low speed for two minutes. Directly after mixing, the flow resistance ratio, Bingham yield stress ( $\tau_0$ ) and plastic viscosity ( $\mu$ ) were measured for each of the matrices. The mini slump test was performed directly after the FlowCyl measurement, and the same paste that had been tested in the FlowCyl was reused in the mini slump cone. The  $\lambda_q$  measurements were performed with the simple test equipment FlowCyl, and the Bingham parameters  $\tau_0$  and  $\mu$  were obtained from Anton Paar rheometer analysis.

The FlowCyl test apparatus was developed by Mørtzell [18] and is a modification of the Marsh cone. The FlowCyl is a cylinder ending in a V-funnel with a narrow nozzle outlet. The inner diameter of the cylinder is 80 mm and the outlet inner diameter is 8 mm (Figure 1). The test principle is analogous to the Marsh cone test principle, where the container is placed vertically in a rack above an electronic scale connected to a computer. While the outlet is closed, the FlowCyl is filled with cement paste up to the level of 15 mm below the top edge. Then, the outlet is opened, and the weight increase is recorded every other second. The dimensionless parameter  $\lambda_q$ , is defined as the difference in flow rate between the test material and an “ideal” fluid with no internal resistance and no external cohesion or friction.

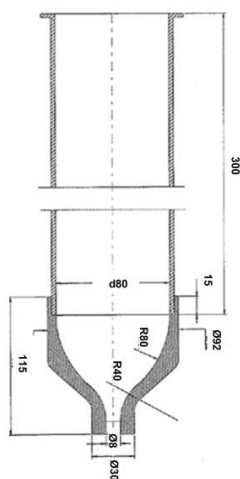


Figure 1 – The geometry of the FlowCyl test apparatus. Illustration adopted from [18].

The Bingham parameters,  $\tau_0$  and  $\mu$ , were measured on 10.5 ml samples at 20 °C by an Anton Paar Physica MCR 300 rheometer equipped with a flat bottom bob-in-a-cup geometry. Such equipment has successfully been used in previous studies to quantify the rheological response of cementitious materials [26-28]. The bob had an outer diameter of 24.580 mm and a length of 50.000 mm. The inner diameter of the cup was 28.901 mm. The gap at the bottom of the bob was set equal to the gap at the side surface. First, the paste was homogenized for 30 seconds at a shear rate of 60 s<sup>-1</sup>, followed by rest for another 30 seconds. Thereafter, the paste was subjected to linearly increasing shear rates from 1 s<sup>-1</sup> to 60 s<sup>-1</sup> over a period of 3 minutes (30 steps of 6 seconds), followed by a step down of shearing from 60 s<sup>-1</sup> to 1 s<sup>-1</sup> for further 3 minutes. The slope of the down-curve (decreasing shear rate) was used to calculate  $\mu$ , while the intercept at zero shear rate was used to calculate  $\tau_0$ .

The truncated mini-cone that was used in this study had a top diameter of 39 mm, a bottom diameter of 89 mm and a height of 70 mm. A smooth plexi glass plate was used as the base for the measurements. The mini-cone was filled with matrix to the level of the top of the cone. Then, the cone was gently lifted and the diameter of the matrix at stoppage was measured in two orthogonal directions. The mini-slump flow value was then calculated as the mean of the two measured diameters.

#### 4. RESULTS AND DISCUSSION

The design of the new empirical equation is developed based on the correlation between single mix design parameters and the measured rheological values. As the mix designs are spanning over a large variation in materials and dosages, several material parameters are varying at the same time, making it difficult to point out a clear rheological trend for each of the individual parameters. However, the five material parameters showing the clearest trend to the measured flow resistance ratio is plotted (Figure 2). In the figure, the mix parameters are normalized based on maximum span of the different parameters. The solid fraction,  $\phi$ , ranges from 0.39 to 0.55 in the experiments, hence,  $\phi = 0.39$  corresponds to 0.0 and  $\phi = 0.55$  corresponds to 1.0. Furthermore,  $w/p$  ranges from 0.29 to 0.57,  $w/c$  from 0.40 to 1.04 and  $w/b$  from 0.40 to 0.81, where  $w$ ,  $p$ ,  $c$  and  $b$  denote water, powder, cement and binder, respectively. Lastly,  $VSSA_{matrix}$  ranges from 285 mm<sup>2</sup>/mm<sup>3</sup> to 551 mm<sup>2</sup>/mm<sup>3</sup>. Note that Figure 2 is an illustration showing the typical trend that was observed for the considered mixes and is a simplification from the true observations. The figure shows the regression lines for the considered parameters. The slopes of the trendlines indicate that the powder- and binder concentration has the strongest relative influence on the flow resistance ratio of our matrices, whereas  $VSSA_{matrix}$  has a relatively weaker influence.

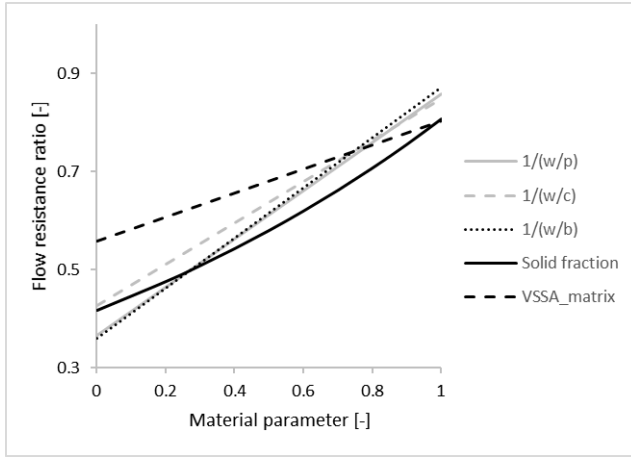


Figure 2 – Illustration of the observed trend between the flow resistance ratio and five different normalized material parameters.

The observed trends between the material parameters and the measured rheology parameters provided useful information with respect to which material parameters the new empirical equation should contain, as well as how each parameter affects the matrix rheology. The new empirical equation is shown in Eq. (3).  $\Gamma$  represents an arbitrary rheology parameter, and the different  $k_x$  factors are obtained by regression analysis using the built in Solver-function in Excel.

$$\Gamma = \left( k_1 \frac{VSSA_{matrix}}{100} - k_2 \phi - k_3 \frac{w}{p} - k_{4,i} \frac{SP}{c} + k_{5,i} \frac{c}{w} + k_6 \frac{bio}{f} + k_7 \frac{FA}{b} + k_8 \frac{s}{b} + k_{9,j} \frac{f}{b} \right)^n \quad (3)$$

where  $w$ ,  $p$ ,  $SP$ ,  $c$ ,  $f$ ,  $b$ ,  $FA$ ,  $s$  and  $bio$  represent mass of water, powder, superplasticizer, cement, filler, binder, fly ash, silica fume and biotite, respectively, and  $\phi$  is the solid fraction of the matrix. The different cement types are indicated by the variable  $i$ , and  $j$  indicates the different filler types. The volume weighed VSSA for all dry materials except silica fume,  $VSSA_{matrix}$ , is described in Section 3.2, see Eq. 2. Although, the material parameter study shows that both the  $w/p$ -ratio and  $\phi$  are best described by the natural logarithm function, the prediction accuracy of the empirical equation was not improved by describing these terms logarithmic in the equation.

One equation was developed for each of the four measured rheological parameters. The results show that the equation for the Bingham plastic viscosity,  $\mu$ , yields the highest prediction accuracy, with an  $R^2 = 0.97$ . The prediction accuracies for the mini slump flow, flow resistance ratio and yield stress are  $R^2 = 0.94$ ,  $R^2 = 0.91$  and  $R^2 = 0.80$ , respectively. As the original empirical equation in [18] predicts  $\lambda_q$ , it is chosen to present the new empirical equation for  $\lambda_q$  for comparison in this paper, as well as the equation for the plastic viscosity, providing the highest accuracy. The  $k_x$  and  $n$  factors for the two empirical equations are presented, as well as the coefficient of determination,  $R^2$  (Table 3).

Table 3 – The  $k_x$  and  $n$  factors for the empirical equations for prediction of flow resistance ratio and plastic viscosity, as well as resulting  $R^2$ -values.

	$n$	$k_1$	$k_2$	$k_3$	$k_4$		$k_5$		$k_6$	$k_7$	$k_8$	$k_9$		$R^2$
$\lambda_q$	1	0.42	2.72	1.47	Std FA	0.06	Std FA	0.31	1.41	0.31	2.15	Fine	0.47	0.91
					Industry	0.25	Industry	0.16				Int.	0.58	
												Coarse	0.47	
												VSI	0.77	
$\mu$	3	0.36	2.49	1.65	Std FA	0.18	Std FA	0.56	0.99	0.81	2.06	Fine	0.72	0.97
					Industry	0.33	Industry	0.46				Int.	0.68	
												Coarse	0.63	
												VSI	0.89	

The equations for the flow resistance ratio and the plastic viscosity are plotted (Figure 3). The figure shows that the prediction accuracy of the flow resistance ratio ( $R^2 = 0.91$ ) is much lower than observed in [18]. However, the coefficient of determination for the plastic viscosity ( $R^2 = 0.97$ ) is only slightly lower than for the three datasets predicted by the original empirical equation ( $R^2 = 0.98-0.99$ ).

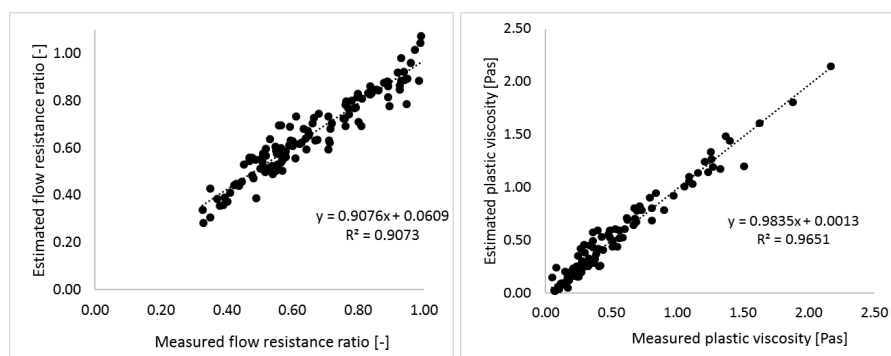


Figure 3 – Measured and estimated values for the flow resistance ratio and the Bingham plastic viscosity.

It is found that the prediction accuracies for the equations may be further improved if the  $k_5$  factor is a two-step function, changing at  $w/c$ -ratio = 0.50. This adjustment of  $k_5$  is considered reasonable to make, as the friction of the cement particles dominates more for low  $w/c$ -ratios, while at high  $w/c$ -ratio viscous flow dominates. In a study of cement grout injectability [29], it was found that fluidity of the grouts at  $w/c$ -ratio below 0.50 is decreasing in such a manner that injection operations could be hindered. It was also found that the rate of evolution of the apparent viscosity increased significantly for  $w/c$ -ratio below 0.50. Hence, it seems reasonable that the  $k_5$  factor changes at  $w/c = 0.5$ . With this adjustment of  $k_5$ , the  $R^2$  values increase to  $R^2 = 0.98$ ,  $R^2 = 0.95$  and  $R^2 = 0.92$  for plastic viscosity, mini slump flow and flow resistance ratio, respectively. A similar two-step strategy was carried out for the  $k_4$  factor, as the SP is known to reach saturation at a certain dosage level. However, the prediction accuracies were only improved by the third decimal via this change, hence  $k_4$  were kept constant for each cement type.

The new empirical model for prediction of flow resistance ratio shows lower prediction accuracy than the original empirical model. However, the FlowCyl test method and the resulting flow resistance ratio are not widely known, neither in Norway nor globally. Also, the cement pastes undergo high shear rates at the outlet of the FlowCyl, overshadowing the effect of the yield stress, making  $\lambda_q$  dominated by the plastic viscosity [30, 31]. Hence, it is considered beneficial that the new empirical equation provides the highest precision for the more known rheological parameters plastic viscosity and mini slump flow. The obtained  $n$  and  $k_x$  factors for the plastic viscosity are listed (Table 4) and the equation is plotted (Figure 4).

Table 4 – The  $n$  and  $k_x$  factors for the empirical equation predicting the plastic viscosity when  $k_5$  differs for  $w/c$ -ratio  $\leq / > 0.50$ .

$n$	$k_1$	$k_2$	$k_3$	$k_4$		$k_5, w/c \leq 0.50$		$k_6$	$k_7$	$k_8$	$k_9$		$R^2$		
3	0.33	0.86	1.52	Std FA	0.20	Std FA	0.29	0.99	0.81	2.06	Fine	0.45	0.98		
				Industry	0.29	Industry	0.25				Int.	0.39			
				$k_5, w/c > 0.50$							Coarse	0.34			
				Std FA	0.21	Industry	0.14				VSI	0.61			

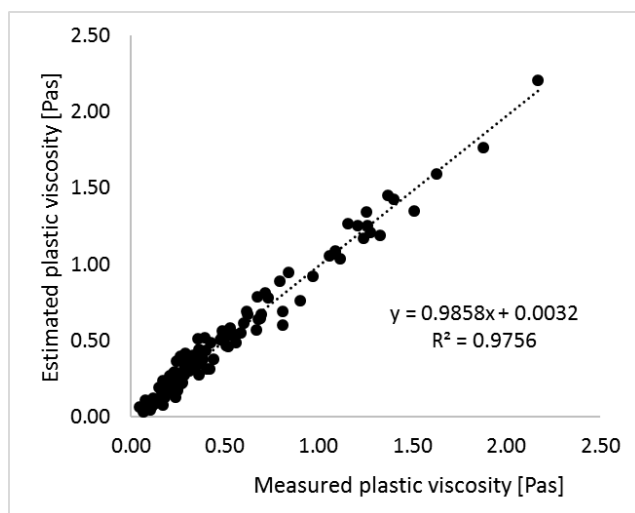


Figure 4 – Correlation between measured and predicted values from the new empirical equation for the plastic viscosity, where  $k_6$  is a two-step function for  $w/c$ -ratio  $\leq / > 0.50$ .

The empirical equation for prediction of plastic viscosity provides an  $R^2 = 0.98$  (Figure 4), which is approximately the same prediction accuracy as the equations presented in [18]. This is a surprisingly good result, considering that the equation is predicting a set of matrices that were tailor made to cover wide spectra of rheology, composition and powder materials. As pointed out in the introduction, the mix program consists of four different crushed fillers, two different cements, biotite, fly ash, silica fume and SP. Large variations occur in both SP dosages,  $w/c$  and  $f_i/b$  ratios. This illustrates that the empirical equation developed in this work is capable of

predicting a wide spectrum of matrices and is a promising proportioning tool for the concrete industry.

A limitation of the empirical equation is that the regression analysis needs to be performed for each set of new materials to obtain their  $k_x$  factors. This means that for the equation to be optimized at a ready mix concrete plant, systematic testing of the given materials must be performed in advance. Also, further research should aim at simplifying the methodology of measuring the VSSA, in terms of comparing the Sedigraph measurements with other simpler and more industrial test methods, such as the Blaine test.

## 5. CONCLUSION

In this paper, 117 matrices are presented, whereas 107 of these contain fillers from manufactured sand. The experimental testing of the matrices provides four rheological parameters: The flow resistance ratio, mini slump flow, Bingham yield stress and Bingham plastic viscosity. An empirical equation for rheology prediction is developed, and its applicability is investigated on the four measured rheological parameters. The results show that the equation provides good correlation to the plastic viscosity, with a coefficient of determination equal to  $R^2 = 0.98$ . Considering the large variety in mix design and materials in the mix program, the prediction accuracy is surprisingly good, and the empirical equation is evaluated to be a promising rheology prediction tool for the concrete industry.

## ACKNOWLEDGEMENT

This paper is based on work performed within the MiKS project (Micro-proportioning with Crushed Sand), which is a Competence Project for the Industry funded by the Research Council of Norway (contract No. 247619) and industrial partners. The authors would like to thank the Research Council of Norway and the industrial partners Norcem AS, Skanska Norge AS and Feiring Bruk AS, for their financial support and for facilitating the interaction between research and industry. Special thanks go to former Ph.D. student in the project, Evgeny Ramenskiy, for performing rheological testing of 51 of the matrices, as well as researcher Malin Sletnes at SINTEF for performing testing of 11 matrices. The authors would also like to thank the master students Patricia Ysabel Sosa and Juni Christine Myhre Foslie for contributing to the testing of the remaining matrices.

## REFERENCES

1. Ferraris C F, Obla K H & Hill R: “The Influence of Mineral Admixtures on the Rheology of Cement Paste and Concrete”. *Cement and Concrete Research*, Vol. 31, No. 2, 2001, pp. 245-255.
2. Krieger I M & Dougherty T J: “A Mechanism for Non-Newtonian Flow in Suspensions of Rigid Spheres”. *Transactions of the society of rheology III*, 1959, pp. 137-152.
3. Chong J S, Christiansen E B & Baer A D: “Rheology of Concentrated Suspensions”. *Journal of applied polymer science*, Vol. 15, 1971, pp. 2007-2021.
4. Mooney M: “The Viscosity of a Concentrated Suspension of Spherical Particles”. *Journal of Colloid Interface Science*, Vol. 6, No. 2, 1951, pp. 162-170.



5. Eilers H: “Die Viskosität von Emulsionen hochviskoser Stoffe als Funktion der Konzentration”. (“The Viscosity of Emulsions of Highly Viscous Materials as a Function of Concentration”). *Kolloid Zeitschrift*, Vol. 97, No. 3, 1941, pp. 313-321 (in German).
6. Quemada D: “Rheology of Concentrated Disperse Systems and Minimum Energy Dissipation Principle”. *Rheologica Acta*, Vol. 16, 1977, pp. 82-94.
7. Robinson J V: “The Viscosity of Suspensions of Spheres”. *Journal of Physical Chemistry*, Vol. 53, No. 7, 1949, pp. 1042-1056.
8. Spangenberg J, Scherer G W, Hopkins A B & Torquato S: “Viscosity of Bimodal Suspensions with Hard Spherical Particles”. *Journal of Applied Physics*, Vol. 116, No. 18, 2014.
9. Damineli B L, John V N, Lagerblad B & Pileggi R G: “Viscosity Prediction of Cement-Filler Suspensions using Interference Model: A Route for Binder Efficiency Enhancement”, *Cement and Concrete Research*, Vol. 84, 2016, pp. 8-19.
10. Buscall R, McGowan I J, Mills P D A, Stewart R F, Sutton D, White L R & Yates G E: “The Rheology of Strongly-Flocculated Suspensions”. *Journal of Non-Newtonian Fluid Mechanics*, Vol. 24, 1987, pp. 183-202.
11. Kapur P C, Scales P J, Boger D V & Healy T W: “Yield Stress of Suspensions Loaded with Size Distributed Particles”. *AIChE Journal*, Vol. 43, 1997, pp. 1171-1179.
12. Scales P J, Johnson S B, Healy T W & Kapur P C: “Shear Yield Stress of Partially Flocculated Colloidal Suspensions”. *AIChE Journal*, Vol. 44, 1998, pp. 538-544.
13. Zhou Z, Solomon M J, Scales P J & Boger D V: “The Yield Stress of Concentrated Flocculated Suspensions of Size Distributed Particles”. *Journal of Rheology*, Vol. 43, 1999, pp. 651-671.
14. Flatt R J & Bowen P: “Yodel: A Yield Stress Model for Suspensions”. *Journal of the American Ceramic Society*, Vol. 89, No. 4, 2006, pp.1244-1256.
15. Powers T C: “The Properties of Fresh Concrete”. Wiley & Sons, New York, USA, 1968, 664 pp.
16. Cepuritis R, Jacobsen S, Smeplass S, Mørtzell E, Wigum B J & Ng S: “Influence of Crushed Aggregate Fines with Micro-Proportioned Particle Size Distributions on Rheology of Cement Paste”. *Cement and Concrete Composites*, Vol. 80, 2017, pp. 64-79.
17. Skare E L, Cepuritis R, Spangenberg J, Ramenskiy E, Mørtzell E, Smeplass S, Jacobsen S: “Microproportioning Paste with Crushed Aggregate Filler by Use of Specific Surface Area”, *Proceedings, The 15<sup>th</sup> International Congress on the Chemistry of Cement, Prague, Czech Republic, 2019*. Ed. Gemrich J. ISSN 2523-935X, 10 pp.
18. Mørtzell E: “Modellering av Delmaterialenes Betydning for Betongens Konsistens”. (“Modelling the Effect of Concrete Part Materials on Concrete Consistency“). (PhD Thesis). Norwegian University of Science and Technology, Department of Structural Engineering, Trondheim, Norway, 1996, 301 pp. (In Norwegian).
19. Cepuritis R: "Development of Crushed Sand for Concrete Production with Micro-proportioning". (PhD Thesis). Norwegian University of Science and Technology, Department of Structural Engineering, Trondheim, Norway, 2016, 386 pp.
20. Bengtsson M & Evertsson CM: “Measuring characteristics of aggregate material from vertical shaft impact crushers”. *Minerals Engineering*, Vol. 19 (15), 2006, pp. 1479-1486.
21. Wallevik O.H: “Den ferske betongens reologi og anvendelse på betong med og uten tilsetning av silikastøv». (Rheology of Fresh Concrete and Application to Concrete With and Without Addition of Silica Fume”)). (PhD Thesis) Norges tekniske høgskole, Trondheim, Norway, 1990, 185 pp.
22. Sheiat S, Ranjbar N, Frellsen J, Skare E L, Cepuritis R, Jacobsen S & Spangenberg J: “Neural Network Predictions of the Simulated Rheological Response of Cement Paste in the FlowCyl”. *Neural Computing & Applications*, Vol. 33, 2021, pp. 13027–13037.

23. Great Wall Mineral, From the GWM Selection [Internet], <<http://greatwallmineral.com/index.asp?Id=3>> [Read 05.04.19]
24. Jacobsen S, Maage M, Smepllass S, Kjellens K O, Sellevold E J, Lindgård J, Cepuritis R, Myrdal R, Bjøntegaard Ø, Geiker M *et al.*: “TKT 4215 Concrete Technology 1”, *Compendium*, Norwegian University of Science and Technology, Department of Structural Engineering, Trondheim, Norway, 2016.
25. Ng S, Mujica H & Smepllass S: “Design of a Simple and Cost-Efficient Mixer for Matrix Rheology Testing”, *Nordic Concrete Research*, Vol. 51, No. 3, 2014, pp. 15-28.
26. Spangenberg J, da Silva W R L, Comminal R, Mollah M T, Andersen T J & Stang H: “Numerical simulation of multi-layer 3D concrete printing”, *RILEM Technical Letters* 6, 2021, pp. 119-123.
27. Comminal R, da Silva W R L, Andersen T J, Stang H & Spangenberg J: “Modelling of 3D concrete printing based on computational fluid dynamics”, *Cement and Concrete Research*, Vol. 138, 106256, 2020, 12 pages.
28. Comminal R, da Silva W R L, Andersen T J, Stang H & Spangenberg J: “Influence of processing parameters on the layer geometry in 3D concrete printing: experiments and modelling”, *RILEM international Conference on Concrete and Digital Fabrication*, 2020, pp.852-862.
29. Rosquoëta F, Alexis A, Khelidj A & Phelipot A: “Experimental Study of Cement Grout: Rheological Behavior and Sedimentation”. *Cement and Concrete Research*, Vol. 33, 2003, pp. 713-722.
30. Cepuritis R, Skare E L, Ramenskiy E, Mørtzell E, Smepllass S, Li S, Jacobsen S & Spangenberg J: “Analysing Limitations of the FlowCyl as a One-Point Viscometer Test for Cement Paste”. *Construction and Building Materials*, Vol. 218, 2019, pp. 333-340.
31. Skare E L, Jacobsen S, Cepuritis R, Smepllass S & Spangenberg J: “Decreasing the Magnitude of Shear Rates in the FlowCyl”. *Proceedings*, 5th fib Congress, Melbourne, Australia, 2018.

## APPENDIX A

### Abbreviations used in the tables:

w/b = water-to-binder ratio by mass.  
 SP = superplasticiser dosage by mass of cement.-.  
 fi/c = filler-to-cement ratio by mass  
 FA/c = fly ash-to-cement ratio by mass  
 s/c = silica fume-to-cement ratio by mass  
 bio/fi = biotite-to-filler ratio by mass

Table 5 – Outline of the different mix designs in Series 1a.

No.	$\frac{w}{b}$	$\frac{sp}{c}$	$\frac{fi}{c}$	$\frac{fa}{c}$	$\frac{s}{c}$	$\frac{bio}{fi}$	Cement	Filler
1	0.40	0.75	0.25	-	-	-	Std FA	Coarse
2	0.40	0.75	0.32	-	-	-	Std FA	Coarse

3	0.40	0.75	0.39	-	-	-	Std FA	Coarse
4	0.55	0.75	0.45	-	-	-	Std FA	Coarse
5	0.55	0.75	0.52	-	-	-	Std FA	Coarse
6	0.55	0.75	0.59	-	-	-	Std FA	Coarse
7	0.70	0.75	0.60	-	-	-	Std FA	Coarse
8	0.70	0.75	0.67	-	-	-	Std FA	Coarse
9	0.70	0.75	0.72	-	-	-	Std FA	Coarse
10	0.40	0.75	0.25	-	-	-	Std FA	Intermediate
11	0.40	0.75	0.32	-	-	-	Std FA	Intermediate
12	0.40	0.75	0.39	-	-	-	Std FA	Intermediate
13	0.55	0.75	0.45	-	-	-	Std FA	Intermediate
14	0.55	0.75	0.52	-	-	-	Std FA	Intermediate
15	0.55	0.75	0.59	-	-	-	Std FA	Intermediate
16	0.70	0.75	0.60	-	-	-	Std FA	Intermediate
17	0.70	0.75	0.67	-	-	-	Std FA	Intermediate
18	0.70	0.75	0.72	-	-	-	Std FA	Intermediate
19	0.40	0.75	0.25	-	-	-	Std FA	Fine
20	0.40	0.75	0.32	-	-	-	Std FA	Fine
21	0.55	0.75	0.45	-	-	-	Std FA	Fine
22	0.55	0.75	0.52	-	-	-	Std FA	Fine
23	0.55	0.75	0.59	-	-	-	Std FA	Fine
24	0.70	0.75	0.60	-	-	-	Std FA	Fine
25	0.70	0.75	0.67	-	-	-	Std FA	Fine
26	0.70	0.75	0.72	-	-	-	Std FA	Fine
27	0.40	1.00	0.25	-	-	-	Std FA	Intermediate
28	0.40	1.00	0.32	-	-	-	Std FA	Intermediate
29	0.40	1.00	0.39	-	-	-	Std FA	Intermediate
30	0.40	1.25	0.25	-	-	-	Std FA	Intermediate
31	0.40	1.25	0.32	-	-	-	Std FA	Intermediate
32	0.40	1.25	0.39	-	-	-	Std FA	Intermediate
33	0.40	1.50	0.25	-	-	-	Std FA	Intermediate
34	0.40	1.50	0.32	-	-	-	Std FA	Intermediate

35	0.40	1.50	0.39	-	-	-	Std FA	Intermediate
36	0.40	1.75	0.25	-	-	-	Std FA	Intermediate
37	0.40	1.75	0.32	-	-	-	Std FA	Intermediate
38	0.40	1.75	0.39	-	-	-	Std FA	Intermediate
39	0.55	1.00	0.45	-	-	-	Std FA	Intermediate
40	0.55	1.00	0.52	-	-	-	Std FA	Intermediate
41	0.55	1.00	0.59	-	-	-	Std FA	Intermediate
42	0.55	1.25	0.45	-	-	-	Std FA	Intermediate
43	0.55	1.25	0.52	-	-	-	Std FA	Intermediate
44	0.55	1.25	0.59	-	-	-	Std FA	Intermediate
45	0.55	1.50	0.45	-	-	-	Std FA	Intermediate
46	0.55	1.50	0.52	-	-	-	Std FA	Intermediate
47	0.55	1.50	0.59	-	-	-	Std FA	Intermediate
48	0.55	1.75	0.45	-	-	-	Std FA	Intermediate
49	0.55	1.75	0.52	-	-	-	Std FA	Intermediate
50	0.55	1.75	0.59	-	-	-	Std FA	Intermediate
51	0.40	0.75	0.32	-	-	0.01	Std FA	Int. + mica
52	0.40	0.75	0.32	-	-	0.02	Std FA	Int. + mica
53	0.40	0.75	0.32	-	-	0.03	Std FA	Int. + mica
54	0.40	0.75	0.32	-	-	0.05	Std FA	Int. + mica
55	0.40	0.75	0.32	-	-	0.10	Std FA	Int. + mica

Table 6 – Outline of the different mix designs in Series 1b.

No.	$\frac{w}{b}$	$\frac{sp}{c}$	$\frac{fi}{c}$	$\frac{fa}{c}$	$\frac{s}{c}$	Cement	Filler
1	0.55	0.75	0.53	0.00	0.04	Std FA	Intermediate
2	0.55	0.75	0.61	0.00	0.04	Std FA	Intermediate
3	0.55	0.75	0.55	0.00	0.09	Std FA	Intermediate
4	0.55	0.75	0.64	0.00	0.09	Std FA	Intermediate
5	0.55	0.75	0.53	0.00	0.04	Std FA	VSI
6	0.55	0.75	0.61	0.00	0.04	Std FA	VSI
7	0.55	0.75	0.78	0.26	0.05	Std FA	VSI

8	0.55	0.75	0.67	0.26	0.05	Std FA	Intermediate
9	0.55	0.75	0.78	0.26	0.05	Std FA	Intermediate
10	0.55	0.75	0.89	0.61	0.14	Std FA	Intermediate
11	0.55	0.75	1.04	0.61	0.14	Std FA	Intermediate
12	0.55	0.75	0.71	0.28	0.11	Std FA	Intermediate
13	0.55	0.75	0.89	0.61	0.14	Std FA	Intermediate
14	0.55	0.75	1.04	0.61	0.14	Std FA	Intermediate

Table 7 – Outline of the different mix designs in Series 2a.

No.	$\frac{w}{b}$	$\frac{sp}{c}$	$\frac{fi}{c}$	$\frac{fa}{c}$	$\frac{s}{c}$	Cement	Filler
1	0.40	0.75	0.28	0.00	-	Industry	Intermediate
2	0.40	1.50	0.28	0.00	-	Industry	Intermediate
3	0.55	0.75	0.51	0.00	-	Industry	Intermediate
4	0.55	0.75	0.59	0.00	-	Industry	Intermediate
5	0.55	1.50	0.51	0.00	-	Industry	Intermediate
6	0.55	1.50	0.59	0.00	-	Industry	Intermediate
7	0.40	1.50	0.36	0.00	-	Industry	Intermediate
8	0.60	0.60	0.17	0.00	-	Industry	Fine
9	0.73	0.60	0.39	0.00	-	Industry	Fine
10	0.55	0.75	0.51	0.00	-	Industry	VSI
11	0.55	0.75	0.59	0.00	-	Industry	VSI
12	0.50	0.60	0.25	0.25	-	Industry	Fine
13	0.50	0.60	0.31	0.54	-	Industry	Fine
14	0.65	0.60	0.25	0.25	-	Industry	Fine
15	0.81	0.60	0.56	0.11	-	Industry	Fine
16	0.76	0.60	0.48	0.23	-	Industry	Fine
17	0.80	0.60	0.64	0.56	-	Industry	Fine
18	0.44	1.50	0.35	0.25	-	Industry	Intermediate

Table 8 – Outline of the different mix designs in Series 2b.

No.	$\frac{w}{b}$	$\frac{sp}{c}$	$\frac{fi}{c}$	$\frac{fa}{c}$	$\frac{s}{c}$	Cement	Filler
1	0.55	0.75	0.53	0.00	0.04	Industry	Intermediate
2	0.55	0.75	0.61	0.00	0.04	Industry	Intermediate
3	0.55	0.75	0.55	0.00	0.09	Industry	Intermediate
4	0.55	0.75	0.64	0.00	0.09	Industry	Intermediate
5	0.51	0.75	0.55	0.00	0.09	Industry	Intermediate
6	0.51	0.75	0.61	0.00	0.04	Industry	Intermediate
7	0.51	1.00	0.64	0.00	0.09	Industry	Intermediate
8	0.51	1.25	0.64	0.00	0.09	Industry	Intermediate
9	0.51	1.50	0.64	0.00	0.09	Industry	Intermediate
10	0.55	0.75	0.67	0.26	0.05	Industry	Intermediate
11	0.55	0.75	0.78	0.26	0.05	Industry	Intermediate
12	0.55	0.75	0.89	0.61	0.14	Industry	Intermediate
13	0.55	0.75	1.04	0.61	0.14	Industry	Intermediate
14	0.55	0.75	0.71	0.28	0.11	Industry	Intermediate
15	0.55	0.75	0.89	0.61	0.14	Industry	Intermediate
16	0.55	0.75	1.04	0.61	0.14	Industry	Intermediate
17	0.42	1.00	0.37	0.26	0.05	Industry	Intermediate
18	0.42	1.25	0.37	0.26	0.05	Industry	Intermediate
19	0.42	1.50	0.37	0.26	0.05	Industry	Intermediate
20	0.55	0.75	0.78	0.26	0.05	Industry	VSI

Table 9 – Outline of the different mix designs in Series 2c.

No.	$\frac{w}{b}$	$\frac{sp}{c}$	$\frac{fi}{c}$	$\frac{fa}{c}$	$\frac{s}{c}$	Cement	Filler
1	0.50	0.60	0.00	0.00	-	Industry	Fine
2	0.45	0.60	0.00	0.00	-	Industry	Fine
3	0.50	0.60	0.00	0.25	-	Industry	Fine
4	0.50	0.60	0.00	0.43	-	Industry	Fine
5	0.50	0.60	0.00	0.54	-	Industry	Fine

6	0.45	0.60	0.00	0.54	-	Industry	Fine
7	0.50	0.60	0.00	0.00	-	Industry	Fine
8	0.53	0.60	0.00	0.23	-	Industry	Fine
9	0.55	0.60	0.00	0.47	-	Industry	Fine
10	0.57	0.60	0.00	0.82	-	Industry	Fine

# Paper III

## **Rheology Modelling of Cement Paste with Manufactured Sand and Silica Fume: Comparing Suspension Models with Artificial Neural Network Predictions**

Skare EL, Sheiati S, Cepuritis R, Mørtzell E, Smepllass S, Spangenberg J, Jacobsen S.

*Construction and Building Materials* 317 (2022) 126114.

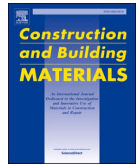






Contents lists available at ScienceDirect

## Construction and Building Materials

journal homepage: [www.elsevier.com/locate/conbuildmat](http://www.elsevier.com/locate/conbuildmat)

# Rheology modelling of cement paste with manufactured sand and silica fume: Comparing suspension models with artificial neural network predictions

Elisabeth Leite Skare<sup>a,b,\*</sup>, Shohreh Sheiati<sup>b</sup>, Rolands Cepuritis<sup>a,c</sup>, Ernst Mørtzell<sup>a,d</sup>, Sverre Smepllass<sup>a,e</sup>, Jon Spangenberg<sup>b</sup>, Stefan Jacobsen<sup>a</sup>

<sup>a</sup> Department of Structural Engineering, Norwegian University of Science and Technology, NO-7491 Trondheim, Norway

<sup>b</sup> Department of Mechanical Engineering, Technical University of Denmark, 2800 Lyngby, Denmark

<sup>c</sup> Norcem AS (HeidelbergCementGroup), R&D Department, Setreveien 2, Postboks 38, NO-3950 Brevik, Norway

<sup>d</sup> NorBetong AS (HeidelbergCementGroup), Lilleakerveien 2A, NO-0283 Oslo, Norway

<sup>e</sup> Skanska Norge AS, Drammensveien 60, PO Box 1175, NO-0107 Oslo, Norway

## ARTICLE INFO

**Keywords:**  
Rheology  
Cement paste  
Manufactured sand  
Artificial neural network

## ABSTRACT

Manufactured sand is increasingly used in concrete and predicting the rheology of such suspensions based on their composition are necessary. In this study, emphasis is on cement pastes with manufactured sand and silica fume. An artificial neural network, namely multilayer perceptron, is compared with nine suspension models: two liquid thickness models, the relative concentration of solids and six relative viscosity models based on the relative concentration of solids. Measurements on 107 mixes with filler (0–125  $\mu\text{m}$ ) from manufactured sand are conducted, acquiring yield stress, plastic viscosity, flow resistance ratio and mini slump flow. None of the suspension models offer good correlations to the measured parameters for all mixes, but an increase in prediction accuracy is seen for subsets of materials, especially mixes without silica fume. The artificial neural network outperforms the suspension models, providing a coefficient of determination between 0.84 and 0.91 for all mixes, thus illuminating a new pathway for cement paste rheology modelling.

## 1. Introduction

Global depletion of good quality construction sand leads to increased use of manufactured sand in concrete, which in contrast to natural sand contains a large number of particles less than 125  $\mu\text{m}$  in diameter [1]. Unless the particle size distribution is improved by suitable technology such as air classification or “wind sieving”, the high number of fines significantly increases the specific surface area of manufactured sand [2], which has a major impact on the rheology of cementitious materials [1,3–4]. In a study of micro-mortars by Westerholm *et al.* [5], the increased volume concentration of fines from manufactured sand was found to increase both yield stress and plastic viscosity. 3D concrete printing is an emerging technology today, being one of the reasons why methods for controlling concrete rheology are becoming increasingly important [6,7]. In [7] the concrete rheology is controlled actively by vibration, while Jones *et al.* [8] add limestone with different median

particle sizes to control rheology of 3D printable cement pastes. The high global interest of ultra-high-performance concrete is also contributing to the increasing need for tailoring rheological properties. Khayat *et al.* [9] state that the most efficient way to control rheological properties of such concretes is by optimization of the proportioning during the material selection, in combination with controlled particle packing density, specific surface area, chemical admixtures, water absorption during hydration and temperature of the mix. Accurately determining the rheological properties of concrete requires a large amount of materials and labor. Ferraris *et al.* [10] stated that measuring rheological properties on cement pastes is a promising approach to predict the rheology of equivalent concrete mixes, and thus this study will focus on cement paste rheology. There is a need for industrially applicable suspension models that are exploiting the fundamental usefulness of studying paste rheology. Such efforts to bridge over from paste studies to concrete proportioning practice have been proposed in the particle – matrix (PM)

\* Corresponding author at: Department of structural Engineering, NTNU, Richard Birkelands vei 1a, 7491 Trondheim, Norway.

E-mail addresses: [Elisabeth.l.skare@ntnu.no](mailto:Elisabeth.l.skare@ntnu.no) (E.L. Skare), [Shoshei@mek.dtu.dk](mailto:Shoshei@mek.dtu.dk) (S. Sheiati), [Rolands.cepuritis@ntnu.no](mailto:Rolands.cepuritis@ntnu.no) (R. Cepuritis), [Ernst.mortzell@norbetong.no](mailto:Ernst.mortzell@norbetong.no) (E. Mørtzell), [Sverre.smepllass@skanska.no](mailto:Sverre.smepllass@skanska.no) (S. Smepllass), [Josp@mek.dtu.dk](mailto:Josp@mek.dtu.dk) (J. Spangenberg), [Stefan.jacobsen@ntnu.no](mailto:Stefan.jacobsen@ntnu.no) (S. Jacobsen).

<https://doi.org/10.1016/j.conbuildmat.2021.126114>

Received 19 March 2021; Received in revised form 6 December 2021; Accepted 13 December 2021

0950-0618/© 2021 Published by Elsevier Ltd.

model [1,11–13]. In the PM-model, the concrete is considered a two phase-system: The particle phase includes all particles larger than 0.125 mm in diameter, and the matrix phase includes water, cement, pozzolanas, admixtures, as well as all particles less than 0.125 mm in diameter. The rheology of the concrete is described by the properties of the two phases and their volumetric relation [11]. Several authors have presented approaches to predict cement paste rheology based on part materials properties and proportions. Krieger and Dougherty [14] developed an equation for the relative suspension viscosity that was shown to have good correlation to measured viscosities on latex and polymer systems. Similar models were proposed by Mooney, Eilers, Robinson, Chong *et al.* and Quemada [15–19]. Powers [20] suggested the lubricating liquid thickness around all particles for modelling suspension rheology, and the method was successfully related to rheology for cement paste and concrete [4,21–22]. An effort to clarify the effect of water reducers in water layer models on fine mortars was investigated by Midorikawa *et al.* [23], where a flocculation number-approach was proposed to replace particles with flocks in the thickness calculation. Though, the thickness was not empirically quantified to rheology [23]. In [24] a yield stress prediction model is proposed by adopting the excess paste theory, where the thickness is assumed constant for different aggregate particle sizes. This is contrary to the observations in [25], where the matrix thickness was found to be proportional to the particle sizes. The relative concentration of solids, i.e. the ratio between volume fraction of solids and maximum packing fraction, has also been found to correlate well with concrete rheology [26]. The maximum packing was calculated numerically, and the relation between packing and rheology was seemingly unaffected by admixture dosage variations. Cepuritis *et al.* [12] showed that the volumetric specific surface area (VSSA) of manufactured sand per unit volume of matrix correlated linearly to measured rheological parameters of cement pastes. Skare *et al.* [13] found that the volume weighted average VSSA of all ingoing matrix powders, denoted  $VSSA_{matrix}$  in this paper, correlated well to rheological properties for cement pastes with widely varying mix compositions. Furthermore, the cement type was found to have a large effect on rheology producing two groups of VSSA-rheology plots [13]. In [27] a generalized viscosity model for cement pastes is proposed, evaluating the steady-state and relaxation responses of the paste by considering the thixotropic behavior, the viscosity-structural relation and the paste microstructure. Numerous other suspension models have been presented in the literature [28–34], but to limit the scope of this study, the focus of the paper is on models where the packing fraction and/or VSSA are central parameters. These models work well for many suspensions, but lack validation of the predictive capabilities for cement paste with manufactured sand and silica fume. The latter is an effective pozzolana frequently used in concrete because of its positive effect on properties as durability and stability [35].

Another approach to model cement paste rheology is by artificial intelligence. Computational techniques are frequently used for prediction of material properties, eschewing the costs and labor from laboratory research [36]. Recently, Zeeshan *et al.* [37] showed that machine learning techniques can be exploited to predict cement paste with nanoclay. Artificial neural network (ANN) is one example of such technique, and several studies show that ANNs can predict experimental rheological results [38,39,40]. However, the literature on the applicability of these techniques in terms of cement paste rheology is still very sparse. In a recent study by Sheiati *et al.* [41] two types of ANNs, i.e. multilayer perceptron (MLP) and radial basis function (RBF), were investigated for prediction of computational fluid dynamics (CFD) results on cement paste rheology. It was found that MLP provided high prediction accuracy even for a sparse training data set, while the accuracy of the RBF reduced significantly for reduced training data. In [42] the predicted viscosity of honey yielded the highest accuracy for MLP, compared to three other investigated ANNs; probabilistic neural network (PNN), recurrent neural network (RNN) and modular neural network (MNN). Hence, it is chosen to investigate cement paste rheology

by MLP in this study.

To advance in the development of more effective and precise models and tools for proportioning of fresh concrete properties, the objective of this paper is to investigate the predictive capabilities of nine semi-empirical suspension models as well as an artificial neural network model, for predicting the rheology of cement pastes with manufactured sand, varying superplasticizer (SP)-dosages, different cement types and with/without pozzolana. The rest of the paper is subdivided into five sections. Section 2 briefly reviews the models, Section 3 introduces the experimental methodology and materials, while the results are presented and analyzed in Section 4. A feature selection of the MLP model is presented in Section 5, and finally, the conclusions are summarized in Section 6.

## 2. Models

### 2.1. Lubricating liquid thickness

Kwan *et al.* [22] stated that the fresh properties of cement pastes mainly are governed by water content, packing density and solid surface area, and showed that the rheological effect of these parameters may be evaluated in terms of the lubricating liquid thickness. They used a wet packing procedure to determine the maximum packing fraction and defined the lubricating liquid thickness as the ratio between the excess fluid volume (EF) and the VSSA. The excess fluid was defined as the fluid in excess to fill up the voids between particles, very similar to what Powers [20] proposed, and in line with [23] and [43]. A larger volume of excess liquid means longer distance between the particles, leading to higher workability [22]. The VSSA is defined as specific surface area per volume of a material. In this study, the VSSA is calculated from the particle size distribution (PSD) obtained from the SediGraph, under the assumption of spherical particles. The combined VSSA for all dry materials in the matrix,  $VSSA_{matrix}$ , is calculated as the sum of the surface area multiplied by its volume percentage for each dry material, and this value is used for calculating the liquid thicknesses. Detailed procedures for obtaining the PSD and the VSSA are given in [1,44], and later rendered by Skare *et al.* in [13]. Two different models describing the lubricating liquid thickness (LT) are investigated here:  $LT_1$  where the void filling fluid (VFF) between the particles at maximum packing is considered as a part of the lubricating liquid, eqn. (1), and  $LT_2$  where the VFF is excluded, eqn. (2). The solid concentration,  $\phi$ , is calculated as the volume of all dry materials divided by the total volume of the mix. The cement paste is considered a three-phase component, consisting of VFF, EF and  $\phi$ .

$$LT_1 = \frac{1 - \phi}{VSSA_{matrix}} = \frac{VFF + EF}{VSSA_{matrix}} \quad (1)$$

$$LT_2 = \frac{1 - \phi - VFF}{VSSA_{matrix}} = \frac{EF}{VSSA_{matrix}} \quad (2)$$

Note that paste in concrete normally contains a certain percentage of air voids, meaning that eqn. (1) and (2) should include the air void content in the numerator [35,45]. However, in this study, the air voids are neglected, as the air void content in the cement paste typically is very low as compared to in paste of concrete, where air voids are captured in between aggregate particles.

### 2.2. Relative concentration of solids

The relative concentration of solids ( $\frac{\phi}{\phi_m}$ ) correlates well with the rheology of suspensions [26] and forms the basis of many predictive models that describe the relative viscosity of suspensions. Chong *et al.* [18] found that the relative viscosity of a monodispersed system correlated remarkably well to  $\frac{\phi}{\phi_m}$  independent of the particle size and temperature. Ferraris and de Larrard [26] showed that the correlation

between the plastic viscosity,  $\mu$ , and  $\frac{\phi}{\phi_m}$  is independent of use of high-range-water reducing admixtures and silica fume. Several other similar studies have been made, substantiating the correlation between  $\frac{\phi}{\phi_m}$  and rheology [44–46]. The yield stress model by Flatt and Bowen [28] is also a function of  $\frac{\phi}{\phi_m}$ , but was excluded in this study due to the uncertain parameters for surface forces and percolation, in spite of recent efforts to apply the model to manufactured sand by Zhu et al [47]. In addition, there is at least one more yield stress model based on  $\frac{\phi}{\phi_m}$  [48]. Hence, the relative concentration of solids seems to be a central parameter for suspension rheology despite that it does not include VSSA. The relative viscosity models in Table 1 are all functions of the relative concentration of solids and were investigated in this study.

The intrinsic viscosities used in this paper were obtained by curve fitting to achieve the best fit between measured and estimated values for each model. The literature on intrinsic viscosities of cement pastes is limited, and it is not a trivial task to evaluate which value that is most representative for the investigated matrices. Russel and Sperry [49] stated that for the Krieger-Dougherty equation, a value of  $[\eta]_{\phi_m} = 2$  often suffices for a good fit. In this study, that would correspond to values in order of  $[\eta] = 3.26 - 4.26$ , as the measured maximum packing ranges between 0.47 and 0.62. Struble and Sun [50] calculated the intrinsic viscosity of different cement pastes, yielding intrinsic viscosities in the range  $[\eta] = 4.5-6.0$ . For spherical particles, on the other hand, the intrinsic viscosity equals 2.5 [50]. The curve fitting method used in this study was previously used by Justnes and Vikan [51]. They investigated the Krieger-Dougherty equation on cement slurries and obtained values of the intrinsic viscosity around 5, though values up to 9.583 were seen for low shear rates in the rheometer. Note that the intrinsic viscosities used in this study are obtained solely to provide the best fit for each investigated model and varies little within each of the four suspension models applying intrinsic viscosity. However, the resulting values for the four different models are in the range 0.53–7.18, provided in Appendix A.

### 2.3. Multilayer perceptron neural networks

A multilayer perceptron based artificial neural network (ANN) is a mathematical technique where interconnected layers of neurons are used to determine the relationship between input and output variables without requiring the explicit physics behind the studied phenomenon. The links between the neurons are weighted to relate the importance of input variables to the output variables. The input layer neurons are

**Table 1**  
Relative suspension viscosity models, based on the relative concentration of solids.

Authors	Equation
Krieger and Dougherty [14]	$\eta_r = \left(1 - \frac{\phi}{\phi_m}\right)^{-[\eta]\phi_m}$
Mooney [15]	$\eta_r = \exp\left(\frac{[\eta]\phi}{1 - \frac{\phi}{\phi_m}}\right)$
Eilers [16]	$\eta_r = \left(1 + 0.5[\eta]\left(\frac{\phi}{1 - \frac{\phi}{\phi_m}}\right)\right)^2$
Robinson [17]	$\eta_r = 1 + [\eta]\left(\frac{\phi}{1 - \frac{\phi}{\phi_m}}\right)$
Chong et al. [18]	$\eta_r = \left(1 + 0.75\left(\frac{\phi_m}{1 - \frac{\phi}{\phi_m}}\right)\right)^2$
Quemada [19]	$\eta_r = \left(1 - \frac{\phi}{\phi_m}\right)^{-2}$

$\eta_r$  = relative viscosity,  $[\eta]$ = intrinsic viscosity,  $\phi$ = packing fraction,  $\phi_m$  = maximum packing fraction

variables that can be altered to optimize a problem and the output layer neurons are quantifications of desired outcomes for a given problem [52]. In this study, the input arguments of the MLP models are the SP/cement-ratio, the silica fume/binder-ratio, the VSSA<sub>matrix</sub>, as well as the volume fractions of water, cement, filler and fly ash. For example, the input arguments for mix 1a-1 are: SP/c = 0.75, silica fume/binder = 0.00, VSSA<sub>matrix</sub> = 394 mm<sup>2</sup>/mm<sup>3</sup>, and the volume fractions of water, cement, filler and fly ash which are 0.48, 0.40, 0.11 and 0.00, respectively. The outputs are the Bingham yield stresses and -plastic viscosities, the flow resistance ratios and the mini slump flows. The experimental data was randomly divided into training data (80%) and testing data (20%), as this is a frequently used split between training and testing data for MLP-models in literature [53–56]. The MLP models were developed from the training data, and their performance was verified on the testing data. All data samples were normalized between 0.1 and 0.9. In addition to the layers of input neurons and output neurons, the MLP models consist of a number of hidden layers of neurons, being the activation functions linking the input neurons to the output neurons [57]. Here, the NEWFF function with *trainlm* training function in MATLAB was used to build the network:

$$net = newff(P, T, S) \tag{3}$$

where  $P$ ,  $T$ , and  $S$  are the input vector, output vector and hidden layer size, respectively.

The number of hidden layers and the number of neurons in each hidden layer were tuned by MATLAB GA Toolbox to increase the speed and efficiency of the neural network [57]. The tuning interval for the number of hidden layers and number of neurons in each layer were defined as 1–2 and 1–20, respectively. To compare the predictive performance and selecting appropriate and robust models, the coefficient of determination,  $R^2$ , was used [58].

## 3. Experiments

### 3.1. Materials data and mix design

The experimental test program consists of 107 cement pastes with manufactured sand, hereinafter referred to as matrices. Originally, 125 mixes were designed, but 8 of the mixes were too viscous to perform testing on, and 10 mixes were without manufactured sand, and hence outside the scope of this paper. Out of the resulting 107 matrices, 41 contained silica fume. Table 2 outlines the main variables of the test series.

Five different fillers were used: Three crushed granitic aggregate fillers from Velde Pukk AS with density 2.65 g/cm<sup>3</sup>, denoted fine, intermediate and coarse; a Vertical Shaft Impactor (VSI) crushed 0/2mm filler from Feiring Bruk with the density 2.75 g/cm<sup>3</sup>, denoted VSI filler; and lastly, an industrial biotite (mica) GW-MB-A230 with the density 2.84 g/cm<sup>3</sup> from Great Wall Mineral [59]. The fillers from Velde Pukk AS differ from each other by being extracted at different cut-sizes in the crusher, where fine, intermediate and coarse is extracted at 63 μm, 125 μm and 500 μm, respectively [1]. The VSI filler was crushed from gneiss and granite and extracted at cut size 2 mm. The fillers from Velde Pukk AS and Feiring Bruk were mechanically sieved at 125 μm.

Two different cement types were used in the mix program: The Norwegian Standard FA cement (Std FA) from Norcem AS, CEM II/B-M 42.5 R, with particle density 3.00 g/cm<sup>3</sup>, and the Norwegian Industry

**Table 2**  
Outline of the different test series.

Series	1a	1b	2a	2b
No. of mixes	55	14	11	27
Description	Standard FA	Standard FA	Industry cement	Industry cement
		+ Silica fume		+ Silica fume

cement from Norcem AS, CEM I 52,5 R, with particle density  $3.13 \text{ g/m}^3$ . The Std FA cement contains 18% fly ash and 4% limestone, and has a modest heat and strength development, while the Industry cement is a rapid hardening Portland cement with rapid heat and strength development [35]. Information about the chemical composition, particle size distributions, fineness and the setting time of the cements is found in Appendix B. Fly ash from Norcem AS and undensified Elkem Microsilica, 940-U, were also included in some of the matrices. The polycarboxylate ether-based superplasticizer Dynamon SR-N from Mapei, with dry solids content of 19.5 %, was used in all the matrices.

The matrices were divided into two main series: Series 1 that consists of Standard FA cement matrices, and Series 2 that consists of Industry cement matrices. Each series was further divided into two subseries, a and b, representing matrices without and with silica fume, respectively, see Table 2. The mix designs were chosen to map a wide span of rheological parameters. Therefore, both matrices within and outside the practical range used in ready mix concrete production appeared in the test program. Appendix C provides detailed information about the mix compositions for all matrices.

### 3.2. Volumetric specific surface area

The PSD analysis was performed with the SediGraph III Plus for all dry powders except silica fume. The dispersing liquid Micromeritics Sedisperse A-12 was used, as this was successfully used to study settling of fly ash, filler and cement with a maximum diameter  $125 \mu\text{m}$  by Sosa in [44].

The measured PSDs and the calculated VSSAs are presented in Fig. 1. A PSD analysis of the silica fume was not performed, due to its small grain sizes. Like in [13], a volumetric specific surface area of  $60\,000 \text{ mm}^2/\text{mm}^3$  was used for the silica fume in this study, based on the assumption of spherical particles with a mean diameter of  $0.05 \mu\text{m}$  and particle density  $2200 \text{ kg/m}^3$  [35].

### 3.3. Mixing and rheology measurements

All matrices were produced in volumes of 2.0 L and mixed according to the procedure by Ng. et al. [60]. Details about the chosen mixing equipment is described in [13]. Later, replica mixes of all matrices were made for packing and fluid viscosity measurements with centrifuge and capillary glass viscometer. For these matrices, the high shear mixing procedure described in [61] was used. The volume of each matrix was chosen to get enough volume of the excess fluid. In [62] it was found

that a volume of 0.4 l was necessary for the matrices with w/c less than 0.5, while 0.2l was sufficient for the matrices with w/c greater than 0.5. All dry materials were premixed by hand for 10 s, followed by wet-mixing by a hand-blender, Phillips ProMix model no. HR 1673, with 800 W power rating. The wet mixing was performed at maximum speed in 30 s, followed by 5 min rest, and then 60 s of maximum speed mixing again. Directly after mixing, the matrices were evenly distributed into an even number of falcon tubes with volume of 45 ml and centrifuged at 4000 rpm for 5 min [63]. After centrifugation, the excess fluid was extracted from the matrix, and used to calculate the maximum packing fraction of the matrix according to eqn. (4) – (6) in [62]. Lastly, the kinematic viscosity of the excess fluid was measured.

### 3.4. Rheology measurements on matrix

Directly after mixing of the 2.0 L matrices, the Anton Paar Physica MCR 300 rheometer and the FlowCyl tests were performed, followed by the mini slump test. A detailed procedure for these tests is described in [12]. The FlowCyl is a vertical pipe with a cone in its end, and the matrices flow through a narrow opening in the cone under gravity. The mass as a function of time is logged and forms the basis for calculating the flow resistance ratio [12]. The flow resistance ratio,  $\lambda_q$ , ranges from 0.0 to 1.0, where 0.0 represents an “ideal fluid” with no internal resistance or external friction and 1.0 represents an extremely viscous fluid that are too viscous to flow through the FlowCyl [35]. The flow resistance ratio is defined as the average ratio between the flow loss of the measured fluid and the theoretical fluid flow of the ideal fluid [35]. Clearly, no such ideal fluid exists, and the authors considers the extremal case of  $\lambda_q = 0.0$  a fluid where the viscosity approaches zero. Mørtzell [11] stated that the theoretical flow rate of an ideal fluid is only governed by the gravity and the geometry of the FlowCyl. Hence, there would be no friction between the fluid and the walls of the FlowCyl and no internal friction in the fluid, and the flow resistance ratio would by definition be equal to zero. In this study, the lowest measured  $\lambda_q$  equaled 0.33, corresponding to a measured plastic viscosity of 0.05 Pas, and the highest measured  $\lambda_q$  equaled 0.99, corresponding to a plastic viscosity of 2.17 Pas. Due to a limited amount of matrix in the current study, the matrices were reused in the mini slump cone after the FlowCyl test was performed. The mini slump – cone had a top diameter of 39 mm, bottom diameter of 89 mm and height of 70 mm. The cone was filled with matrix and lifted vertically so the matrix started flowing. When the matrix stopped flowing, its diameter was measured in two perpendicular directions, and the average value was used.

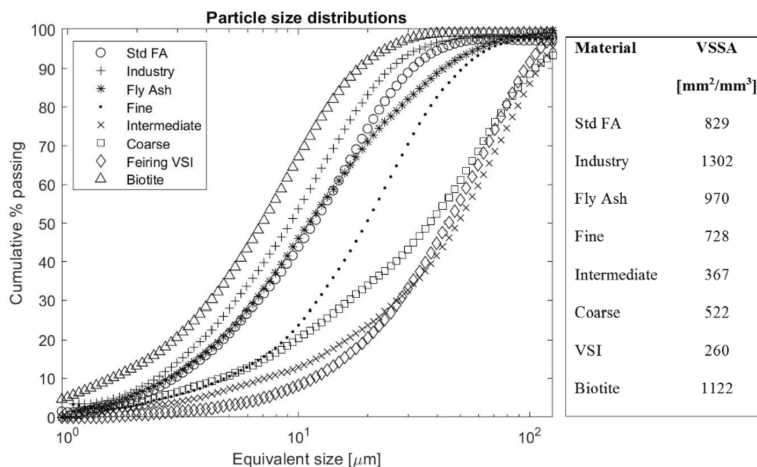


Fig. 1. PSDs and VSSAs of all dry materials except silica fume.

The yield stress,  $\tau_0$ , and plastic viscosity,  $\mu$ , were calculated according to the Bingham model using the flow curve (shear stress vs shear rate) obtained by the rheometer [64]. The rheometer was installed with bob-in-a-cup geometry, and the geometry of the bob was as described in [12]. Such equipment has successfully been used for rheology quantification of cementitious materials in previous studies [65–67]. The matrices were sheared at a shear rate of  $60 \text{ s}^{-1}$  for 30 s, then at rest for 30 s, followed by linearly increasing shear rates from  $1 \text{ s}^{-1}$  to  $60 \text{ s}^{-1}$  over a period of 3 min (30 steps of 6 s). Thereafter, the shear rate decreased in steps from  $60 \text{ s}^{-1}$  to  $1 \text{ s}^{-1}$  for 3 min. The plastic viscosity was calculated as the slope of the down-curve (linearly decreasing shear rate) and the yield stress as the intercept at zero shear rate of the down-curve [64]. Fig. 2 illustrates typical down-curves obtained from the rheometer for cement pastes from the experimental study with both low and high Bingham parameters, i.e., mix 1a-46 and 1a-3, respectively. The cement paste presented in Fig. 2 (a) yields  $\tau_0 = 0.57 \text{ Pa}$  and  $\mu = 0.14 \text{ Pas}$ , while the cement paste in Fig. 2 (b) measures  $\tau_0 = 23.98 \text{ Pa}$  and  $\mu = 1.40 \text{ Pas}$ .

The repeatability of the measurements was determined by repeated mixing and testing of mix 1a-2. Table 3 summarizes the repeatability results.

### 3.5. Maximum packing fraction and the relative concentration of solids

The maximum packing fraction,  $\phi_m$ , was measured on the replica mixes by centrifugation of a known volume of matrix [63]. During centrifugation, the excess fluid expelled from the matrix, forming a liquid layer on top of the compacted matrix in the tube. The volume of the excess fluid was found by weighing the fluid after pouring it off from the tubes. It was assumed that in addition to water, the liquid consisted of some solid particles from the matrix. This solid content was found by evaporating the excess fluid at  $40 \text{ }^\circ\text{C}$ . The density of the fluid was obtained by the simple assumption that the solid particles were composed by 50% fines and 50% solid content from the polymers, resulting in an average solid density of  $1.85 \text{ g/cm}^3$  [62,68]. The maximum packing fraction was calculated from eqn. (4), where the total solid fraction of the matrix,  $\phi$ , was calculated from the mix proportions and the individual powder particle densities:

$$\phi_m = \frac{\phi}{VFF + \Phi} = \frac{\phi}{1 - EF} \quad (4)$$

The accuracy of the maximum packing measurements was estimated based on repeated measurement of four matrices. The maximum error equaled 5.8%, while the average error for the four matrices equaled 1.68%.

### 3.6. Viscosity of interstitial pore solution - $\eta_{fluid}$

The kinematic viscosity measurements of the interstitial pore solution were performed using two different glass viscometers, ASTM D2515 size no. 50 with a capillary diameter 0.44 mm, and ASTM D2515 size no.

**Table 3**  
Repeatability of the rheology measurements.

Repeatability test no.	$\tau_0$ [Pa]	$\mu$ [Pas]	Mini slump flow [mm]	$\lambda_q$ [-]
1	14.65	1.31	15.5	0.92
2	12.02	1.24	16.2	0.93
3	15.49	1.23	16.0	0.92
4	13.75	1.29	15.3	0.94
5	15.45	1.24	15.2	0.92
Mean	14.27	1.26	15.64	0.92
Standard deviation, $\sigma$	1.45	0.04	0.44	0.01
Coefficient of variation, CV [%]	10.1	2.9	2.8	0.9

75 with a capillary diameter of 0.54 mm. It was necessary to use two different viscometer sizes due to the variation in the expelled excess fluids ability to flow through the capillary of the glass viscometer. An overview of which viscometer that was used for each matrix is found in Appendix C. The excess fluids of the matrices that were tested with the viscometer size no. 50 were filtered after centrifugation, using a cellulose filter with mesh size  $0.45 \mu\text{m}$ . The excess fluids of the other matrices were unfiltered. For all matrices, the test setup and sample preparation were done according to the ASTM D2515-66 Standard [69]. Three viscosity measurements were performed for each matrix [62,68]. The maximum coefficient of variation between similar matrices was 8.2%. However, out of all matrices, a coefficient of variation of more than 0.88% was only seen twice.

## 4. Results and discussion

Firstly, the correlations between the predicted and measured rheology values for all mixes are investigated. The correlations are described by their  $R^2$ -values, listed in Table 4. As the models in Table 1

**Table 4**  
Coefficients of determination,  $R^2$ , for predicted and measured values for all matrices.

	$R^2$ $\mu$	$R^2$ $\tau_0$	$R^2$ $\lambda_q$	$R^2$ Mini slump flow
All matrices	All matrices	All matrices	All matrices	All matrices
LT <sub>1</sub>	0.05	0.52	0.05	0.39
LT <sub>2</sub>	0.36	0.46	0.39	0.44
$\Phi/\Phi_{max}$	0.55	0.01	0.60	0.07
K-D	0.59	–	–	–
Mooney	0.56	–	–	–
Eilers	0.57	–	–	–
Robinson	0.55	–	–	–
Chong	0.56	–	–	–
Quemada	0.56	–	–	–
MLP	$0.91 \pm 0.07$	$0.84 \pm 0.10$	$0.88 \pm 0.09$	$0.87 \pm 0.09$

K-D = Krieger and Dougherty

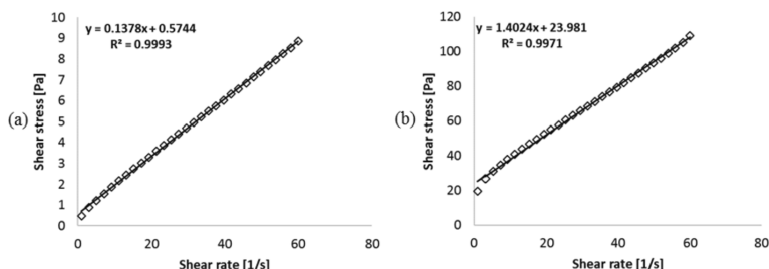


**Fig. 2.** Typical down-curves of cement pastes tested in the rheometer. The straight lines and the corresponding equations represent the linear regressions applied on the data to extract the Bingham parameters. The illustration includes flow curves of cement pastes yielding both (a) low Bingham parameters and (b) high Bingham parameters.

are developed for viscosity prediction, they are only compared with the plastic viscosity. The  $R^2$ -values for all models except the MLP model, are obtained from regression analysis in Excel, using the Solver function to obtain the minimum sum of squares. The exponential, linear, logarithmic and power law function fits are compared, and the equation providing the highest  $R^2$  is chosen. For the MLP model, the prediction accuracy is calculated as the average accuracy of 100 randomly selected training datasets for the considered case.

Table 4 shows that the MLP model provides far better correlations to all the four rheology parameters, than the other models. The coefficient of determination for the MLP model is in the range of 0.84 – 0.91, while the best coefficient of determination for the nine other models is 0.60. The best correlation for the MLP model is found for the plastic viscosity, with an  $R^2 = 0.91$ .

It is clear that the nine suspension models are not suitable for rheology prediction of all matrices in the presented test program. As two different cement types are used in the test program, it is of interest to investigate whether the models improve when considering matrices with each of the cement types, individually. Note that all mix designs contain either Standard FA or Industry cement, not a combination of both cement types. As described in section 3.1, Standard FA cement has a modest heat and strength development, while Industry cement is rapid hardening, meaning faster loss of workability. Table 5 provides the  $R^2$ -values for Series 1 (matrices with Standard FA cement) and 2 (matrices with Industry cement).

Table 5 shows that when considering Series 1 and 2 individually, the MLP model is the only model that can predict the rheology of matrices with Standard FA cement (Series 1). However, the maximum coefficient of determination for matrices with Industry cement (Series 2) is 0.76, which at best can be said to give values in the same order of magnitude as the measured values. Hence, none of the investigated models can predict the rheological behavior of the matrices in Series 2. Even the MLP model that provides quite good correlations to all matrices (Series 1 + 2) is not suited for prediction of Series 2 alone. This can be a result of either a material effect or sample size effect, as Series 2 has fewer matrices than Series 1 (38 and 69 matrices, respectively). These effects were investigated by performing the MLP analysis for an equal number of random selected samples from each series, see Fig. 3. The difference between the Standard FA and Industry cement matrices with equal number of samples indicate that the prediction accuracy of the dataset is affected by both sample size and material effects, but with a slight dominance of the latter.

When it comes to the material effect, the observed difference between matrices with Standard FA and Industry cement might be attributed to a different SP interaction with the cements. Justnes and Ng [69] showed that plasticizers interact more strongly with  $C_3A$  (aluminate) than other clinker phases. Bogue calculations [35] based on the oxide compositions in Appendix B, show that the Standard FA cement contains approximately 13.8 %  $C_3A$ , while Industry cement contains

approximately 8.7 %  $C_3A$ . This shows that the SP interacts more strongly with Standard FA cement than Industry cement. Another possible reason for the observed difference between the cement types is that the VSSA of Industry cement is higher than that of Standard FA cement. In [13], the two cement types were found to have the clearest effect in the relation rheology as function of VSSA, after silica fume, compared to the other dry materials. Maeyama et al. [43] showed that powders with high specific surface area are more prone to flocculation. Hence, a possible consequence of the high VSSA of Industry cement is higher degree of flocculation. Though SP was added in all mixes, not all mixes reached SP-saturation in terms of complete surface adsorption. This was discussed in [70], where it was shown that variations in yield stress clearly related to SP-dosage. Hence, we think that there are differences in dispersion due to this effect. A third reason, which is investigated in detail below, is that in contrast to the Standard FA matrices, most of the Industry matrices contain silica fume.

To investigate whether addition of silica fume affects the prediction accuracy, individual analyses of each subseries were done. The  $R^2$  values for the subseries 1a, 1b, 2a and 2b are listed in Table 6, where *a* indicates mixes without silica fume, and *b* mixes with silica fume. The relative viscosity models are all functions of  $\frac{\phi}{\phi_m}$ , and show approximately the same correlation to the estimated values as  $\frac{\phi}{\phi_m}$  alone, and are therefore not included in the table. The MLP analysis is not performed for each subseries due to too few matrices in each series. Instead, a total analysis for all matrices without silica fume, i.e. Series 1a and 2a, and all matrices with silica fume, i.e. Series 1b and 2b, is performed, and these results are listed to the right in Table 6.

Table 6 shows that  $\frac{\phi}{\phi_m}$  does not provide a good fit for any of the rheological parameters. Both liquid thickness models provide a better fit for the flow resistance ratio and plastic viscosity than the yield stress and mini slump flow, which is in line with [13], where it was found that the correlation between the  $VSSA_{matrix}$  and yield stress or mini slump flow is weaker than for  $VSSA_{matrix}$  and plastic viscosity or flow resistance ratio. However, the liquid thickness models break down when adding silica fume, which is attributed to its very high VSSA. The liquid thickness is inversely proportional to the  $VSSA_{matrix}$ , thus the matrices with silica fume obtain a significantly lower calculated liquid thickness than matrices without silica fume. The authors are aware that an assumed VSSA of silica fume of 60 000  $m^2/kg$  is higher than normally seen in literature, which is typically 13 000 – 30 000  $m^2/kg$  [71]. However, independent of which value that is chosen, the VSSA of silica fume would be an order of magnitude higher than the other dry materials, hence it is not believed that this assumption would affect the main results from this study.

Another possible reason that the models struggle to predict matrices with silica fume, is that the energy needed to disperse particles is decreasing when silica fume is introduced [72–73]. In addition, as silica fume particles are spherical, the “ball bearing effect” could also play a

**Table 5**  
Coefficients of determination,  $R^2$ , for predicted and measured values for Series 1 and 2.

Series	$R^2$		$\tau_0$		$\lambda_q$		Mini slump flow	
	$\mu$		1	2	1	2	1	2
	1	2						
LT <sub>1</sub>	0.02	0.17	0.50	0.40	0.01	0.27	0.29	0.40
LT <sub>2</sub>	0.35	0.42	0.53	0.31	0.33	0.53	0.43	0.44
$\Phi/\Phi_{max}$	0.68	0.57	0.06	0.05	0.74	0.61	0.14	0.22
K-D	0.71	0.54	–	–	–	–	–	–
Mooney	0.66	0.47	–	–	–	–	–	–
Eilers	0.68	0.53	–	–	–	–	–	–
Robinson	0.64	0.53	–	–	–	–	–	–
Chong	0.66	0.52	–	–	–	–	–	–
Quemada	0.66	0.52	–	–	–	–	–	–
MLP	0.91 ± 0.09	0.76 ± 0.21	0.91 ± 0.09	0.76 ± 0.18	0.94 ± 0.05	0.75 ± 0.18	0.90 ± 0.12	0.74 ± 0.20

K-D = Krieger and Dougherty

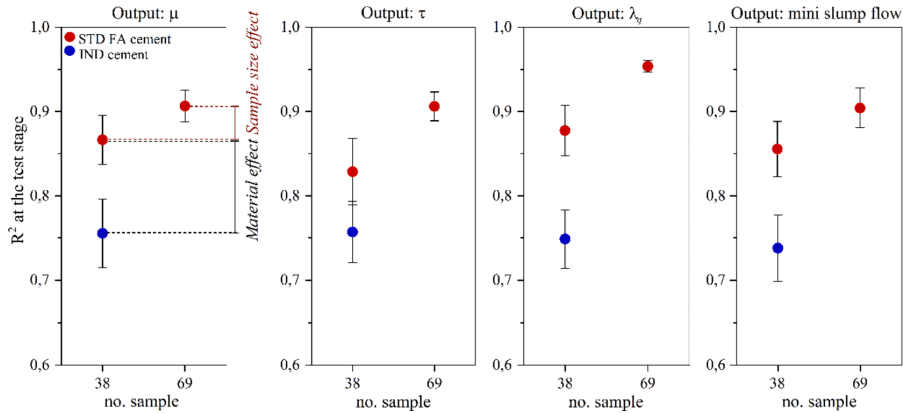


Fig. 3. A comparison between the Standard FA (Std FA) and Industry (IND) cement matrices to investigate the impact of sample size.

Table 6

Coefficient of determination for measured and estimated values for Series 1a 1b, 2a and 2b. (1a + 2a: Without silica fume, 1b + 2b: With silica fume).

	Series	No. of matrices	R <sup>2</sup>	LT <sub>1</sub>	LT <sub>2</sub>	Φ/Φ <sub>m</sub>	Series	No. of matrices	R <sup>2</sup> MLP
μ	1a	55	0.91	0.83	0.75	1a + 2a	73	0.89 ± 0.14	
	1b	14	0.04	0.01	0.30				
	2a	18	0.77	0.67	0.62				
	2b	20	0.01	0.02	0.15				
τ <sub>0</sub>	1a	55	0.52	0.38	0.32	1a + 2a	73	0.84 ± 0.15	
	1b	14	0.74	0.39	0.30				
	2a	18	0.08	0.09	0.06				
	2b	20	0.09	0.00	0.32				
λ <sub>q</sub>	1a	55	0.94	0.89	0.84	1a + 2a	73	0.92 ± 0.08	
	1b	14	0.06	0.01	0.34				
	2a	18	0.81	0.73	0.69				
	2b	20	0.04	0.01	0.06				
Mini slump flow	1a	55	0.59	0.44	0.36	1a + 2a	73	0.91 ± 0.10	
	1b	14	0.65	0.34	0.35				
	2a	18	0.46	0.33	0.27				
	2b	20	0.13	0.03	0.14				

role. These two effects can contribute to a less viscous matrix, which is not explicitly accounted for in any of the models.

The best correlation from Table 6 is seen between liquid thickness model 1 and the flow resistance ratio for Series 1a. The correlation is surprisingly good, particularly considered the varying SP-dosage in the series. Varying dispersion between the individual matrices is expected to affect the lubricating effect of the liquid around the particles, but apparently, the interpretation of the mode of action of the lubricating liquid layer is not straightforward and needs to be investigated more.

Overall, the MLP models provide the best predictions. However, they also start to struggle when adding silica fume (Series 1b and 2b). The best correlation for these matrices is found for the MLP model vs flow resistance ratio, yielding an R<sup>2</sup> = 0.79. The results in Table 6 also illustrate that the predictions of the MLP models do not diminish when including Industry cement. The reason why the MLP model could not accurately predict Series 2 (i.e. the matrices with Industry cement) in Table 5 was that more than 50% of the matrices also included silica fume. In this regard, it should be noted that a part of the decrease in model accuracy when adding silica fume, see Table 6, is attributed to the reduced sample size, similar as was seen in the analysis of the two cement types in Fig. 3. However, the advantage of the MLP model is that it is based on experience and can continuously be improved as the experimental dataset increases. In addition, it is a flexible model that can be fitted to many different datasets, meaning that it easily can be expanded to account for new materials. On the other hand, the

shortcoming of this model is that the physical aspects of the other models are lost. Also, as the model is tailor-made for a given dataset, the model will break down for matrices outside the considered dataset, unless the model gets updated. In general, the ANN prediction has three limitations. Firstly, the models cannot produce their own database, hence requiring an experimental or numerical database for training [41]. Secondly, ANNs can only predict values within the network training domain, demanding training data over the whole performance range of the system [41]. Lastly, the choice of initial parameters has a major impact on the training outcome [41].

### 5. Feature selection

Neighborhood Component Feature Selection (NCFS) was conducted to map the importance of the input variables for prediction with MLP. NCFS solves a multi-objective optimization problem to obtain the optimum weights that minimize the mean loss of the neighborhood component analysis (NCA) regression model, eqn. (5). The optimum weights provide information regarding the importance of the input variables [74].

$$\min_w \frac{1}{n} \sum_{p=1}^N L_p + \Gamma \sum_{i=1}^n w_i^2 \tag{5}$$

where *n* is the number of input variables, *N* is the number of data, *w<sub>i</sub>* is the weight of the NCA regression model for the *i*th input variable, *L<sub>p</sub>* is



the loss of the NCA regression model for the  $p$ th data, and  $\Gamma$  is a parameter determined by the user. Note that  $L_p$  is the expected value of the difference between the  $p$ th output data and the predicted output data for the  $p$ th input data using the NCA regression model. Fig. 4 shows the inputs rank according to their importance by NCFs, where the weight of non-relevant inputs is zero. However, it should be noted that the robustness of NCFs can be reduced by sampling uncertainty. Therefore, the importance of input variables varies depending on the sampled dataset.

Fig. 4 shows that the importance of the input parameters varies for

the four analyses, but common for all is the importance of water and superplasticizer. This is not surprising, as it is common knowledge within the field of concrete technology that water and superplasticizer affect rheology strongly. Also, these two parameters are the only ones that are included in all the presented mix designs. For the dry materials, on the other hand, no general trend is found for all output variables. This is probably partly because none of the dry materials are constituents in all mixes, and partly due to the fact that the input parameters are affected by each other, and their effect on the output parameters are dependent on their volumetric relations.

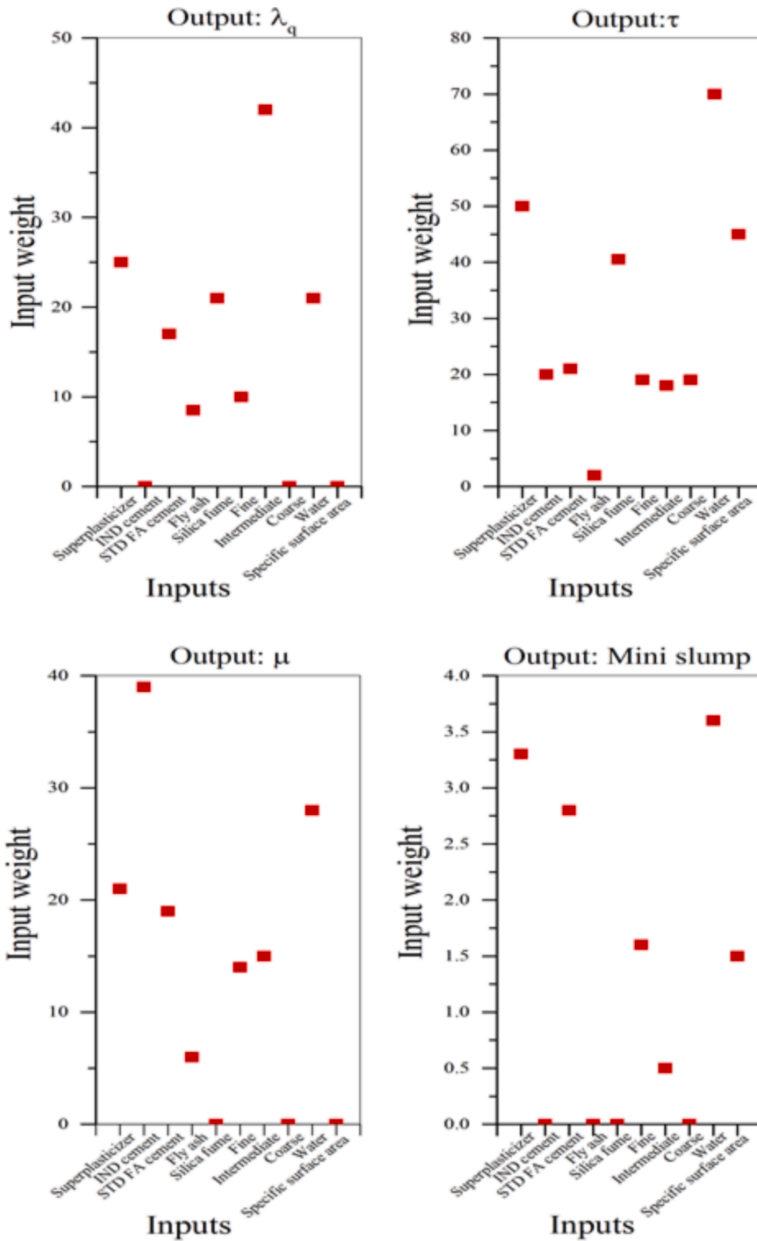


Fig. 4. Importance of the input variables for the prediction of the four rheology parameters with MLP. Input weight =  $w_i$  in eqn. (5).

## 6. Conclusion

In this study, the ability of ten different models to predict rheology of cement pastes with manufactured sand and silica fume was investigated. The investigated models were two different liquid thickness models, the relative concentration of solids, six different viscosity models by Krieger and Dougherty, Mooney, Eilers, Robinson, Chong and Quemada, and lastly an MLP model. The predicted parameters were compared with the Bingham yield stress and plastic viscosity, the flow resistance ratio and the mini slump flow, obtained by laboratory testing. The MLP model was clearly better than the other models in predicting the behavior of all matrices, with a coefficient of determination of  $R^2 = 0.84 - 0.91$  for the four investigated rheological parameters. The nine suspension models provided at best an  $R^2 = 0.60$  for all matrices. When considering each cement type individually, the correlations improved for matrices with Standard FA cement, as opposed to matrices with Industry cement, with the exception of predictions from the liquid thickness models and the correlation between the relative concentration of solids and mini slump flow. Although the MLP model provided high prediction accuracy for all mixes, it only obtained an  $R^2 = 0.76$  for mixes with Industry cement, which is partly due to smaller sample size and partly due to material effect. The material effect could either come from that Standard FA cement interacts more strongly with SP than Industry cement, or that Industry cement has higher VSSA than Standard FA cement. Lastly, it could be because a majority of the Industry cement matrices contain silica fume, which was found to weaken the prediction accuracy. A highlight for liquid thickness model 1 was its ability to predict the flow resistance ratio of the matrices without Industry cement and silica fume with  $R^2 = 0.94$ . Like for many of the other models, the accuracy of this model especially diminished when adding silica fume, which was speculated to be attributed to three effects; 1) the very high VSSA of silica fume; 2) the decrease in energy that is needed to disperse particles when adding silica fume; and 3) the ball bearing effect of the round silica fume particles. Nevertheless, overall, the MLP model outperformed all the suspensions models for the matrices investigated in this study, which indicates that artificial neural network predictions are a promising avenue to follow when it comes to cement paste rheology.

### CRedit authorship contribution statement

**Elisabeth Leite Skare:** Formal analysis, Investigation, Visualization, Writing – original draft, Visualization. **Shohreh Sheiati:** Software, Methodology, Visualization, Writing – review & editing, Writing – original draft. **Rolands Cepuritis:** Resources. **Ernst Mørtzell:** Resources, Supervision. **Sverre Smepllass:** Supervision. **Jon Spangenberg:** Conceptualization, Supervision, Writing – review & editing. **Stefan Jacobsen:** Project administration, Conceptualization, Supervision, Resources, Writing – review & editing.

### Declaration of Competing Interest

The authors declare that they have no known competing financial interests or personal relationships that could have appeared to influence the work reported in this paper.

### Acknowledgement

This paper is based on work performed within the MiKS project (Micro-proportioning with Crushed Sand), which is a Competence Project for the Industry funded by the Research Council of Norway (contract no. 247619) and the industrial partners Norcem AS, Skanska Norge AS and Feiring Bruk AS. The authors would like to thank Harald Justnes, Serina Ng, Tone Østnor, Ove Loraas and Steinar Seehuus for helpful discussions and guidance in the laboratory. We would also thank former Ph.D.-student Evgeny Ramenskiy for performing some of the rheological testing, as well as Laboratory Engineer Tone H. Nilsen and

the master students Metathip Sihaklang and David Nicolas for performing centrifuge packing measurement, extracting excess fluid and measuring dynamic viscosity on all mixes.

## References

- [1] R. Cepuritis, Development of Crushed Sand for Concrete Production with Micro-proportioning, Norwegian University of Science and Technology, Ph.D.-thesis, 2016.
- [2] R. Cepuritis, S. Jacobsen, T. Onnela, Sand production with VSI crushing and air classification: Optimising fines grading for concrete production with microproportioning, ISSN 0892-6875, Miner Eng 78 (1–14) (2015), <https://doi.org/10.1016/j.mineng.2015.03.025>.
- [3] D.P. Bentz, C.F. Ferraris, M.A. Galler, A.S. Hansen, J.M. Guynn, Influence of particle size distributions on yield stress and viscosity of cement-fly ash pastes, Cem. Concr. Res. 42 (2) (2012) 404–409, <https://doi.org/10.1016/j.cemconres.2011.11.006>.
- [4] H.W. Reinhardt, T. Wüstholtz, About the influence of the content and composition of the aggregates on the rheological behaviour of self-compacting concrete, Mater. Struct. 39 (7) (2006) 683–693, <https://doi.org/10.1617/s11527-006-9102-3>.
- [5] M. Westerholm, B. Lagerblad, E. Forsberg, Rheological properties of micromortars containing fines from manufactured aggregates, Mater. Struct. 40 (6) (2007) 615–625, <https://doi.org/10.1617/s11527-006-9173-1>.
- [6] N. Roussel, J. Spangenberg, J. Wallevik, R. Wolfs, Numerical simulations of concrete processing: From standard formative casting to additive manufacturing, Cem. Concr. Res. 135 (2020) 106075, <https://doi.org/10.1016/j.cemconres.2020.106075>.
- [7] J.G. Sanjayan, R. Jayathilakage, P. Rajeev, Vibration induced active rheology control for 3D concrete printing, Cem. Concr. Res. 140 (2021) 106293, <https://doi.org/10.1016/j.cemconres.2020.106293>.
- [8] Jones SZ, Bentz DP, Martys NS, George WL, Thomas A (2019) Rheological Control of 3D Printable Cement Paste and Mortars. Wangler T., Flatt R. (eds) First RILEM International Conference on Concrete and Digital Fabrication – Digital Concrete 2018. RILEM Bookseries, vol 19. Springer, Cham. [https://doi.org/10.1007/978-3-319-99519-9\\_7](https://doi.org/10.1007/978-3-319-99519-9_7).
- [9] K.H. Khayat, W. Meng, K. Vallurupalli, L.e. Teng, Rheological properties of ultra-high-performance concrete — An overview, Cem. Concr. Res. 124 (2019) 105828, <https://doi.org/10.1016/j.cemconres.2019.105828>.
- [10] C.F. Ferraris, K.H. Obla, R. Hill, The influence of mineral admixtures on the rheology of cement paste and concrete, Cem. Concr. Res. 31 (2) (2001) 245–255.
- [11] E. Mørtzell, Modellering av delmaterialenes betydning for betongens konsistens, Norwegian University of Science and Technology, Ph.D.-thesis, 1996.
- [12] R. Cepuritis, S. Jacobsen, S. Smepllass, E. Mørtzell, B.J. Wigum, S. Ng, Influence of crushed aggregate fines with micro-proportioned particle size distributions on rheology of cement paste, ISSN 0958-9465, Cem. Concr. Compos. 80 (64–79) (2017), <https://doi.org/10.1016/j.cemconcomp.2017.02.012>.
- [13] E.L. Skare, R. Cepuritis, J. Spangenberg, E. Ramenskiy, E. Mørtzell, S. Smepllass, S. Jacobsen, Microproportioning paste with crushed aggregate filler by use of specific surface area. 15<sup>th</sup> Int. Congress Chem. Cem. (2019).
- [14] I.M. Krieger, T.J. Dougherty, A Mechanism for Non-Newtonian Flow in Suspensions of Rigid Spheres, Trans. Soc. Rheol. III (1959) 137–152, <https://doi.org/10.1122/1.548848>.
- [15] M. Mooney, The viscosity of a concentrated suspension of spherical particles, J. Colloid Interface Sci. 6 (2) (1951) 162–170, [https://doi.org/10.1016/0095-8522\(51\)90036-0](https://doi.org/10.1016/0095-8522(51)90036-0).
- [16] H. Eilers, Die Viskosität von Emulsionen hochviskoser Stoffe als Funktion der Konzentration, Kolloid Z 97 (3) (1941) 313–321, <https://doi.org/10.1007/BF01503023>.
- [17] J.V. Robinson, The viscosity of suspensions of spheres, J. Phys. Chem. 53 (7) (1949) 1042–1056, <https://doi.org/10.1021/j150472a007>.
- [18] J.S. Chong, E.B. Christiansen, A.D. Baer, Rheology of Concentrated Suspensions, J. Appl. Polym. Sci. 15 (1971) 2007–2021, <https://doi.org/10.1002/app.1971.070150818>.
- [19] D. Quemada, Rheology of concentrated disperse systems and minimum energy dissipation principle, Rheol. Acta 16 (1) (1977) 82–94, <https://doi.org/10.1007/BF01516932>.
- [20] T.C. Powers, The properties of fresh concrete, Wiley & Sons, New York, 1968.
- [21] Y. Ghasemi, Aggregates in Concrete Mix Design, Lulea University of Technology, 2017. Licentiate Thesis.
- [22] A.K.H. Kwan, W.W.S. Fung, H.H.C. Wong, Water film thickness, flowability and rheology of cement-sand mortar, Adv. Cem. Res. 22 (1) (2010) 3–14, <https://doi.org/10.1680/adcr.2008.22.1.3>.
- [23] T. Midorikawa, G.I. Pelova, J.C. Walraven, Application of “the water layer model” to self-compacting mortar with different size distribution of fine aggregate, 2<sup>nd</sup> Int Symp Self-Compact Concr. 237–246 (2001), ISBN 4-901514-04-0.
- [24] J.H. Lee, J.H. Kim, J.Y. Yoon, Prediction of the yield stress of concrete considering the thickness of excess paste layer, Constr. Build. Mater. 173 (2018) 411–418.
- [25] W.Q. Zuo, J.P. Liu, Q. Tian, W. Xu, W. She, P. Feng, C.W. Miao, Optimum design of low-binder self-compacting concrete based on particle packing theories, ISSN 0950-0618, Constr. Build. Mater. 163 (938–948) (2018), <https://doi.org/10.1016/j.conbuildmat.2017.12.167>.
- [26] C. Ferraris, F. de Larrard, Testing and modelling of fresh concrete rheology, 9780266909552, Natl. Inst. Stand. Technol. 6094 (ISBN13) (1998), <https://doi.org/10.6028/NIST.IR.6094>.

- [27] B. Choi II, J.H. Kim, T.Y. Shin, Rheological model selection and a general model for evaluating the viscosity and microstructure of a highly-concentrated cement suspension, ISSN 0008-8846, Cem. Concr. Res. 123 (105775) (2019), <https://doi.org/10.1016/j.cemconres.2019.05.020>.
- [28] R.J. Flatt, P. Bowen, Yodel: a yield stress model for suspensions, J. Am. Ceram. Soc. 89 (4) (2006) 1244-1256, <https://doi.org/10.1111/j.1551-2916.2005.00888.x>.
- [29] D. Loewke, P. Schiessl, Robustness of cement suspensions – superplasticizer adsorption, particle separation and interparticle forces. 3rd Int. RILEM Symp. Rheol. Cem. Suspens. Fresh Concr. 45-54 (2009). ISBN: 978-2-35158-091-2.
- [30] R. Buscall, L.J. McGowan, P.D.A. Mills, R.F. Stewart, D. Sutton, L.R. White, G. E. Yates, The rheology of strongly-flocculated suspensions, ISSN 0377-0257, J. Non-Newton Fluid Mech. 24 (183-202) (1987), [https://doi.org/10.1016/0377-0257\(87\)85009-7](https://doi.org/10.1016/0377-0257(87)85009-7).
- [31] P.C. Kapur, P.J. Scales, D.V. Boger, T.W. Healy, Yield stress of suspensions loaded with size distributed particles, AIChE J. 43 (5) (1997) 1171-1179, <https://doi.org/10.1002/aic.690430506>.
- [32] P.J. Scales, S.B. Johnson, T.W. Healy, P.C. Kapur, Shear yield stress of partially flocculated colloidal suspensions, AIChE J. 44 (3) (1998) 538-544, <https://doi.org/10.1002/aic.690440305>.
- [33] Z. Zhou, M.J. Solomon, P.J. Scales, D.V. Boger, The yield stress of concentrated flocculated suspensions of size distributed particles, J. Rheol. 43 (3) (1999) 651-671, <https://doi.org/10.1122/1.551029>.
- [34] B.L. Damineli, V.N. John, B. Lagerblad, R.G. Pileggi, Viscosity prediction of cement-filler suspensions using inference model: A route for binder efficiency enhancement, ISSN 0008-8846, Cem. Concr. Res. 84 (8-19) (2016), <https://doi.org/10.1016/j.cemconres.2016.02.012>.
- [35] S. Jacobsen, M. Maage, S. Smeplass, K.O. Kjellsen, E.J. Sellevold, J. Lindgård, R. Cepuritis, R. Myrdaal, Ø. Bjøntegaard, M. Geiker, et al., TKT 4215 Concrete Technology 1, Norwegian University of Science and Technology, Compendium, 2016.
- [36] A. Ahmadi Nadooshan, M. Hemmat Esfe, M. Afrand, Prediction of rheological behavior of SiO<sub>2</sub>-MWCNTs/10W40 hybrid nanolubricant by designing neural network, J. Therm. Anal. Calorim. 131 (3) (2018) 2741-2748, <https://doi.org/10.1007/s10973-017-6688-3>.
- [37] Z. Tariq, M. Murtaza, M. Mahmoud, Development of New Rheological Models for Class G Cement with Nanoclay as an Additive Using Machine Learning Techniques, ACS Omega 5 (28) (2020) 17646-17657, <https://doi.org/10.1021/acsomega.0c02122>.
- [38] M. Hemmat Esfe, S. Saedodin, N. Sina, M. Afrand, S. Rostami, Designing an artificial neural network to predict thermal conductivity and dynamic viscosity of ferromagnetic nanofluid, Int. Commun. Heat Mass Transfer 68 (2015) 50-57.
- [39] M. Afrand, K. Nazari Najafabadi, N. Sina, M.R. Safaei, A.S. Kherbeet, S. Wongwiset, M. Dahari, Prediction of dynamic viscosity of a hybrid nano-lubricant by an optimal artificial neural network, Int. Commun. Heat Mass Transfer 76 (2016) 209-214.
- [40] H. Karimi, F. Yousefi, M.R. Rahimi, Correlation of viscosity in nanofluids using genetic algorithm-neural network (GA-NN), Heat Mass Transfer 47 (11) (2011) 1417-1425, <https://doi.org/10.1007/s00231-011-0802-z>.
- [41] S. Sheiati, N. Ranjbar, J. Frellsen, E.L. Skare, R. Cepuritis, S. Jacobsen, J. Spangenberg, Neural network predictions of the simulated rheological response of cement paste in the FlowCyl, Neural Comput. & Applic. 33 (19) (2021) 13027-13037, <https://doi.org/10.1007/s00521-021-05999-4>.
- [42] M.L.E. Roberto, F.J. Tanleque-Alberto, M.V. Fas, M. Oroian, Physicochemical and rheological characterization of honey from Mozambique, LWT - Food Sci. Tech. 86 (2017) 108-115, <https://doi.org/10.1016/j.lwt.2017.07.053>.
- [43] A. Maeyama, K. Maruyama, T. Midorikawa, N. Sakata, Characterization of powder for self-compacting concrete, Int. Workshop Self-Compact Concr. 191-200 (1998).
- [44] P.Y. Sosa, Particle Size Distribution and Specific Surface Area Measurements with X-ray SediGraph on Filler, Cement and Fly Ash, Norwegian University of Science and Technology, 2017. Master's thesis.
- [45] S. Jacobsen, B. Arntsen, Aggregate packing and -void saturation in mortar and concrete proportioning, Mater. Struct. 41 (4) (2008) 703-716, <https://doi.org/10.1617/s11527-007-9275-4>.
- [46] J. Spangenberg, G.W. Scherer, A.B. Hopkins, S. Torquato, Viscosity of bimodal suspensions with hard spherical particles, J. Appl. Phys. 116 (18) (2014) 184902, <https://doi.org/10.1063/1.4901463>.
- [47] J. Zhu, X. Shu, J. Tang, T. Li, Q. Ran, J. Liu, Effect of microfines from manufactured sand on yield stress of cement paste, Constr. Build. Mater. 267 (2021) 120987, <https://doi.org/10.1016/j.conbuildmat.2020.120987>.
- [48] X. Chateau, G. Ovarlez, K.L. Trung, Homogenization approach to the behavior of suspensions of noncolloidal particles in yield stress fluids, J. Rheol. 52 (2) (2008) 489-506, <https://doi.org/10.1122/1.2838254>.
- [49] H. Justnes, H. Vikan, Viscosity of Cement Slurries as a Function of Solids Content, Annu. Trans. Nordic. Rheol. Soc. 13 (2005) 75-82.
- [50] W.B. Russel, P.R. Sperry, Effect of microstructure on the viscosity of hard sphere dispersions and modulus composites, Prog. Org. Coat. 23 (1994) 305-325, [https://doi.org/10.1016/0033-0655\(94\)87001-2](https://doi.org/10.1016/0033-0655(94)87001-2).
- [51] L. Struble, G.K. Sun, Viscosity of Portland cement paste as a function of concentration, Adv. Cem. Based Mat. 2 (2) (1995) 62-69, [https://doi.org/10.1016/1065-7355\(95\)90026-8](https://doi.org/10.1016/1065-7355(95)90026-8).
- [52] M.A. DeRousseau, J.R. Kasprzyk, W.V. Srubar, Computational design optimization of concrete mixtures: A review, Cem. Concr. Res. 109 (2018) 42-53.
- [53] Z. Car S.B. Segota N. Andelić I. Lorenčin V. Mrzljak (2020) Modeling the Spread of COVID-19 Infection Using a Multilayer Perceptron- Comput. Math. Methods Med. 10 pages Article ID 5714714 2020 10.1155/2020/5714714.
- [54] S. Miller, K. Curran, T. Lunney, Multilayer Perceptron Neural Network for Detection of Encrypted VPN Network Traffic, 11.06.18-12.06.18, in: 2018 International Conference On Cyber Situational Awareness, Data Analytics And Assessment (Cyber SA), 2018, <https://doi.org/10.1109/CyberSA.2018.8551395>.
- [55] S. Savalia, E. Vahid, Cardiac Arrhythmia Classification by Multi-Layer Perceptron and Convolution Neural Networks, Bioengineering 5 (2):35 (2018) 12 pages, <https://doi.org/10.3390/bioengineering5020035>.
- [56] M. Ajjj, S. Pratihari, S.R. Nayak, T. Hanne, D.S. Roy, Off-line signature verification using elementary combinations of directional codes from boundary pixels, Neural Comput. & Applic. (2021), <https://doi.org/10.1007/s00521-021-05854-6>.
- [57] David Tian, Jiamel Deng, Gopika Vinod, T.V. Santhosh, Hissam Tawfik, A constraint-based genetic algorithm for optimizing neural network architectures for detection of loss of coolant accidents of nuclear power plants, Neurocomputing 322 (2018) 102-119.
- [58] Rong Cai, Taihao Han, Wenyu Liao, Jie Huang, Dawang Li, Aditya Kumar, Hongyan Ma, Prediction of surface chloride concentration of marine concrete using ensemble machine learning, Cem. Concr. Res. 136 (2020) 106164, <https://doi.org/10.1016/j.cemconres.2020.106164>.
- [59] Great Wall Mineral, From the GWM Selection, <http://greatwallmineral.com/index.asp?Id=3>. Accessed 05.04.19.
- [60] S. Ng, H. Mujica, S. Smeplass, Design of a simple and cost-efficient mixer for matrix rheology testing, Nordic Concr. Res. 51 (3) (2014) 15-28.
- [61] R. Cepuritis, S. Jacobsen, B. Pedersen, H.V. Vikan, K. De Weerd, Rheology of matrix and SCC with different mineral fillers and admixtures. COIN Project report 41, 2012.
- [62] M. Sihaklang, Micro-proportioning modelling with measurements of maximum particle packing in filler modified cement paste and viscosity of paste fluid, Norwegian University of Science and Technology, 2019. Master's thesis.
- [63] S. Ng, Kinematic viscosity of filler pore solution with and without superplasticizers, Memo, SINTEF, Norway, 2016.
- [64] M. Stieger, The Rheology Handbook: for Users of Rotational and Oscillatory Rheometers, Vincentz Network, Hannover. 12 (5) (2002) 232, <https://doi.org/10.1515/arh-2002-0029>.
- [65] J. Spangenberg, W.R.L. da Silva, R. Comminal, M.T. Mollah, T.J. Andersen, H. Stang, Numerical simulation of multi-layer 3D concrete printing, RILEM Tech. Letters 6 (2021) 119-123.
- [66] Raphael Comminal, Wilson Ricardo Leal da Silva, Thomas Juul Andersen, Henrik Stang, Jon Spangenberg, Modelling of 3D concrete printing based on computational fluid dynamics, Cem. Concr. Res. 138 (2020) 106256, <https://doi.org/10.1016/j.cemconres.2020.106256>.
- [67] R. Comminal, W.R.L. da Silva, T.J. Andersen, H. Stang, J. Spangenberg, Influence of processing parameters on the layer geometry in 3D concrete printing: experiments and modelling, RILEM int. Conf. Concr. Digital Fabr. 852-862 (2020).
- [68] D. Nicolas Engineer Assistant Internship Report, IMT Mines Alès 2018.
- [69] ASTM, D2515-66 Standard Specification for Kinematic Glass Viscometers 33 (1966) p.
- [70] R. Cepuritis, E.L. Skare, E. Ramenskij, E. Mortsell, S. Smeplass, S. Li, S. Jacobsen, J. Spangenberg, Analysing limitations of the FlowCyl as a one-point viscometer test for cement paste, ISSN 0950-0618, Constr. Build. Mat. 218 (333-340) (2019), <https://doi.org/10.1016/j.conbuildmat.2019.05.127>.
- [71] Daman K. Panesar, Chapter 3: Supplementary cementing materials in Developments in the Formulation and Reinforcement of Concrete (Second Edition), in: Developments in the Formulation and Reinforcement of Concrete, Elsevier, 2019, pp. 55-85, <https://doi.org/10.1016/B978-0-08-102616-8.00003-4>.
- [72] Billberg P (2006) Form Pressure Generated by Self-Compacting Concrete — Influence of Thixotropy and Structural Behaviour at Rest. Ph.D.-thesis, Kungliga Tekniska Högskolan. ISSN 1103-4270.
- [73] R.J. Pugh, L. Bergström, Surface and Colloid Chemistry in Advanced Ceramics Processing, 1st ed., CRC Press, 1994.
- [74] H. Kim, T.H. Lee, T. Kwon, Normalized neighborhood component feature selection and feasible-improved weight allocation for input variable selection, ISSN 0950-7051, Knowl.-Based Syst. 218 (106855) (2021), <https://doi.org/10.1016/j.knsys.2021.106855>.

## Paper IV

**FlowCyl: one-parameter cement paste rheology test developed at NTNU, Norway**  
Cepuritis R, Skare EL, Jacobsen S, Spangenberg J, Smeplass S, Mørtzell E.  
*Rhéologie* 35 (2019) pp. 20-24.

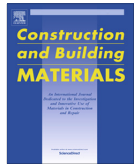
This paper is not included in NTNU Open due to copyright



# Paper V

**Analysing limitations of the FlowCyl as a one-point viscometer test for cement paste**  
Cepuritis R, Skare EL, Ramenskiy E, Mørtzell E, Smeplass S, Li S, Jacobsen S, Spangenberg J.  
*Construction and Building Materials* 218 (2019) pp. 333-340.





## Analysing limitations of the FlowCyl as a one-point viscometer test for cement paste



Rolands Cepuritis<sup>a,b,\*</sup>, Elisabeth L. Skare<sup>a,c</sup>, Evgeny Ramenskiy<sup>a,c</sup>, Ernst Mørtzell<sup>a,e</sup>, Sverre Smepllass<sup>a,d</sup>, Shizhao Li<sup>c</sup>, Stefan Jacobsen<sup>a</sup>, Jon Spangenberg<sup>c</sup>

<sup>a</sup> Department of Structural Engineering, Norwegian University of Science and Technology, NO-7491 Trondheim, Norway

<sup>b</sup> Norcem AS (HeidelbergCementGroup), R&D Department, Setreveien 2, Postboks 38, NO-3950 Brevik, Norway

<sup>c</sup> Department of Mechanical Engineering, Technical University of Denmark, 2800 Lyngby, Denmark

<sup>d</sup> Skanska Norge AS, Drammensveien 60, PO Box 1175, NO-0107 Oslo, Norway

<sup>e</sup> NorBetong AS (HeidelbergCementGroup), Heggstadmyra 6, NO-7080 Heimdal, Norway

### HIGHLIGHTS

- The average difference between experimental and numerical flow resistance ratio is 6.5% and 4.6%.
- All measurements collapse on the same curve in the flow resistance ratio vs. plastic viscosity plot.
- Flow resistance ratio can characterize cement pastes if the superplasticiser dosage is constant.

### ARTICLE INFO

#### Article history:

Received 14 September 2018

Received in revised form 15 May 2019

Accepted 18 May 2019

Available online 25 May 2019

#### Keywords:

Rheology  
Cement paste  
FlowCyl  
Yield stress  
Plastic viscosity

### ABSTRACT

The FlowCyl is a simple flow viscometer – a modification of the Marsh Cone test apparatus – developed to quantify the flow behaviour of cement pastes. The FlowCyl gives a one-parameter characterisation of rheology called the flow resistance ratio or  $\lambda_Q$ , which is defined as the average ratio between the flow loss of a measured fluid and theoretical flow of an ideal fluid. This paper reports a study on the limitations of the FlowCyl and apparent flow resistance ratio. The investigation includes rheological measurements of cement pastes incorporating crushed aggregate fines with a diameter below 125  $\mu\text{m}$  and development of a numerical model in order to analyse the flow condition inside the FlowCyl. The numerical simulations are carried out both with the Bingham- and Herschel-Bulkley material model of the rheometer data. A comparison with the experimental  $\lambda_Q$  results illustrates that only a minor error is introduced when describing the flow of cement paste in the FlowCyl with a two-parameter model (Bingham material model) as compared to a three-parameter model (Herschel-Bulkley model). The results also show that the one-parameter characterisation (*i.e.*  $\lambda_Q$ ) mainly correlates to the plastic viscosity in the Bingham material model, while the yield stress only correlates if the dosage of superplasticizer per mass of cement is kept constant. The numerical simulations show that high shear rates at the outlet of the FlowCyl are responsible for the difference in the correlations.

© 2019 Elsevier Ltd. All rights reserved.

### 1. Introduction

As pointed out by Ferraris et al. [1], determining rheology properties by testing concrete is not always practical, easy, and economical, because execution of numerous concrete tests requires a large amount of material and manpower. Therefore, there is a need for simpler and easier laboratory approaches. It has been demonstrated that rheological measurements of cement paste can be used as a reasonable indicator of concrete rheology [1–3].

Fresh cement paste is a fluid that, just like concrete, exhibits a yield stress, requiring a minimum stress to initiate flow. Below the yield stress, cement paste behaves like a solid, which typically is a result of a three-dimensional microstructure at low stresses [4]. Above the yield stress, cement paste on the contrary deforms as a fluid according to a viscosity function that is shear rate dependent. The rheological behaviour of cement paste can be quantified by the usage of a rheometer, for example, with a parallel plate, cone and plate, coaxial cylinder, or Couette geometry [5]. The shear stress (or viscosity) as a function of shear rate and a best-fit match to the data determines the appropriate constitute law, *e.g.* the Bingham- or Herschel-Bulkley (H-B) material model [5].

\* Corresponding author.

E-mail address: [rolands.cepuritis@ntnu.no](mailto:rolands.cepuritis@ntnu.no) (R. Cepuritis).



As pointed out by Shaughnessy and Clark [6], measuring the rheological properties of cement paste is not a straightforward task, and substantial care must be taken prior, during and after the measurements. The most common measurement techniques, procedures and challenges were recently thoroughly reviewed by some of the authors of this paper. The review can be found in the following reference [7]. Although highly accurate rheometers are available, simple empirical test methods for rheological examination of cement paste are also quite popular, for both research and industrial purposes. This is due to relatively complex procedures of performing measurements with the rheometers, but even more importantly due to their cost. One of the most popular of the applied empirical methods include a range of mini slump-cone geometries that mainly provide the single empirical parameter, slump flow (spread diameter of the mixture), which relates to the yield stress of the cement paste [1,8]. Another set of tests are the orifice viscometers, where the fresh cement paste flows out of different funnel-shaped containers through a narrow orifice. The mass flux or flow time is registered as the test result. Some of the most popular orifice viscometers are the Marsh cone [9,10], mini V-funnel [1], and FlowCyl [2,3,11].

The FlowCyl test characterizes the rheological behaviour of cement pastes via one parameter, the flow resistance ratio (denoted  $\lambda_Q$ ), which is described in more detail later in the paper. This test method has been successfully used to predict the workability of conventional (vibrated) normal-weight concrete mixes with consistencies of up to about 240 mm of slump, which was based on natural sand and cement paste with relatively low fines content [2]. Later, the same was shown to be possible for lightweight aggregate concrete that was based on natural sand and coarse lightweight aggregates [3]. However, in a series of further studies [11–13] it was demonstrated that the FlowCyl test result has limitations when applied to self-compacting concrete (SCC) mixes and mixes incorporating high amounts of crushed sand fines when the amount of superplasticiser was below the assumed saturation level. In the study, by Mørtzell and Smeplass [11] the hypothesis was that the proportioning model where the FlowCyl is used to characterise the viscous phase of the concrete (filler modified cement paste = matrix) would work even better with the matrix-dominated SCC mixes. Then the workability of the SCC mixes tested would be a unique function of the flow resistance ratio of the matrix determined with the FlowCyl and the volume of the matrix according to the Particle-Matrix concrete proportioning model [2]. However, the results revealed that to achieve a slump-flow measurement of approx. 650 mm, the necessary matrix volume was 40–80 l/m<sup>3</sup> lower for the mixes based on the high-strength ordinary Portland cement (OPC) than for the regular OPC mixes, when all other parameters (including  $\lambda_Q$  values) were comparable. In other words, the researchers did not find a simple correlation between the flow resistance ratio of the matrix and the workability of the SCC. Smeplass and Mørtzell [11] suggested that the problem potentially was in the measuring device used for the characterisation of the matrix, i.e. the FlowCyl. They theorized that the problem with the FlowCyl was that it gives only a single value, whereas the matrix is at least a two-parameter fluid and thus there is a need to get a more fundamental understanding of the limitations of this equipment.

In this paper, the objective is for the first time to analyse the limitations of the flow resistance ratio when used as a one-point parameter to describe the flow behaviour of fresh filler modified cement paste. Hereto, FlowCyl and rheometer measurements of filler modified cement pastes that cover a broad interval of flowabilities are performed and correlated. In addition, a numerical model is employed to simulate the FlowCyl tests and thereby assist in understanding/estimating the error that is introduced by going

from a three-parameter (H-B material model:  $\tau = \tau_0 + K\dot{\gamma}^n$ , where  $\tau_0$  is H-B yield stress [Pa],  $K$  is consistency factor [Pa s<sup>n</sup>] and  $n$  is flow index [-]) to a two-parameter (Bingham material model:  $\tau = \tau_0 + \mu\dot{\gamma}$ , where  $\tau_0$  is Bingham's yield stress [Pa],  $\mu$  is Bingham's plastic viscosity [Pa s], while  $\tau$  and  $\dot{\gamma}$  are the corresponding yield stress [Pa] and shear rate [1/s]) to a one-parameter (flow resistance ratio) flow characterization of cement pastes.

## 2. Experiments

### 2.1. Materials

Three different types of crushed aggregate fines were included in the cement pastes in order to obtain cement pastes with different rheological behaviour. All of the crushed fines originated from the same granitic rock type (typical mineralogical composition of the parent rock: feldspar 48%, quartz 48%, amphibolite 2%, mica 1%, chlorite 1%) and were produced in the same way. The production process included four steps of rock crushing followed by a system of air-classification that was utilised to extract the generated fines from the crushed aggregates. The three types of crushed fines were extracted at different steps in the air-classification process and thus the main difference between them was their PSD. The different types of fines were denoted as (F)-PSD, (C)-PSD and (I)-PSD. The maximum particle size for all three types of fines was adjusted to be the same by mechanical sieving via a sieve with square opening of 125  $\mu\text{m}$  edge length. The PSD of the fines, see Fig. 1, was determined by a SediGraph, which is a PSD measurement tool that measures the particle sedimentation speed through x-ray absorption and calculates the equivalent particle diameter based on Stoke's law [14]. The oven-dry particle density for all of the crushed fines was determined with a helium pycnometer to be the same, i.e. 2.65 g/cm<sup>3</sup>.

Blended cement with a particle density of 3.0 g/cm<sup>3</sup> incorporating 18.1% of fly-ash and 5% of gypsum (CEM II/B-M 42.5 R) from Norcem AS was used in all the cementitious mixes. The mineralogical composition of the clinker of the cement was C<sub>3</sub>S: 61.0%; C<sub>2</sub>S: 14.2%; C<sub>3</sub>A: 8.8%; C<sub>4</sub>AF: 9.3%; free CaO: 1.7%; other minerals: 5.0%. The Na<sub>2</sub>O-eq. content of the cement was 1.3%. The Blaine value was determined to be 422 m<sup>2</sup>/kg and the PSD of the cement determined with the SediGraph is shown in Fig. 1. Polycarboxylate ether (PCE) based superplasticiser (SP) Dynamon SR-N (solids content of 19.5%; liquid density of 1.05 g/cm<sup>3</sup>) from Mapei was used.

### 2.2. Cement paste compositions

An overview of the studied filler modified cement paste compositions is given in Table 1. The mixes were divided into "A"-series and "B"-series. The "A"-series represents mixes where three different w/c ratios (0.4, 0.55 and 0.70) were combined with the three different types of crushed fines. In addition, for every w/c ratio, three different f/c ratios were employed. The w/c and f/c ratios were chosen with the goal of covering the range that is practically used in ready-mix concrete production with crushed sand in Norway. For the "A"-series mixes the dosage of SP was fixed at 0.75% of the total cement mass. In the "B"-series, the SP dosage was varied for the

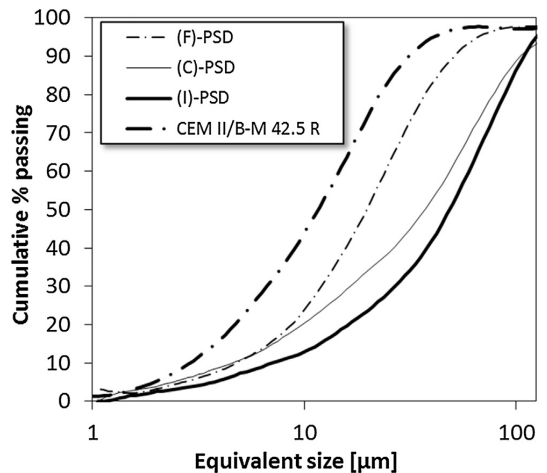


Fig. 1. PSDs of the crushed aggregate fines and cement used for the experiments.

**Table 1**  
Overview of the studied filled modified cement paste compositions.

Mix No.	w/c	SP [%]	fi/c	PSD	Solid volume fraction $\Phi_s$	Mix No.	w/c	SP [%]	fi/c	PSD	Solid volume fraction $\Phi_s$
A-1	0.4	0.75	0.28	(C)	0.516	B-1	0.40	1.00	0.28	(I)	0.516
A-2	0.4	0.75	0.36	(C)	0.531	B-2	0.40	1.00	0.36	(I)	0.531
A-3	0.4	0.75	0.44	(C)	0.545	B-3	0.40	1.00	0.44	(I)	0.545
A-4	0.55	0.75	0.51	(C)	0.477	B-4	0.40	1.25	0.28	(I)	0.515
A-5	0.55	0.75	0.59	(C)	0.490	B-5	0.40	1.25	0.36	(I)	0.530
A-6	0.55	0.75	0.67	(C)	0.502	B-6	0.40	1.25	0.44	(I)	0.545
A-7	0.7	0.75	0.68	(C)	0.444	B-7	0.40	1.50	0.28	(I)	0.515
A-8	0.7	0.75	0.76	(C)	0.456	B-8	0.40	1.50	0.36	(I)	0.530
A-9	0.7	0.75	0.82	(C)	0.464	B-9	0.40	1.50	0.44	(I)	0.544
A-10	0.4	0.75	0.28	(I)	0.516	B-10	0.40	1.75	0.28	(I)	0.515
A-11	0.4	0.75	0.36	(I)	0.531	B-11	0.40	1.75	0.36	(I)	0.530
A-12	0.4	0.75	0.44	(I)	0.545	B-12	0.40	1.75	0.44	(I)	0.544
A-13	0.55	0.75	0.51	(I)	0.477	B-13	0.55	1.00	0.51	(I)	0.477
A-14	0.55	0.75	0.59	(I)	0.490	B-14	0.55	1.00	0.59	(I)	0.490
A-15	0.55	0.75	0.67	(I)	0.502	B-15	0.55	1.00	0.67	(I)	0.502
A-16	0.7	0.75	0.68	(I)	0.444	B-16	0.55	1.25	0.51	(I)	0.477
A-17	0.7	0.75	0.76	(I)	0.456	B-17	0.55	1.25	0.59	(I)	0.490
A-18	0.7	0.75	0.82	(I)	0.464	B-18	0.55	1.25	0.67	(I)	0.502
A-19	0.4	0.75	0.28	(F)	0.516	B-19	0.55	1.50	0.51	(I)	0.477
A-20	0.4	0.75	0.36	(F)	0.531	B-20	0.55	1.50	0.59	(I)	0.490
A-21	0.4	0.75	0.44	(F)	0.545	B-21	0.55	1.50	0.67	(I)	0.502
A-22	0.55	0.75	0.51	(F)	0.477	B-22	0.55	1.75	0.51	(I)	0.477
A-23	0.55	0.75	0.59	(F)	0.490	B-23	0.55	1.75	0.59	(I)	0.489
A-24	0.55	0.75	0.67	(F)	0.502	B-24	0.55	1.75	0.67	(I)	0.502
A-25	0.7	0.75	0.68	(F)	0.444						
A-26	0.7	0.75	0.76	(F)	0.456						
A-27	0.7	0.75	0.82	(F)	0.464						

Abbreviations used in the table:

w/c = water-to-cement ratio by mass.

SP = superplasticiser dosage by mass of cement.

fi/c = crushed fines-to-cement ratio by volume.

PSD = particle size distribution of the crushed fines.

mixes with (I)-PSD fines and w/c ratio 0.4 and 0.55 from the "A"-series, i.e. A10-A15. The SP dosage was increased to 1.0%, 1.25%, 1.5% and 1.75% of the total cement mass.

### 2.3. Methods

Mixing of the filler modified cement pastes was carried out following a routine investigated and described by Ng, et al. [15]. This routine was chosen because, as reported by Ng, et al. [15], it provides a level of shear rates in the fresh mix that remedy too excessive temperature rise and/or air entrainment during the material preparation. The FlowCyl and rheometer measurements were started exactly 10 min after beginning the mixing procedure.

The test setup for the FlowCyl and its geometry is presented in Fig. 2. The FlowCyl measurements followed the same routine as reported in [16]. During a measurement, the FlowCyl is filled with cement paste up to the level of 15 mm below the top edge, while the outlet is blocked. Then the outlet is opened and the mass of the cement paste in the bowl under the FlowCyl is registered with a sampling rate of 2 s. Subsequently, the volumetric flow is analysed from the cement paste has a height of 35 cm in the FlowCyl until it reaches 15 cm in order to extract the flow resistance ratio (i.e.  $\lambda_Q$ ), which is a dimensionless single parameter proposed by Mørtzell [2] that characterise the flowability of the cement paste. The flow resistance ratio is defined as the difference in volumetric flow rate between the tested material (fresh cement paste) and an "ideal" fluid [2] with no internal flow resistance and no external cohesion or friction, i.e. the flow rate for an ideal fluid is only affected by gravity (the actual expected volumetric flow rate, as function of the fluid height in the FlowCyl is provided in the references [2,3]). It is given by the expression:

$$\lambda_Q = F_t/F_i, \quad (1)$$

where  $F_t$  is the average difference between the theoretical flow rate of an "ideal" fluid and the measured flow rate of the tested cement paste; and  $F_i$  is the average flow rate of the "ideal" fluid. By definition, the "ideal" fluid has a  $\lambda_Q$  value of 0.0, while the theoretical upper limit of the  $\lambda_Q$  value for a viscous fluid is 1.0 [2,3]. More details on the FlowCyl and the mathematical derivation of  $\lambda_Q$  can be found in [2,3,11].

The rheometer measurements were done on a Physica MCR 300 rheometer (Anton Paar) with a bob-in-a-cup geometry, see Fig. 3. The geometry and the used measurement routine were the same, as reported in [17]. Mathematical regression was applied on the measured down (decreasing shear rate) flow-curve data in order to obtain the Bingham and H-B material model parameters [5]. In [17], also details

about the uncertainty for both the Physical MCR 300 rheometer and FlowCyl measurements can be found. It was shown in [17] that for very similar cement pastes as studied in this paper, the standard deviation for 5 repeated measurements on the same mix composition, was approximately 0.9 MPa and 0.01 Pa·s for the Bingham parameters and 0.01 units for the flow resistance ratio.

### 3. Numerical model

In the literature, numerical models have successfully been utilized to analyse different topics related to fresh cementitious materials, e.g. flow in reinforced formwork [18–20], gravity induced aggregate migration [21–24], flow of fibers [25,26], pumping [27], and flow conditions in rheological characterization tools [28,29]. As mentioned in the introduction, in this study a computational fluid dynamics (CFD) model was used to analyse the flow behaviour in the FlowCyl. The CFD model was developed in the commercial software Flow3D that has been found to be very applicable for simulations of fresh cementitious materials [30]. Flow3D utilizes the finite volume method to discretize the mass- and momentum conservation equations and the generalized minimal residual method in order to solve for the pressure and velocity. The interface between the cement paste and air was tracked by the volume of fluid method [31], which is a free surface tracking algorithm that in an Eulerian frame is considered very accurate [32]. In Fig. 4, the model version of the FlowCyl at time zero is illustrated. The inner surface of the FlowCyl was modelled with a wall boundary condition (zero-velocity/no-slip) and the numerically predicted flow resistance ratio was calculated in a similar way as for the experiments, except that the flow rate was determined based on the remaining volume in the simulated domain. A preliminary validation of the CFD model was presented in [13] where it was shown that the simulations predicted the flow resistance ratio within 10% accuracy for five different cement pastes, when assuming that the cement pastes could be described by the Bingham

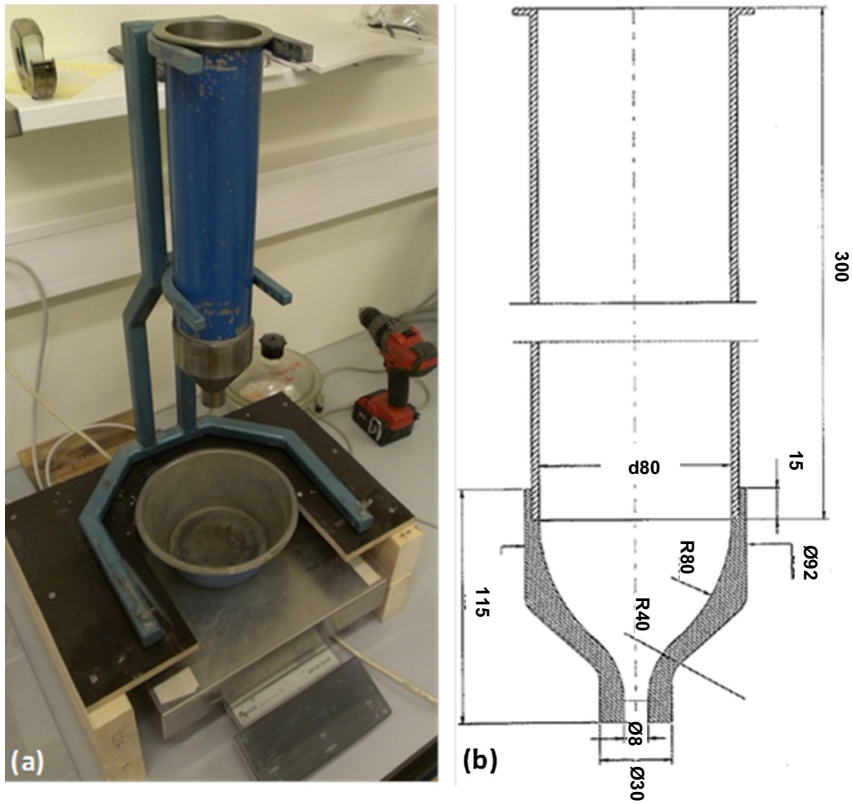


Fig. 2. (a) The FlowCyl test apparatus; (b) the exact geometry of the FlowCyl test apparatus. Note that the lengths and radii are given in mm.

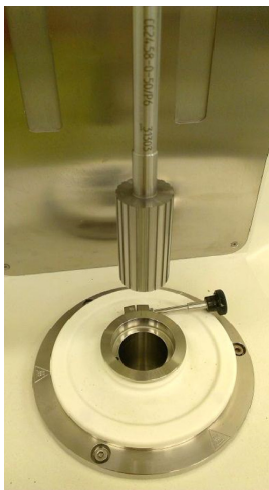


Fig. 3. The bob-in-a-cup geometry used for the experiments. The surfaces of the bob have been roughened to prevent slip.

material model. In this study, both the Bingham- and H-B material model [33] were used to describe the flow behaviour of all 52 cement pastes in order to compare their performance.



Fig. 4. The model version of the FlowCyl at time zero [37].

#### 4. Results and discussion

In Table 2, the rheological parameters for the Bingham- and H-B material model are presented for all 52 cement pastes together with the experimental- and two numerical flow resistance ratios.

**Table 2**  
Experimental and numerical results.

Mix No.	Flow resistance ratio $\lambda_Q$			Bingham model parameters		Herschel–Bulkley model parameters			Mix No.	Flow resistance ratio $\lambda_Q$			Bingham model parameters		Herschel–Bulkley model parameters		
	M	F-3D (B)	F-3D (HB)	$\tau_0$ [Pa]	$\mu$ [Pas]	$\tau_{HB}$ [Pa]	c [Pas <sup>n</sup> ]	p [Pa]		M	F-3D (B)	F-3D (HB)	$\tau_0$ [Pa]	$\mu$ [Pas]	$\tau_{HB}$ [Pa]	c [Pas <sup>n</sup> ]	p [Pa]
A-1	0.890	0.866	0.887	9.36	1.09	9.39	1.09	1.00	B-1	0.810	0.822	0.810	7.11	0.72	6.99	0.74	0.99
A-2	0.920	0.891	0.906	14.27	1.26	14.40	1.12	1.01	B-2	0.849	0.869	0.849	8.32	0.97	8.59	0.92	1.01
A-3	0.960	0.920	0.929	23.98	1.40	20.67	2.25	0.89	B-3	0.873	0.894	0.873	11.34	1.12	11.16	1.16	0.99
A-4	0.580	0.628	0.605	2.72	0.26	2.23	0.37	0.91	B-4	0.780	0.798	0.780	4.15	0.62	4.71	0.51	1.05
A-5	0.590	0.678	0.647	5.02	0.31	3.40	0.76	0.80	B-5	0.792	0.814	0.792	4.42	0.68	5.53	0.47	1.09
A-6	0.650	0.713	0.693	4.85	0.38	3.77	0.65	0.88	B-6	0.814	0.826	0.814	4.59	0.80	5.13	0.69	1.03
A-7	0.390	0.481	0.458	1.69	0.10	0.86	0.36	0.72	B-7	0.755	0.766	0.755	3.52	0.53	3.78	0.48	1.03
A-8	0.410	0.493	0.474	1.76	0.11	1.02	0.33	0.75	B-8	0.767	0.791	0.767	1.69	0.62	3.32	0.33	1.15
A-9	0.430	0.509	0.473	1.84	0.12	1.08	0.34	0.77	B-9	0.820	0.844	0.820	1.91	0.90	4.50	0.45	1.16
A-10	0.840	0.871	0.861	11.04	0.84	9.26	1.26	0.91	B-10	0.753	0.773	0.753	1.64	0.56	2.85	0.34	1.12
A-11	0.890	0.883	0.905	16.79	1.09	14.34	1.67	0.90	B-11	0.731	0.751	0.731	1.63	0.49	2.68	0.30	1.12
A-12	0.950	0.922	0.927	25.95	1.33	19.70	3.01	0.81	B-12	0.782	0.801	0.782	1.43	0.69	3.28	0.36	1.15
A-13	0.570	0.623	0.605	2.73	0.25	2.14	0.39	0.90	B-13	0.554	0.553	0.554	1.39	0.17	1.20	0.22	0.95
A-14	0.570	0.648	0.618	3.73	0.27	2.75	0.52	0.85	B-14	0.581	0.562	0.581	1.64	0.20	1.30	0.28	0.92
A-15	0.550	0.643	0.596	4.40	0.25	3.22	0.56	0.81	B-15	0.569	0.565	0.569	1.44	0.19	1.31	0.22	0.97
A-16	0.350	0.431	0.397	1.19	0.07	0.67	0.23	0.75	B-16	0.513	0.483	0.513	1.04	0.13	0.57	0.25	0.85
A-17	0.380	0.481	0.431	1.49	0.10	0.81	0.30	0.74	B-17	0.551	0.534	0.551	1.00	0.17	0.73	0.23	0.93
A-18	0.490	0.557	0.521	1.86	0.17	1.08	0.38	0.81	B-18	0.598	0.592	0.598	1.23	0.23	1.08	0.26	0.97
A-19	0.930	0.921	0.917	16.45	1.37	13.61	2.04	0.91	B-19	0.501	0.433	0.501	0.75	0.12	0.39	0.21	0.87
A-20	0.990	0.950	0.950	32.15	1.88	21.63	4.81	0.78	B-20	0.519	0.508	0.519	0.57	0.14	0.39	0.18	0.94
A-21	1.000	1.000	0.987	75.05	3.36	33.84	17.90	0.62	B-21	0.557	0.520	0.557	0.64	0.18	0.55	0.20	0.98
A-22	0.720	0.776	0.764	6.13	0.52	4.68	0.87	0.88	B-22	0.474	0.397	0.474	0.69	0.10	0.19	0.24	0.81
A-23	0.770	0.791	0.796	8.02	0.60	6.37	1.00	0.88	B-23	0.478	0.453	0.478	0.43	0.10	0.18	0.16	0.89
A-24	0.830	0.822	0.842	9.87	0.73	9.13	0.90	0.95	B-24	0.518	0.467	0.518	0.41	0.14	0.27	0.17	0.95
A-25	0.520	0.565	0.551	2.08	0.18	1.60	0.30	0.88									
A-26	0.580	0.607	0.552	2.64	0.23	2.14	0.35	0.90									
A-27	0.600	0.650	0.627	3.54	0.28	2.73	0.48	0.87									

Abbreviations used in the table:

M = measured flow resistance ratio  $\lambda_Q$ .

F-3D (B) = flow resistance ratio obtained with the Flow3D CFD model, using the Bingham material model.

F-3D (HB) = flow resistance ratio obtained with the Flow3D CFD model, using H-B material model.

4.1. Bingham material model vs. H-B material model

The objective of this study is, as mentioned in the introduction, to evaluate whether the flow resistance ratio can be used as a single parameter to describe the flowability of cement paste. However, in order to get to this point, it is necessary to quantify the error that is introduced by going from a three-parameter model (the H-B material model) to a two-parameter model (the Bingham material model). The quantification of this error is carried out by the numerical model. In Fig. 5, the difference between the experimental flow resistance ratio and the two numerical predictions are presented. The plot illustrates that for either of the two numerical predictions, the difference does not exceed 30% in the  $\lambda_Q$  range of 0.3 to 1.0, and the agreement improves when increasing the flow resistance ratio. As reported in [34], a typical range of measurable  $\lambda_Q$  for cements pastes will vary between 0.30 and 0.75, which also corresponds well to the range of values measured for the pastes studied in the paper. The improvement in the observed difference between the measured and predicted values might be a consequence of the no-slip boundary condition and/or the rheological approximation functions favouring a slow flow. Furthermore, Fig. 5 demonstrates that generally the best agreement is obtained, when using the H-B material model in the numerical simulations. The average difference in absolute values for the Bingham and H-B material model is 6.5 and 4.6%, respectively, thus illustrating that an additional error of approx. 2% can be expected when assuming the two-parameter material model instead of the three-parameter material model. This error is specific for the flow condition in the FlowCyl where the shear rates can vary in the order of 0 – 290 1/s, see Fig. 6 that presents simulation results for mix No. A-6. Note that these shear rates are experienced at a height of 25 cm, which

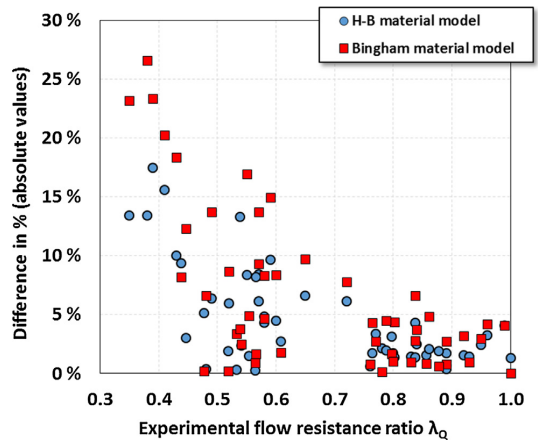


**Fig. 5.** The difference in percentage between the experimental and numerical flow resistance ratio obtained with both the Bingham- and H-B material model. The difference is presented in absolute values. The average difference for the Bingham material model is 6.5%, while it is 4.6% for the H-B material model.

is in the middle of the measuring interval, and that greater shear rates are experienced at the start of the measuring interval (35 cm), as the hydrostatic head is larger. Within the shear rate interval 0 – 290 1/s, the two material models approximate the measured rheological data as seen in Fig. 7 for mix No. A-6. The rheometer experiments are carried out up until a shear rate of 60

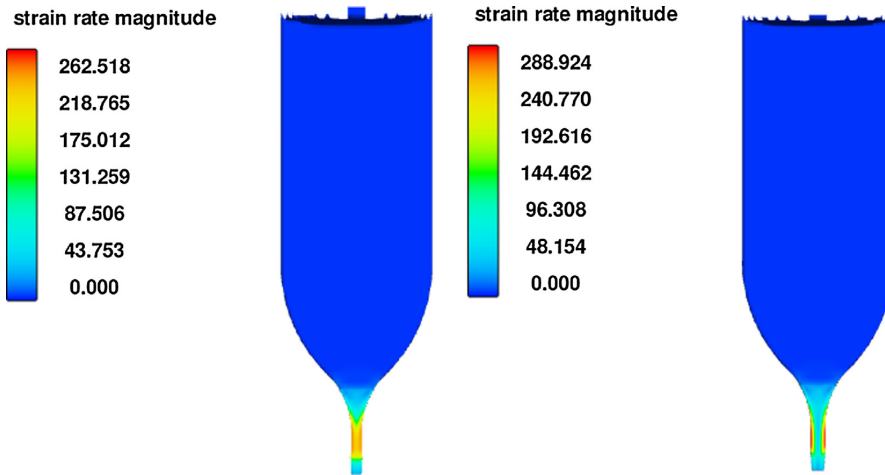


Fig. 6. The shear rate magnitude in the cross section of the FlowCyl for mix No. A-6 at a height of 25 cm: left) Bingham material model right) H-B model. Note that the strain rates are in 1/s.

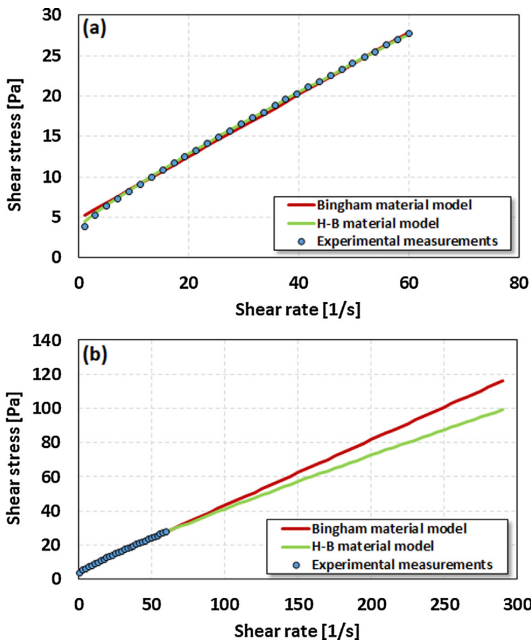


Fig. 7. The rheological measurements for mix No. A-6 together with the fits based on the Bingham and H-B model: a) plotted until a shear rate of 60 1/s, b) plotted until a shear rate of 290 1/s.

1/s, whereas the shear rates in the FlowCyl are greater, as predicted by the numerical simulations, see Fig. 6. This is a source of error that leads to a difference between the experimental and numerical flow resistance ratio. In addition, there could also be a potential error associated with how good the models are able to approximate the actual rheological response of the materials, which was found to be more precise in the case of the H-B model, see Fig. 6. Fig. 7 shows that at shear rates above 60 1/s, the material models start to deviate from each other, which is the main reason for the

difference in the predicted flow resistance ratios between the two models shown in Fig. 5. The shear rate interval experienced by the cement paste during concrete mixing and placement is in the order 0–70 1/s [35]. This upper shear rate limit is less than the one experienced in the FlowCyl, which indicates that modifying the flowrate in the FlowCyl to lower the shear rate is relevant.

4.2. Effect of the rheological properties on the measured flow resistance ratio

Knowing that the error that is introduced going from the H-B- to the Bingham material model is relatively sparse (see previous section), the rest of the analysis focus on going from a two-parameter (the Bingham material model) to a one-parameter (the flow resistance ratio) flow characterization. In Figs. 8 and 9, the

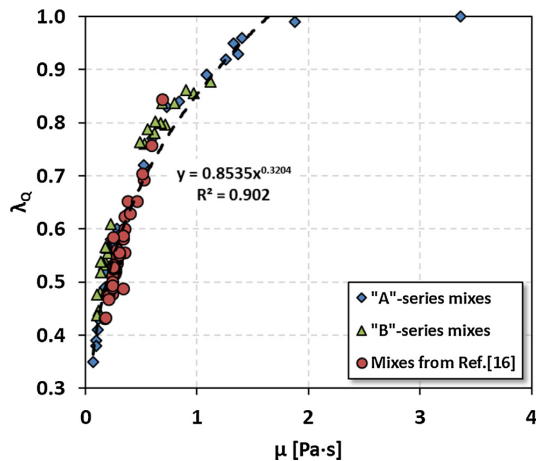


Fig. 8. Flow resistance ratio vs. plastic viscosity for all the experiments and mixes from Ref. [16]. Note that the experimental point corresponding to  $\lambda_Q = 1$  represents a cement paste matrix that was not flowing in the FlowCyl equipment, and this is in fact its rheological parameters are outside the measurement range of the equipment.

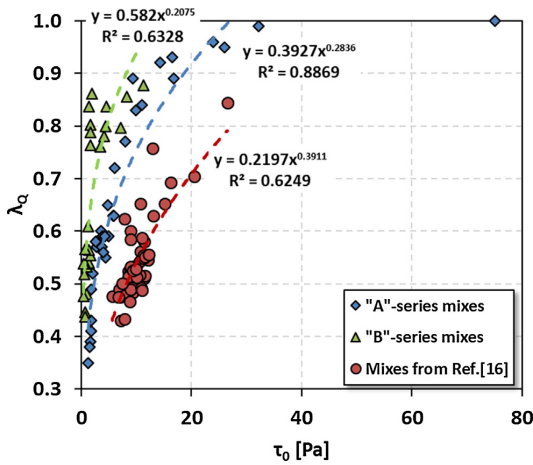


Fig. 9. Flow resistance ratio vs. Bingham's yield stress for all the experiments and mixes from Ref. [16]. Note that the experimental point corresponding to  $\lambda_Q = 1$  represents a cement paste matrix that was not flowing in the FlowCyl equipment, and this is in fact its rheological parameters are outside the measurement range of the equipment.

experimental flow resistance ratio is plotted as function of the plastic viscosity and yield stress, respectively. In the figures, additional 42 results from a previous study [16] are included in order to cover a broader rheological interval. The mixes in [16] were carried out with ten different types of fillers,  $f/c$  ratios by volume ranging from 0.4 to 0.5, a  $w/c$  ratio of 0.5, and constant SP dosage of 0.50% per mass cement. Fig. 8 shows that all the measurements collapse on the same curve in the flow resistance ratio vs. plastic viscosity plot, whereas Fig. 9 shows that the same trend is not the case for the flow resistance ratio vs. yield stress plot. This illustrates that the plastic viscosity dominates the flow resistance ratio, a finding that theoretically was predicted by the numerical model as seen in [13]. This can be illustrated by the following example where the apparent viscosity is calculated for mix No. A-6 at the outlet as well as for two hypothetical cement pastes; one where the yield stress is increased with 50% and another where the plastic viscosity is increased with 50%, both as compared to mix No. A-6. The three cement pastes have the following rheological properties: 1)  $\tau_0 = 4.85$  Pa and  $\mu = 0.38$  Pas; 2)  $\tau_0 = 7.28$  Pa and  $\mu = 0.38$  Pas; and 3)  $\tau_0 = 4.85$  Pa and  $\mu = 0.57$  Pas. The apparent viscosity is calculated for the three cement pastes at a representative shear rate of  $150 \text{ s}^{-1}$ . This value is obtained by considering the shear rates at a height of 25 cm (i.e. the middle of the measuring interval) and then taking the average shear rate over the cross section in the bottom of the FlowCyl.

$$\begin{aligned} \mu_{app,1} &= \tau / \dot{\gamma} = \tau_0 / \dot{\gamma} + \mu = 4.85 / 150 + 0.38 = 0.412 \text{ Pas}; \\ \mu_{app,2} &= \tau / \dot{\gamma} = \tau_0 / \dot{\gamma} + \mu = 7.28 / 150 + 0.38 = 0.429 \text{ Pas}; \\ \mu_{app,3} &= \tau / \dot{\gamma} = \tau_0 / \dot{\gamma} + \mu = 4.85 / 150 + 0.57 = 0.602 \text{ Pas}. \end{aligned}$$

The above examples show that a 50% increase in the yield stress (from 4.85 Pa to 7.28 Pa) only makes the apparent viscosity increase by approx. 4%, whereas a 50% increase in the plastic viscosity (from 0.38 Pas to 0.57 Pas) makes the apparent viscosity increase by approx. 50%. This example explains why the flow resistance ratio primarily depends on the plastic viscosity of the materials in the FlowCyl. The reason for the dominance is owed to the fact that the cement paste experiences high shear rates at the outlet, see Fig. 6, which is a region of the FlowCyl that has a great influence on the flow rate and thereby the flow resistance ratio. These

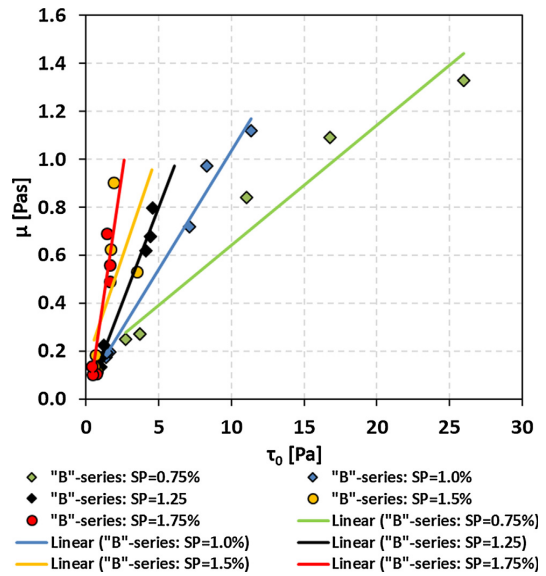


Fig. 10. Plastic viscosity vs. yield stress for "B"-series mixes where the SP dosage per cement mass was varied.

high shear rates lead to apparent viscosities (the viscosity felt by the flowing cement paste) that are dominated by the plastic viscosity in the Bingham material model. As a result, one can state that the flow resistance ratio can be used as a one-parameter characterization of cement paste rheology, as long as the shear rates that the cement paste undergoes in the given application are high. However, this statement only covers a part of the usefulness/limitations of the flow resistance ratio. This is because it is generally accepted that the SP is mainly affecting the yield stress [36], whereas the plastic viscosity is mainly affected by the solid fraction [37]. Therefore, we conducted the "B"-series in this study. Fig. 10 shows the plastic viscosity vs. yield stress of the B-series. It illustrates that the SP dosage per cement mass primarily affects the yield stress, as expected, and thereby the slope of the linear relationship between the plastic viscosity and yield stress. Consequently, one single curve cannot represent the flow resistance ratio vs. yield stress measurements, because the flow resistance ratio does not capture the effect of the change in the yield stress. Hence, the SP-dosage per cement mass affects the usefulness of the flow resistance ratio as a one parameter characterization. Further research should therefore look for ways to make the flow resistance ratio more sensitive to the yield stress, e.g. by lowering the rate of shear in the FlowCyl.

### 5. Conclusions

For the cement pastes investigated experimentally and numerically in this study, the following main conclusions can be drawn with respect to the limitations of the FlowCyl and appertaining flow resistance ratio:

- The average difference between the experimental and numerical flow resistance ratio is 6.5% and 4.6% with the Bingham and H-B material model, respectively. Thus, indicating that an additional error of approx. 2% can be expected when assuming that the cement paste can be described with the two-parameter material model (Bingham material model) instead of the three-parameter material model (H-B material model);

- All the measurements collapse on the same curve in the flow resistance ratio vs. plastic viscosity plot, which is not the case for the flow resistance ratio vs. yield stress plot. This illustrates that the flow resistance ratio is dominated by the plastic viscosity. This finding is supported by the numerical model that predicts very high shear rates at the outlet. As a consequence, it is argued that the flow resistance ratio can be used as a one-parameter characterization of cement paste rheology, when the shear rates that the cement paste undergoes in a given application are high.
- The SP dosage per mass cement changes the slope of the apparent linear relationship between the yield stress and plastic viscosity. For that reason, it is also argued that the flow resistance ratio can distinguish between the flowability of cement pastes if the SP dosage per mass cement is kept constant.
- Further work will be targeted at changing the FlowCyl design to decrease the shear rate at the outlet and thereby enable the one-parameter flow resistance ratio to become sensitive to variations in the yield stress.

### Declaration of Competing Interest

None.

### Acknowledgements

The study presented in this paper is performed within the MiKS project – Mikroproporsjonering med Knust Sand (Norwegian for Micro-proportioning with Crushed Sand), which is a KPN (Competence Project for the Industry) funded by the Research Council of Norway (RCN) contract No. 247619 and industrial partners. The authors would like to thank the RCN and the industrial partners (Norcem AS, Skanska Norge AS and Feiring Bruk AS) for their financial contribution to the research.

### References

- [1] C. Ferraris, K. Obla, R. Hill, The influence of mineral admixtures on the rheology of cement paste and concrete, *Cem. Concr. Res.* 31 (2) (2001) 245–255.
- [2] E. Mørtzell, Modelling the Effect of Concrete Part Materials on Concrete Consistency (Ph.D.), Norwegian University of Science and Technology (In Norwegian), 1996.
- [3] S. Smeplass, BE96-3942/R12 Applicability of the Particle-Matrix Model to LWAC, EuroLightCon, Brussels, 2000.
- [4] J. Wallevik, Rheological properties of cement paste: thixotropic behaviour and structural breakdown, *Cem. Concr. Res.* 39 (2009) 14–29.
- [5] T. Mezger, The Rheology Handbook: For users of Rotational and Oscillatory Rheometers, Vincentz Network, Hannover, 2006.
- [6] R. Shaughnessy, P. Clark, The rheological behaviour of fresh, *Cem. Concr. Res.* 18 (1988) 327–341.
- [7] D. Feys, R. Cepuritis, S. Jacobsen, K. Lesage, E. Secrieru, A. Yahia, Measuring rheological properties of cement pastes: most common techniques, procedures and challenges, *RILEM Tech. Lett.* 2 (2017) 129–135.
- [8] N. Roussel, C. Stefani, R. Leroy, From mini-cone test to Abrams cone test: measurement of cement-based materials yield stress using slump tests, *Cem. Concr. Res.* 35 (2005) 817–822.
- [9] N. Roussel, R. Le Roy, The Marsh cone: a test or a rheological apparatus?, *Cem Concr. Res.* 35 (2005) 823–830.
- [10] R. Le Roy, N. Roussel, The Marsh Cone as a viscometer: theoretical analysis and practical limits, *Mater. Struct.* 38 (January-February) (2005) 25–30.
- [11] S. Smeplass, E. Mørtzell, The applicability of the particle matrix model to self compacting concrete, *Nordic Concr. Res.* 26 (2001).
- [12] T. Hammer, J. Wallevik, On the correlation between rheology of paste, mortar and concrete Chicago, Proceedings of the Second North American Conference on the Design and Use of Self-Consolidating Concrete (SCC) and the Fourth International RILEM Symposium on Self-Compacting Concrete, 2005.
- [13] R. Cepuritis, E. Ramenskiy, E. Mørtzell, S. Smeplass, H. Kjos-Hanssen, S. Li, S. Jacobsen, J. Spangenberg, FlowCyl: one-parameter characterisation of matrix rheology Tromsø, Norway, Proceedings of the Second Concrete Innovation Conference (2nd CIC), 6–8 March, 2017.
- [14] H. Merkus, Particle Size Measurements. Fundamentals, Practice, Quality, Springer Science+Business Media B.V., Dordrecht, 2009.
- [15] S. Ng, H. Mujica, S. Smeplass, Design of a simple and cost-efficient mixer for matrix rheology testing, *Nordic Concr. Res.* 51 (3) (2014) 15–28.
- [16] R. Cepuritis, Development of Crushed Sand for Concrete Production with Micro-Proportioning (Ph.D.), Norwegian University of Science and Technology, Trondheim, 2016.
- [17] R. Cepuritis, S. Jacobsen, S. Smeplass, E. Mørtzell, B. Wigum, S. Ng, Influence of crushed aggregate fines with micro-proportioned particle size distributions on rheology of cement paste, *Cem. Concr. Compos.* 80 (2017) 64–79.
- [18] K. Vasilic, W. Schmidt, H. Kühne, F. Haamkens, V. Mechtcherine, N. Roussel, Flow of fresh concrete through reinforced elements: experimental validation of the porous analogy numerical method, *Cem. Concr. Res.* 88 (2016) 1–6.
- [19] K. Vasilic, B. Meng, H. Kühne, N. Roussel, Flow of fresh concrete through steel bars: a porous medium analogy, *Cem. Concr. Res.* 41 (2011) 496–503.
- [20] S. Jacobsen, R. Cepuritis, Y. Peng, M. Geiker, J. Spangenberg, Visualizing and simulating flow conditions in concrete form filling using pigments, *Constr. Build. Mater.* 49 (2013) 328–342.
- [21] L. Shen, L. Struble, D. Lange, Modelling dynamic segregation of self-consolidation concrete, *ACI Mater. J.* (2009) 375–380.
- [22] J. Spangenberg, N. Roussel, J. Hattel, H. Stang, J. Skocek, M. Geiker, Flow induced particle migration in fresh concrete: theoretical frame, numerical simulations and experimental results on model fluids, *Cem. Concr. Res.* (2012) 633–641.
- [23] J. Spangenberg, N. Roussel, J. Hattel, E. Sarmiento, G. Zirgulis, M. Geiker, Patterns of gravity induced aggregate migration during casting of fluid concretes, *Cem. Concr. Res.* (2012) 1571–1578.
- [24] J. Wallevik, W. Mansour, O. Wallevik, OpenFOAM casting solver with segregation, International RILEM conference on materials, systems and Structures in Civil Engineering, Conference segment on Fresh Concrete, RILEM Publications S.A.R.L. ISBN: 978-2-35158-184-1, 22-24 August, Technical University of Denmark, Lyngby, Denmark, 2016.
- [25] O. Svec, G. Zirgulis, J. Bolander, H. Stang, Influence of formwork surface on the orientation of steel fibres within self-compacting concrete and on the mechanical properties of cast structural elements, *Cem. Concr. Compos.* 50 (2014) 60–72.
- [26] L. Martinie, J.-F. Lataste, N. Roussel, Fiber orientation during casting of UHPFRC: electrical resistivity measurements, image analysis and numerical simulations, *Mater. Struct.* 48 (2015) 947–957.
- [27] H. Le, E. Kadri, S. Aggoun, J. Vierendeels, P. Troch, G. De Schutter, Effect of lubrication layer on velocity profile of concrete in a pumping pipe, *Mater. Struct.* 48 (2008) 3991–4003.
- [28] J. Wallevik, Minimizing end-effects in the coaxial cylinders viscometer: viscoplastic flow inside the ConTec BML Viscometer 3, *J. Non-Newtonian Fluid Mech.* (2008) 116–123.
- [29] A. Gram, J. Silfverbrand, B. Lagerblad, Obtaining rheological parameters from flow test – analytical, computational and lab test approach, *Cem. Concr. Res.* 63 (2014) 29–34.
- [30] N. Roussel, A. Gram, M. Cremonesi, L.K.K. Ferrara, V. Mechtcherine, S. Shyshko, J. Skocek, J. Spangenberg, O. Svec, L. Thrane, K. Vasilic, Numerical simulations of concrete flow: a benchmark comparison, *Cem. Concr. Res.* 79 (2016) 265–271.
- [31] C. Hirt, B. Nichols, Volume of fluid (VOF) method for the dynamics of free boundaries, *J. Comput. Phys.* (1981) 201–225.
- [32] R. Comminal, J. Spangenberg, J. Hattel, Cellwise conservative unsplit advection for the volume of fluid method, *J. Comput. Phys.* (2015) 582–608.
- [33] E. Mitsoulis, Flows of viscoplastic materials: models and computations, *Rheol. Rev.* (2007) 135–178.
- [34] S. Smeplass, R. Cepuritis, Chapter 4 - Fresh, concrete - proportioning, in: TKT 4215 Concrete Technology 1, Course Compendium, Norwegian University of Science and Technology, Trondheim, 2016, pp. 4.1–4.41.
- [35] R. Helmuth, L. Hills, D. Whitting, S. Bhattacharja, Abnormal Concrete Performance in the Presence of Admixtures. PCA R&D Serial No. 2006, Portland Cement Association, Skokie, 2006.
- [36] O. Wallevik, J. Wallevik, Rheology as a tool in concrete science: the use of rheographs and workability boxes, *Cem. Concr. Res.* 41 (12) (2011) 1279–1288.
- [37] H. Barnes, J. Hutton, K. Walters, Introduction to Rheology, Elsevier Science Publishers B.V., Amsterdam, 1993.

# Paper VI

**Neural network predictions of the simulated rheological response of cement paste in the FlowCyl**  
Sheiati S, Ranjbar N, Frelsen J, Skare EL, Cepuritis R, Jacobsen S, Spangenberg J.  
*Neural Computing and Applications* 33 (2021) pp. 13027-13037.







# Neural network predictions of the simulated rheological response of cement paste in the FlowCyl

Shohreh Sheiati<sup>1</sup> · Navid Ranjbar<sup>1,2,3</sup> · Jes Frellsen<sup>4</sup> · Elisabeth L. Skare<sup>1,5</sup> · Rolands Cepuritis<sup>5,6</sup> · Stefan Jacobsen<sup>5</sup> · Jon Spangenberg<sup>1</sup>

Received: 6 July 2020 / Accepted: 31 March 2021 / Published online: 22 April 2021  
© The Author(s), under exclusive licence to Springer-Verlag London Ltd., part of Springer Nature 2021

## Abstract

For the past decades, computational fluid dynamics (CFD) simulations have been shown as a promising approach for understanding the complex flow behavior of concrete. However, their application is often limited due to the computationally heavy analysis. In this study, two artificial neural networks, multi-layer perceptron and radial basis function, are trained by results of a CFD model that simulates the cement flow in the FlowCyl equipment. Both models were investigated for predicting single values of volume loss over a predetermined duration as well as the full volume loss versus time curves. The results show that after training the neural networks can accurately substitute the predictions of the CFD model for both single values and the full curves. For the multi-layer perceptron, accurate predicts are even obtained after substantial reducing the training data, which illustrates that a coupling between a CFD model and a neural network can significantly decrease the overall calculation time.

**Keywords** Cement paste · Rheology · Computational fluid dynamics · Artificial neural network

## 1 Introduction

The complex nature of concrete rheology has for decades been extensively studied as it is a key parameter for obtaining proper concrete structures. These studies include

development of low- [1] and high-tech [2] equipment for rheological quantification as well as the determination of flow behaviors during transport [3], pumping [4], and placement [5]. In recent years, computational fluid dynamics (CFD) has been increasingly applied to

✉ Shohreh Sheiati  
shoshei@mek.dtu.dk

✉ Navid Ranjbar  
naran@mek.dtu.dk

Jes Frellsen  
jefr@dtu.dk

Elisabeth L. Skare  
elisabeth.l.skare@ntnu.no

Rolands Cepuritis  
rolands.cepuritis@ntnu.no

Stefan Jacobsen  
stefan.jacobsen@ntnu.no

Jon Spangenberg  
josp@mek.dtu.dk

<sup>2</sup> Department of Health Technology, Technical University of Denmark, 2800 Lyngby, Denmark

<sup>3</sup> Department of Civil, Environmental and Geomatic Engineering, University College London, London WC1E 6BT, UK

<sup>4</sup> Department of Applied Mathematics and Computer Science, Technical University of Denmark, 2800 Lyngby, Denmark

<sup>5</sup> Department of Structural Engineering, Norwegian University of Science and Technology, NO-7491 Trondheim, Norway

<sup>6</sup> Norcem AS (HeidelbergCement), NO-3950 Brevik, Norway

<sup>1</sup> Department of Mechanical Engineering, Technical University of Denmark, 2800 Lyngby, Denmark

understand concrete rheology as it provides a virtual window into the material and process [6]. CFD models have been used to study concrete flow phenomena such as the effect of lubrication layers on velocity profiles inside pumping pipes [7] as well as the flow behavior in reinforced areas of large-scale laboratory castings [8–10]. In addition, CFD models have been used to predict local variations in aggregate volume fractions [11–13] and orientation of fibers [14, 15]. In other studies, these models have been used to understand the flow behavior of cementitious material in equipment utilized to measure its rheological behavior e.g., inside the ConTec BML Viscometer 3 [16] or in the FlowCyl [17], which is a modified version of the March Cone. The challenge for CFD models is that they often require a dedicated experimental setup to be validated [18] and that they can be computationally heavy and thus takes a long time to run [19]. The latter becomes even more pronounced when the models are exploited to investigate a large parameter space or when coupled with an optimization algorithm [20]. Consequently, CFD models are used infrequently in the concrete industry despite their great potential. Researchers are continuously trying to find solutions that can speed-up CFD simulations. One such solution is to manipulate the governing equations (i.e., the mass and momentum conservation equations) in order to reduce the number of unknowns (e.g., the streamfunction formulation for two-dimensional problems [21, 22]). Another solution is to couple the CFD model with an artificial neural network (ANN) that learns from the simulations and eventually predicts the flow patterns with good accuracy, but substantially faster. A typical ANN is composed of an arbitrary number of elements named neurons connected to each other by weighted vectors that are arranged in the input, output, and hidden layers [23, 24]. The number of input and output neurons is equal to the number of input and output variables, respectively, while the number of hidden neurons is chosen depending on the problem at hand. The performance of a neural network critically depends on its architecture. If a network is not complicated enough it would underfit to the training set, while a network that concentrates too much on detailed information would overfit the training set [25]. In both cases, the neural network would have a poor generalization performance on unseen data [26]. Evolutionary algorithms such as genetic algorithms (GA) [27, 28] have been widely used to optimize the neural network architecture in different applications. Previous studies show that GAs outperform random search and trial and error methods [29], because GAs find the optimal solution using the evolutionary process, which follows the idea of survival of solutions with better quality evolve from previous generations [30]; whereas, random search methods generate and utilize random solutions to find a better solution, and trial

and error methods find a better solution among a number of solutions generated using different configuration parameter tuning by the user. With this setup, the ANN imitates the learning and reasoning ability of the human brain. The coupling between CFD models and ANNs is a relatively unexplored research topic. One such study was recently exemplified in an aerodynamics related problem, where the nonuniform steady laminar velocity field was predicted around an objective that changed geometry [31]. This enabled a calculation speed-up of two and four orders of magnitude as compared to a Graphics Processing Unit (GPU)- and Central Processing Unit (CPU)-based CFD solver, respectively. In another investigation, a similar coupling was used to carry out real-time simulations of a three-dimensional smoke plume, and in this case, the calculation time was also substantially reduced [32]. Although CFD models and ANNs previously have been coupled, there exists no literature where such coupling is used to analyze the rheological behavior of fluids. Therefore, in this study, two artificial neural network models in different structures are exploited to predict the CFD simulated rheological response of cement pastes in the FlowCyl equipment. The objectives of the study are to investigate the accuracy of the predictions as well as to study how few of the time-consuming CFD simulations the ANNs require for training without reducing its predictive capabilities. The rest of the paper is divided into four sections. Firstly, a brief introduction to the FlowCyl measurements is provided. This is followed by an overview of the applied methodology. Subsequently, the results of the study are presented and discussed, and finally, conclusive remarks are summarized.

## 2 Experimental measurements and computational fluid dynamic model

The FlowCyl equipment (Fig. 1a) is designed to characterize the rheological behavior of cement pastes. The test is carried out by filling up the FlowCyl to a height of 360 mm. Subsequently, the mass flow out of the equipment is recorded as a function of time (Fig. 1b) from which a single parameter (viz. the flow resistance ratio) describing the flowability of the cement paste can be deduced [33, 34]. In addition, for each cement paste composition the rheological parameters, shear stress ( $\tau$ ) and plastic viscosity ( $\mu$ ), were measured using a rheometer. In a recent study [17], the FlowCyl was simulated with a CFD model, and it was illustrated that the model was able to predict the mass flow versus time (and thus the flow resistance ratio) based on the yield stress and plastic viscosity, which were measured experimentally, Fig. 1b. A total number of 51 simulations

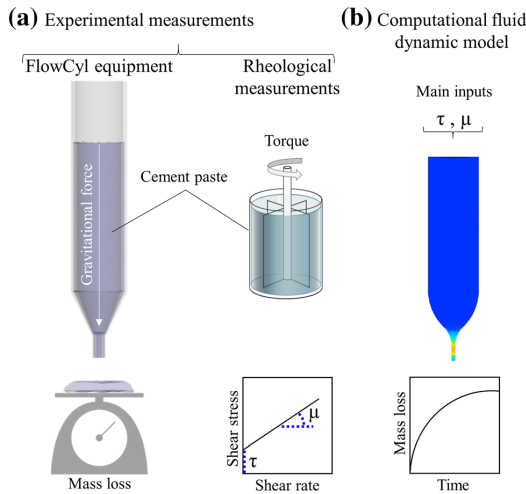


**Fig. 1** a Schematic of FlowCyl equipment and rheological measurements, b computational fluid dynamic model using experimental inputs

were performed in this study, and each simulation took approximately 12 h.

### 3 Methodology

An overview of the methodology used in this study is shown in Fig. 2. As illustrated, several ANNs were set up to predict the CFD simulated rheological response of the cementitious material inside the FlowCyl from [17]. All the ANNs were set up using the neural network Toolbox of MATLAB version 9.4(R2018a). The details of each step of the methodology and the different ANNs are described in this section.

#### 3.1 Dataset

The input parameters in all the ANNs were the two rheological parameters:  $\tau$  and  $\mu$ . These two parameters were obtained experimentally in the previous study for 51 mix compositions and used as the key parameters in the CFD modeling of cement paste [17]. Of all mixes [17], one mix was excluded from the current study ( $\tau = 75.05$  Pa and  $\mu = 3.36$  Pas), since no flow was observed experimentally. The target variables were obtained from the CFD simulations and the ANNs used them for training. The target variables are described in more detail in the following subsections. The ANNs used 70 and 30% of the dataset for training and testing, respectively.

#### 3.2 Preprocessing

The data preprocessing involved normalization of the input and target variables in order to improve solver stability and modeling performance [35]. To this end, all input and target values were scaled to the range between 0.1 and 0.9 by the following Eq. (1) [36]:

$$N_i = 0.8 \left( \frac{X_i - X_{\min}}{X_{\max} - X_{\min}} \right) + 0.1 \quad (1)$$

where  $X_i$  is the original data,  $X_{\min}$  and  $X_{\max}$  are the minimum and maximum value of the original data set, respectively, and  $N_i$  is the normalized value.

#### 3.3 Applied methods

Two methods were employed in order to predict the simulated flow behavior of the cementitious material inside the FlowCyl:

1. *The single point method (SPM)* where the target of the ANNs was a single value describing the volume of the cementitious material leaving the FlowCyl in the time interval 5 and 25 s, see Fig. 3a.
2. *The full curve method (FCM)* where the target was a curve describing the volume loss as a function of time, Fig. 3a. In this method, the ANNs were designed to predict the curve by a quadratic equation with coefficients  $a$ ,  $b$ , and  $c$ . The latter was forced to be zero to ensure no mass flow at  $t = 0$ . The advantage of this model is to achieve volume loss at any desired time, while it is not applicable for SPM. Notably, in the applied methods the volume losses are simulated, which can be directly compared to the mass losses obtained by the FlowCyl by multiplying with the density of each considered matrix.

#### 3.4 Structure

The performance of three different ANN structures was investigated, see Fig. 3b–d. In all cases, the ANNs had two inputs ( $\mu$  and  $\tau$ ). One structure was setup using the SPM (i.e., the target was the volume loss between 5 and 25 s). While two structures were applied for the FCM: (1) one ANN with two targets ( $a$  and  $b$ ); and (2) two ANNs with each one target.

#### 3.5 Artificial neural network models

Two different neural network models were tested and compared in this study:

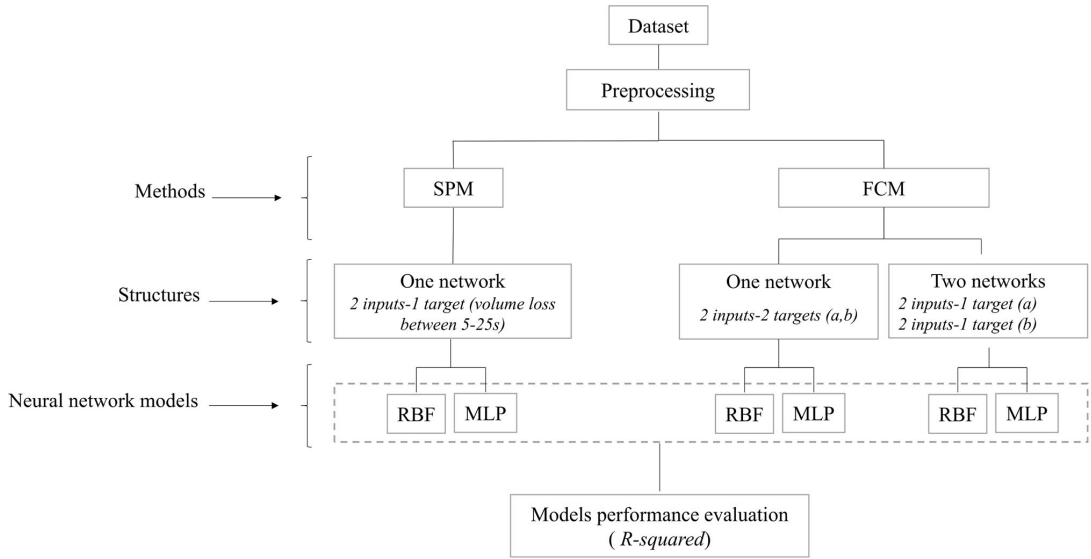


Fig. 2 An overview of the methodology used in this study

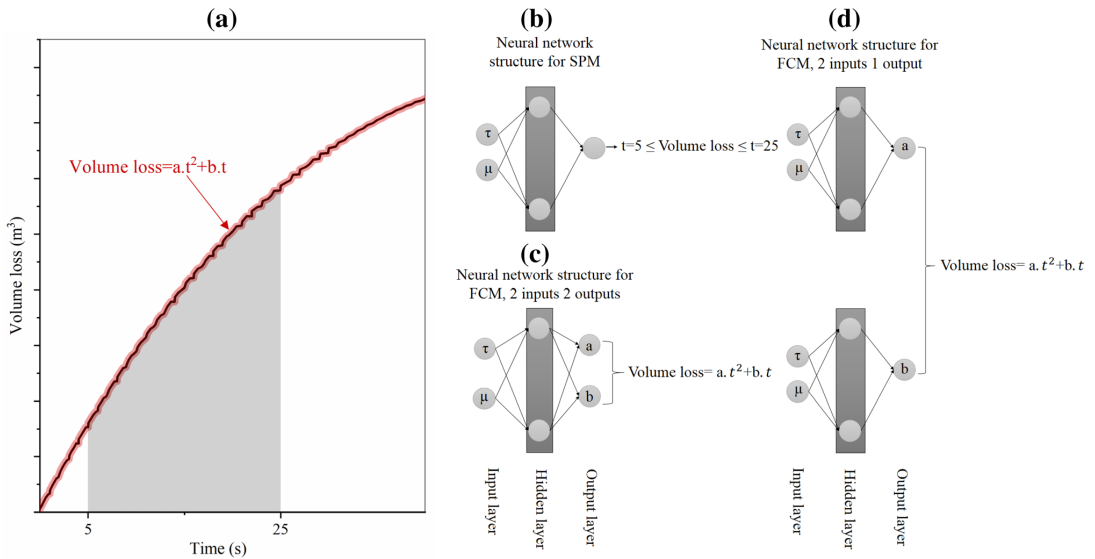


Fig. 3 a CFD-simulation of the typical volume loss through the FlowCyl as a function of time; b schematic ANN structure for SPM; c first FCM structure—one ANN with two targets; d Second FCM structure—two ANNs with each one target

1. The multilayer perceptron (MLP) model is fully connected; meaning that all input neurons are linked to each of the neurons of the hidden layer and similarly they are connected to each of the targets. Mathematically, the relationship between each hidden neuron and the input variables is expressed as:

$$h_i = \sigma(w_i^T x) \tag{2}$$

where  $x = [x_1, \dots, x_p]^T$  is the vector of  $p$  input variables,  $w_i = [w_{i,1}, \dots, w_{i,p}]^T$  are the weights corresponding to each input variables, and  $\sigma$  is a nonlinear activation function.

The sigmoid function is used as the activation function of the network:

$$\sigma(w_i^T x) = \frac{1}{1 + e^{-w_i^T x}} \tag{3}$$

The predicted target  $\hat{Y}$  is related to the hidden neurons  $h$ ,

$$\hat{Y} = g(\beta^T h) \tag{4}$$

where  $h = [h_1, \dots, h_k]^T$  is the vector of hidden neuron values and  $\beta = [\beta_1, \dots, \beta_k]^T$  is the weight matrix between the hidden neurons and target neurons. Fig. 4a shows a schematic of a typical MLP model with four input variables, a hidden layer with three hidden neurons, and a single target. Here, the NEWFF function in MATLAB was used with Levenberg-Marquardt, trainlm, as training function to build the network, as Eq. (5):

$$\text{net} = \text{newff}(P, T, S) \tag{5}$$

where  $P$ ,  $T$  and  $S$  are the input vector, target vector and hidden layer size, respectively. There is a possibility to increase the number of hidden layers when the data are complex in nature. The effects of the number of hidden layers are investigated. The number of hidden layer neurons is tuned by MATLAB GA Toolbox via coefficients and associated weights in order to increase the speed and efficiency of the system. The number of hidden layer neurons was tuned in the interval 1–20.

2. *The radial basis function (RBF) model* also captures interactions among input and target variables via a hidden layer that consist of RBF neurons. Each  $j$ th RBF neuron maintains spread ( $\sigma_j$ ) and basis function  $\phi_j$  with  $c_j$  center. The nonlinear basis functions  $\phi_j$  are the radial distance functions of the input from the center of the  $j$ th RBF neuron. In this work, the most commonly used Gaussian basis function was employed as:

$$\phi_j(x) = e^{-\frac{\|x - c_j\|^2}{2\sigma_j^2}} \tag{6}$$

where  $\|x - c_j\|$  represents the distance between the input vector and the center of  $j$ th RBF neuron. The parameter  $\sigma_j$  is known as spread of the radial basis function and used for the corresponding width of the  $j$ th hidden neuron representing the scale of the density distribution. Having the input variable of  $P$ , and the RBF neuron number of  $h$ , the  $i$ th output  $y_i(x)$  of the RBF neural network is:

$$y_i(x) = \sum_{j=1}^h \phi_j(x) \times w_{i,j} \tag{7}$$

where  $w_{i,j}$  is the connection weight between the  $j$ th RBF neuron and the  $i$ th target neuron. A schematic of the RBF network is described in Fig. 4b. In this study, the RBF neural network was trained and implemented by the NEWRB function in MATLAB and it is given by:

$$\text{net} = \text{newrb}(P, T, \text{GOAL}, \text{SPREAD}, \text{MN}) \tag{8}$$

where  $P$ ,  $T$ , GOAL, SPREAD, and MN are the input vector, target vector, error goal, spread value, and number of neurons, respectively. Here, the number of hidden layer neurons and the value of spread is tuned by the MATLAB GA Toolbox in the interval 1–20 and 0–1, respectively.

The ANNs accuracy was evaluated based on the coefficient of determination ( $R^2$ ):

$$R^2 = 1 - \frac{\sum_{i=1}^n (y_{\text{CFDvalues},i} - y_{\text{ANNvalues},i})^2}{\sum_{i=1}^n (y_{\text{CFDvalues},i} - \bar{y}_{\text{CFDvalues}})^2} \tag{9}$$

where subscript ‘ANN values’ refers to the predictions made by the ANN, while subscript ‘CFD values’ refers to

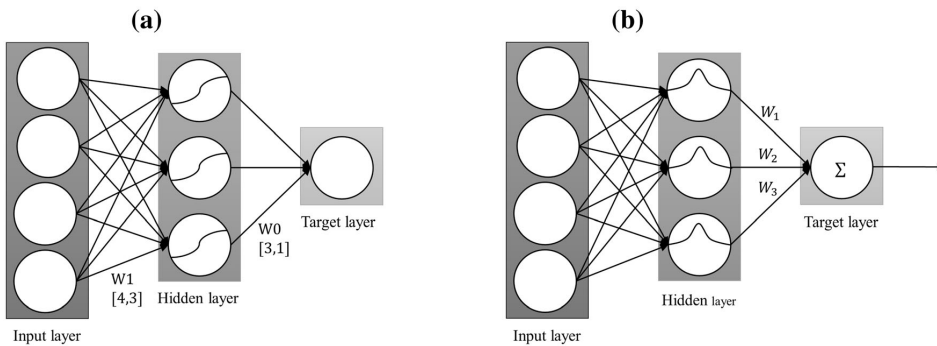


Fig. 4 A schematic of a typical a MLP and b RBF models.3.7 Performance indexes

the CFD results or in the case of the FCM, the best fit to the CFD results.

## 4 Results and discussion

### 4.1 Predicting the volume loss between 5 and 25 s using SPM

Table 1 shows the effects of one, two and three MLP hidden layers for the prediction of the volume loss between 5 and 25 s using SPM. As observed, all architectures perform similarly. Thus, to reduce the computational cost of the network, one hidden layer with three neurons is selected for the rest of analysis. The best performance for the RBF model is obtained with fourteen neurons with the spread of 0.7 in the hidden layer. The error goal for both MLP and RBF was set to 0.1 mean-squared-error (MSE) as an absolute zero value may cause overfitting.

In Fig. 5, the CFD results and ANN predictions of the volume loss versus yield stress and plastic viscosity are shown. Both ANN models are in good agreement with the simulation results. The  $R^2$ -value is 99.9% for both models, which indicate that the predictions are highly accurate. In [17], it was found that the plastic viscosity of the cement paste is dominating the rheological response in the Flow-Cyl. The relationship between the plastic viscosity and volume loss has a non-complex polynomial behavior and this might be the reason for the MLP model obtaining such high accuracy with only one hidden layer and few neurons, because the MLP model is good at approximating regions of the solution space with a linear description. On the other hand, this non-complex polynomial behavior has an opposite effect on the number of required neurons used by the RBF model. This type of ANN model uses the Euclidean distances between inputs and weights in combination with the Gaussian kernel activation function, which makes the RBF neurons perform well locally (i.e., when the weights are close to the inputs), but less good when having to extrapolate. Thus, relatively many neurons are needed to minimize extrapolation when having to cover the polynomial behavior of the plastic viscosity versus volume loss relationship. In contrast, if the yield stress would have dominated the volume loss, a lower number of RBF

neurons might have been sufficient, as this relationship has a more clustered behavior as compared to the plastic viscosity versus volume loss relationship.

### 4.2 Predicting the volume loss as a function of time, FCM

An example of a typical volume loss versus time curve predicted by the ANN models is shown in Fig. 6. The prediction of the MLP and RBF model is more or less identical for the selected example and they both accurately predict the rheological response of the cement paste in the FlowCyl equipment. In Table 2, the  $R^2$ -values at the test stage for the  $a$  and  $b$  coefficients of the quadratic equation are shown for the MLP and RBF model using both one and two ANNs. Similar to the SPM, no improvement was observed with deeper MLPs. Thus, the MLP model with one hidden layer and a number of neurons that are fewer than that of RBF is selected. All  $R^2$ -values are above 99%, again indicating that both models provide highly accurate predictions. The results in the table also illustrate that there is not a substantial improvement by utilizing two ANNs instead of one. Therefore, in the rest of this paper, only a structure of one ANN is used for the FCM.

In order to further evaluate the performance of the FCM results, the determined quadratic equations are used to estimate the volume loss between 5 and 25 s. Figure 7 shows the predicted values for the fitted CFD data. Since a curve fitting is the prerequisite of the FCM model to obtain the quadratic equation parameters, there is an inevitably small difference between the CFD and fitted CFD results. The error is as a result of rounding the quadratic equation parameters and this influence the ANN models. Based on these results,  $R^2$ -values at test stage are found and compared with the SPM results, see Table 3. For simplicity, the  $R^2$ -values of FCM are given as the mean of  $R^2$  for the targets  $a$  and  $b$ . The FCM based  $R^2$ -values are slightly lower than those of the SPM, which is expected, as this evaluation is carried out on a sub time interval of the curve predicted by the FCM. Nevertheless, the  $R^2$ -values at the test stage of the FCM are still  $\sim 99\%$ , thereby providing accurate predictions.

**Table 1**  $R^2$  at the test stage for the two ANN models using the SPM

Model	Parameters	$R$ -squared at the test stage
MLP	1 hidden layer with 3 neurons	0.999
	2 hidden layers with 4 and 5 neurons each	0.998
	3 hidden layers with 4, 3, and 5 neurons each	0.998
RBF	1 hidden layer with 14 neurons and spread value of 0.7	0.998

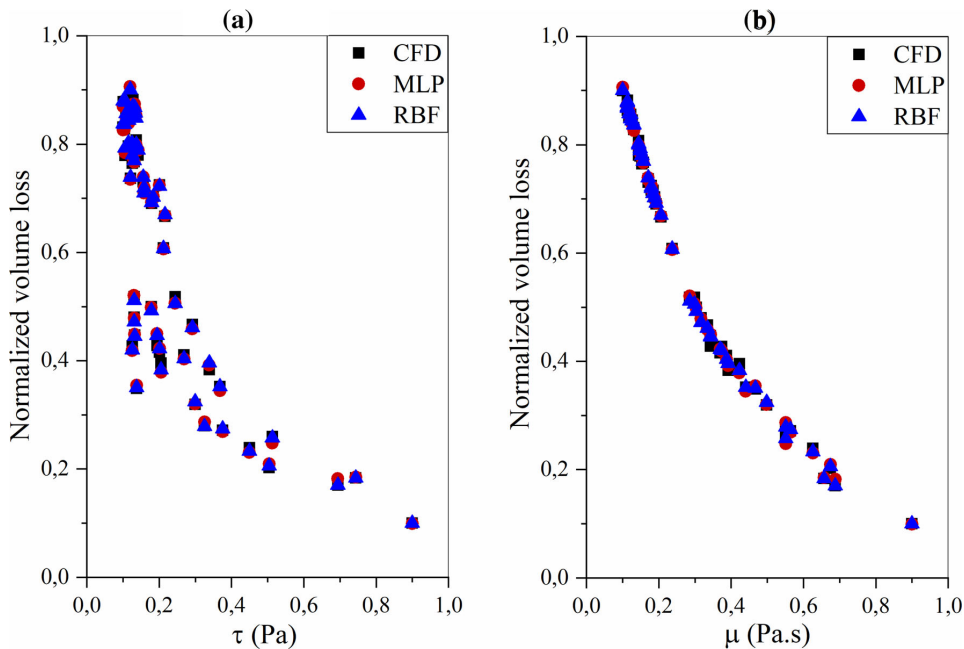


**Fig. 5** CFD results and ANN predictions of the volume loss as a function of **a**  $\tau$ , and **b**  $\mu$

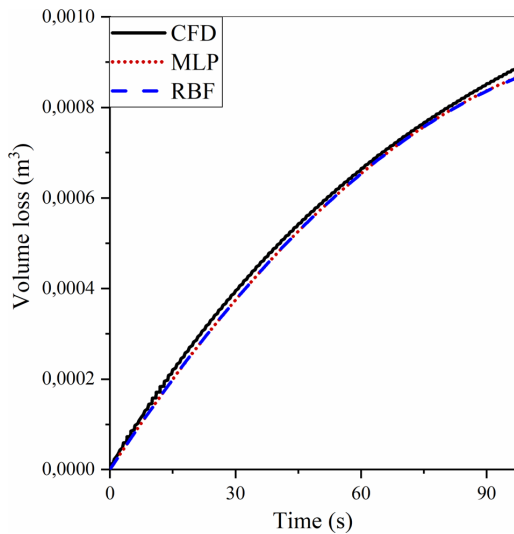


**Fig. 6** CFD results and ANN predictions of the volume loss versus time curve for a selected case ( $\tau = 23.98$  and  $\mu = 1.4$ )

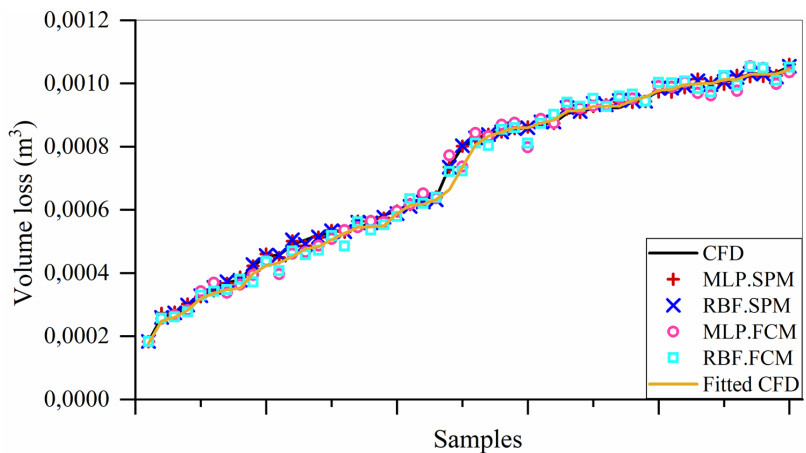
### 4.3 Influence of training data on the accuracy of predictions

As previously mentioned, it is of interest to reduce the training data for the ANNs, since it is generated through the time-consuming CFD simulations, but only as long as this reduction does not lead to a substantial loss in accuracy of the predictions. In order to make such investigation, the training data are reduced in intervals of 5 input data from 35 (i.e., 70% of the full dataset that was used in the previous investigations) to 10. For each value, the ANN models are executed twenty times with randomly chosen training data to get a sound statistical basis for the evaluation. In Fig. 8, the  $R^2$ -values at the test stage for the two ANN models using the SPM is shown for different numbers of training data. As expected, both ANNs predictive capability reduces with a reduced number of training data, but the reduction is minimal for the MLP model. When utilizing 10 input data (i.e., a reduction of  $\sim 70\%$ ) for training in the MLP model, the averaged  $R^2$ -value is above 95%, indicating that the predictions are still accurate. Furthermore, the standard deviation at 10 input data is only 1%, which illustrates that the chosen input data only has little effect on the precision of the MLP model. Consequently, this analysis demonstrates that the rheological response of the investigated cement pastes in the FlowCyl could have been accurately predicted with a substantially



**Table 2** The optimum number of neurons and  $R^2$ -values at the test stage for the MLP and RBF models using both one and two ANNs to predict the volume loss versus time curve

Structure	model	Target	Parameters	$R^2$ -squared at the test stage	
One ANN	MLP	$a$	1 hidden layer with 9 neurons	0.995	
		$b$		0.997	
		$a$	2 hidden layer with 7 and 10 neurons	0.994	
		$b$		0.997	
		$a$	3 hidden layer with 5, 5, and 5 neurons	0.995	
		$b$		0.998	
	RBF	$a$	1 hidden layer with 14 neurons and spread value of 0.9	0.993	
		$b$		0.995	
Two ANNs	MLP	$a$	1 hidden layer with 3 neurons	0.998	
			2 hidden layers with 10 and 4 neurons each	0.996	
			3 hidden layers with 7, 5, and 2 neurons each	0.998	
		$b$	1 hidden layer with 10 neurons	0.988	
			2 hidden layers with 7 and 7 neurons	0.988	
			3 hidden layers with 8,5, and 6 neurons	0.991	
		RBF	$a$	1 hidden layer with 13 neurons and spread value of 0.8	0.992
			$b$	1 hidden layer with 14 neurons and spread value of 1	0.996

**Fig. 7** A comparison between SPM and FCM method in prediction of volume loss between 5 and 25 s by MLP and RBF models

reduced CFD simulation effort, if the CFD model had been coupled with an MLP based ANN. This reduction in computational effort, of course, needs to be evaluated against the overhead in time required to set up the ANN and finding the appropriate model. In comparison to the performance of the MLP model, the averaged  $R^2$ -value at the test stage of the RBF model reduces to less than 80% when using 25 input data, which clearly illustrates that the RBF model is not ideal when utilized to reduce the number of CFD simulations. The reason for the quicker reduction

in  $R^2$ -value for the RBF model is due to its limited ability to extrapolate. A property that becomes increasingly important when removing a part of the training data. The  $R^2$ -values at the test stage for the FCM at different numbers of training data are shown in Fig. 9. Comparing the MLP and RBF model provides a similar picture as for the SPM. Thereby, again illustrating that the MLP model with greater advance can be used to reduce the CFD simulation effort while providing accurate predictions of the volume loss versus time curve.

**Table 3**  $R^2$ -values at the test stage for the SPM and FCM in predicting the volume loss between 5 and 25 s by using both the MLP and RBF model

Method		ANN model		$R^2$
SPM	FCM	MLP	RBF	
×		×		0.999
×			×	0.998
	×	×		0.992
	×		×	0.989

### 5 Limitation

Although, the ANN can predict the process in less computational time than CFD, it has three major limitations; first, ANN models need a numerical or experimental database to be trained by, since they are not able to produce their own database. Second, the ANNs are not able to predict the values which are outside of the network training domain, therefore the range of training data should be illustrative of the whole performing range of the system [37, 38]. Third, the training outcome depends significantly on the choice of initial parameters such as the number of

hidden layers, the number of hidden neurons, and type of activation functions.

### 6 Conclusion

This study demonstrates the first important step of utilizing predictive machine learning models within the field of computational concrete rheology. Two artificial neural networks, MLP and RBF, were trained by the outputs of a CFD model that simulated cement flow in the FlowCyl equipment. Both models were investigated for predicting single values of volume loss between 5 and 25 s as well as the full volume loss versus time curves using a novel method, called FCM method. The results showed that both MLP and RBF model were able to predict the simulated rheological response of cement paste, if the majority of the dataset was used for training. In fact, the two models were both able to predict the volume loss between 5 and 25 s as well as the full volume loss versus time curve with  $R^2$ -values at the test stage above 99%. When the training data were reduced, it was shown that the RBF model quickly lost its precision, while in the case of the MLP model, it was possible to reduce the training data with 70% and still have an  $R^2$ -value at the test stage above 95%.

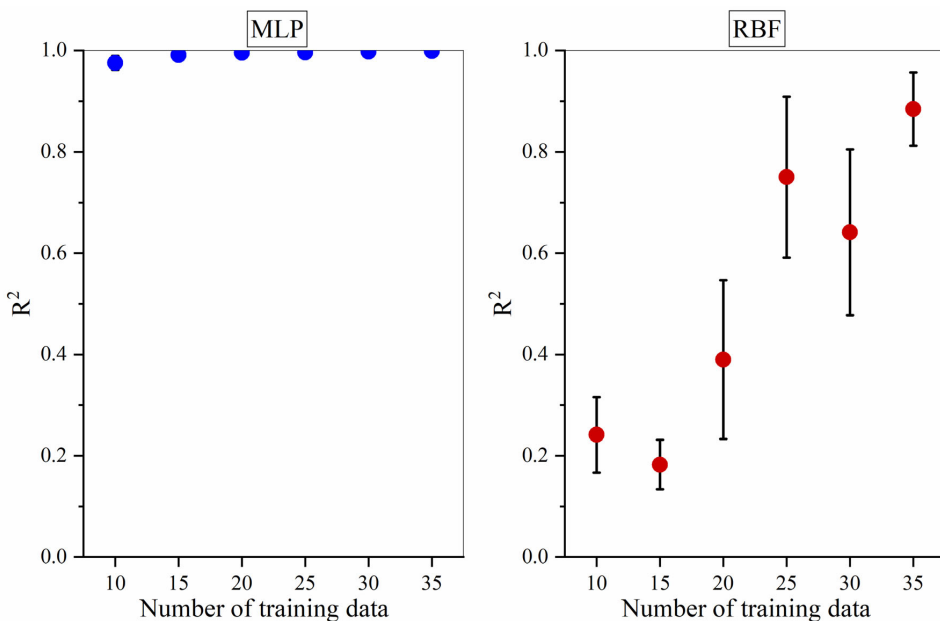


**Fig. 8** Influence of sample size on  $R^2$ -values at the test stage when predicting the volume loss between 5 and 25 s by the MLP and RBF model using the SPM

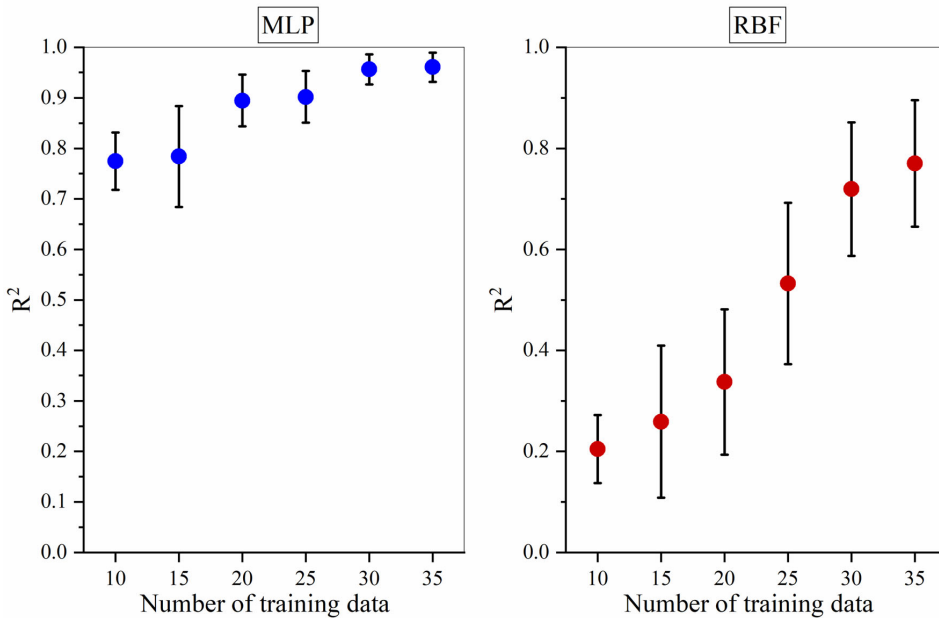


**Fig. 9** Influence of sample size on  $R^2$ -values at the test stage when predicting the volume by the MLP and RBF model using the FCM

exemplifies that it is possible to substantially reduce the number of required flow simulations of cementitious materials in a study if the CFD model is coupled with the appropriate ANN. Consequently, this is a step in the right direction to reduce CFD simulations in a parametric study, which is paramount if CFD should be more widely used in the concrete industry. In this study, however, the presented numerical experiments worked well with standard neural network structures, activation- and error-functions. The use of more advanced activation functions for MLP, such as, SPOCU [39], might lead to a more successfully trained network and could assist in the reduction of the computational effort especially for a big data scenario [40]. These could be the topic of future research.

**Acknowledgment** The study presented in this paper is performed within the MiKS project – Mikroproportionering med Knust Sand (Norwegian for Micro-proportioning with Crushed Sand), which is a KPN (Competence Project for the Industry) funded by the Research Council of Norway (RCN) Contract No. 247619 and industrial partners. The authors would like to thank the RCN and the industrial partners (Norcem AS, Skanska Norge AS and Feiring Bruk AS) for their financial contribution to the research. N. Ranjbar has received funding from the European Union’s Horizon 2020 research and innovation program under the Marie Skłodowska-Curie Grant Agreement No. 713683 (COFUNDfellowsDTU).

## Declarations

**Conflict of interest** The authors declare that they have no conflict of interest.

## References

1. Roussel N (2007) The LCPC BOX: a cheap and simple technique for yield stress measurements of SCC. *Mater Struct* 40(9):889–896
2. Wallevik OH (1990) The rheology of fresh concrete and its application on concrete with and without silica fume, Norway: NTH Trondheim
3. Amziane S, Ferraris CF, Koehler EP (2005) Measurement of workability of fresh concrete using a mixing truck. *J Res Nat Inst Stand Technol* 110(1):55
4. Choi M et al (2013) Lubrication layer properties during concrete pumping. *Cem Concr Res* 45:69–78
5. Spangenberg J et al (2012) Patterns of gravity induced aggregate migration during casting of fluid concretes. *Cem Concr Res* 42(12):1571–1578
6. Roussel N et al (2016) Numerical simulations of concrete flow: a benchmark comparison. *Cem Concr Res* 79:265–271
7. Le HD et al (2015) Effect of lubrication layer on velocity profile of concrete in a pumping pipe. *Mater Struct* 48(12):3991–4003
8. Vasilic K et al (2016) Flow of fresh concrete through reinforced elements: experimental validation of the porous analogy numerical method. *Cem Concr Res* 88:1–6

9. Vasilic K et al (2011) Flow of fresh concrete through steel bars: a porous medium analogy. *Cem Concr Res* 41(5):496–503
10. Jacobsen S et al (2013) Visualizing and simulating flow conditions in concrete form filling using pigments. *Constr Build Mater* 49:328–342
11. Shen L, Struble L, Lange D (2009) Modeling dynamic segregation of self-consolidating concrete. *ACI Mater J* 106(4):375
12. Spangenberg J et al (2012) Flow induced particle migration in fresh concrete: theoretical frame, numerical simulations and experimental results on model fluids. *Cem Concr Res* 42(4):633–641
13. Wallevik JE, Mansour W, Wallevik OH (2016) OpenFOAM casting solver with segregation. In: International RILEM conference on materials, systems and structures in civil engineering, conference segment on fresh concrete, RILEM publications SARL. Technical University of Denmark, Lyngby, Denmark
14. Švec O et al (2014) Influence of formwork surface on the orientation of steel fibres within self-compacting concrete and on the mechanical properties of cast structural elements. *Cement Concr Compos* 50:60–72
15. Martinie L, Lataste J-F, Roussel N (2015) Fiber orientation during casting of UHPFRC: electrical resistivity measurements, image analysis and numerical simulations. *Mater Struct* 48(4):947–957
16. Wallevik JE (2008) Minimizing end-effects in the coaxial cylinders viscometer: viscoplastic flow inside the ConTec BML viscometer 3. *J Nonnewton Fluid Mech* 155(3):116–123
17. Cepuritis R et al (2019) Analysing limitations of the FlowCyl as a one-point viscometer test for cement paste. *Constr Build Mater* 218:333–340
18. Serdeczny MP et al (2018) Experimental validation of a numerical model for the strand shape in material extrusion additive manufacturing. *Addit Manuf* 24:145–153
19. Chetverushkin B et al (2004) *Parallel computational fluid dynamics 2003: advanced numerical methods, software and applications*. Elsevier, Amsterdam
20. Spangenberg J et al. (2011) Optimization of casting process parameters for homogeneous aggregate distribution in self-compacting concrete: a feasibility study. In: 2011 IEEE congress of evolutionary computation (CEC), IEEE
21. Kupferman R (2001) A central-difference scheme for a pure stream function formulation of incompressible viscous flow. *SIAM J Sci Comput* 23(1):1–18
22. Comminal R, Spangenberg J, Hattel JH (2015) Robust simulations of viscoelastic flows at high Weissenberg numbers with the streamfunction/log-conformation formulation. *J Nonnewton Fluid Mech* 223:37–61
23. Tu JV (1996) Advantages and disadvantages of using artificial neural networks versus logistic regression for predicting medical outcomes. *J Clin Epidemiol* 49(11):1225–1231
24. Monjezi M et al (2010) Predicting blast-induced ground vibration using various types of neural networks. *Soil Dyn Earthq Eng* 30(11):1233–1236
25. Liu C, Zhao Z, Wen G (2019) Adaptive neural network control with optimal number of hidden nodes for trajectory tracking of robot manipulators. *Neurocomputing* 350:136–145
26. Czajkowski M, Kretowski M (2019) Decision tree underfitting in mining of gene expression data: an evolutionary multi-test tree approach. *Expert Sys Appl* 137:392–404
27. Sánchez D, Melin P (2014) Optimization of modular granular neural networks using hierarchical genetic algorithms for human recognition using the ear biometric measure. *Eng Appl Artif Intell* 27:41–56
28. Idrissi MAJ et al. (2016) Genetic algorithm for neural network architecture optimization. In: 2016 3rd international conference on logistics operations management (GOL), IEEE
29. Tian D et al (2018) A constraint-based genetic algorithm for optimizing neural network architectures for detection of loss of coolant accidents of nuclear power plants. *Neurocomputing* 322:102–119
30. Mia M, Dhar NR (2019) Prediction and optimization by using SVR, RSM and GA in hard turning of tempered AISI 1060 steel under effective cooling condition. *Neural Comput Appl* 31(7):2349–2370
31. Guo X, Li W, Iorio F (2016) Convolutional neural networks for steady flow approximation. In: Proceedings of the 22nd ACM SIGKDD international conference on knowledge discovery and data mining
32. Tompson J et al. (2017) Accelerating eulerian fluid simulation with convolutional networks. In: International conference on machine learning, PMLR
33. Cepuritis R (2016) Development of crushed sand for concrete production with micro-proportioning. Norwegian University of Science and Technology, Trondheim
34. Mørtsell E (1996) Modelling the effect of concrete part materials on concrete consistency. PhD, Norwegian University of Science and Technology (In Norwegian)
35. Sola J, Sevilla J (1997) Importance of input data normalization for the application of neural networks to complex industrial problems. *IEEE Trans Nucl Sci* 44(3):1464–1468
36. Naderpour H, Kheyroddin A, Amiri GG (2010) Prediction of FRP-confined compressive strength of concrete using artificial neural networks. *Compos Struct* 92(12):2817–2829
37. Tafarroj MM, Daneshazarian R, Kasaieian A (2019) CFD modeling and predicting the performance of direct absorption of nanofluids in trough collector. *Appl Therm Eng* 148:256–269
38. Mohanraj M, Jayaraj S, Muraleedharan C (2015) Applications of artificial neural networks for thermal analysis of heat exchangers—a review. *Int J Therm Sci* 90:150–172
39. Kiseľák J et al (2020) SPOCU: scaled polynomial constant unit activation function. *Neural Comput Appl* 33:1–7
40. Kallioras NA, Lagaros ND (2020) DL-SCALE: a novel deep learning-based model order upscaling scheme for solving topology optimization problems. *Neural Comput Appl* 2020:1–20



## Paper VII

### **Decreasing the Magnitude of Shear Rates in the FlowCyl**

Skare EL, Jacobsen S, Cepuritis R, Smeplass S, Spangenberg J.

*Proceedings for the International Federation for Structural Concrete 5th International FIB Congress (2018).*



# Decreasing the Magnitude of Shear Rates in the FlowCyl

Elisabeth Leite Skare<sup>1,2,3</sup>, Stefan Jacobsen<sup>4</sup>, Rolands Cepuritis<sup>5,6</sup>, Sverre Smepllass<sup>4,7</sup> and Jon Spangenberg<sup>8</sup>

<sup>1</sup>Ph.D. candidate, Norwegian University of Science and Technology, NO-7491 Trondheim, Norway

<sup>2</sup>Ph.D. candidate, Technical University of Denmark, 2800 Lyngby, Denmark

<sup>3</sup>Concrete Technologist, Norbetong AS (HeidelbergCement Group), NO-7080 Heimdal, Norway

<sup>4</sup>Professor, Norwegian University of Science and Technology, NO-7491 Trondheim, Norway

<sup>5</sup>Post doc. fellow, Norwegian University of Science and Technology, NO-7491 Trondheim, Norway

<sup>6</sup>Project Manager, Norcem AS (HeidelbergCement Group), NO-3950 Brevik, Norway

<sup>7</sup>Chief Adviser, Skanska Norge AS, NO-0107 Oslo, Norway

<sup>8</sup>Associate Professor, Technical University of Denmark, 2800 Lyngby, Denmark

## Abstract:

FlowCyl is an experimental setup (similar to the Marsh cone) that quantifies rheological properties of cement pastes via a parameter called flow resistance ratio. In a previous study by the authors, it was found that the high shear rates in the FlowCyl affects the flow resistance ratio to be dominated by the plastic viscosity of the cement paste. In this numerical study, we use a computational fluid dynamics model to analyse how the magnitude of shear rates can be reduced in the FlowCyl by changing its geometry (i.e. the height as well as the thickness of both the cylinder and outlet) in order to make the flow resistance ratio also dependent on the yield stress of the cement paste. The numerical model solves the continuity and momentum conservation equation based on the finite volume method. We simulate a Bingham material with yield stress 4.85 Pa and plastic viscosity of 0.38 Pas. The results illustrate that the magnitude of the shear rates can be substantially reduced by decreasing the height of the FlowCyl, as this reduces the hydrostatic head. Increased outlet opening from 8 to 12 mm increases max shear rates whereas the Marsh Cone has lower max shear rates than the FlowCyl.

**Keywords:** Cement Paste, FlowCyl, Modelling, Rheology

## 1. Introduction

Rheological properties of cement pastes may be described by the flow resistance ratio,  $\lambda_Q$ . The flow resistance ratio is representing the difference between the accumulated flow flowing through a narrow opening as a function of time in a test material and in an ideal fluid without internal flow resistance (Mørtzell, Maage & Smepllass 1996). By definition, the ideal fluid has a flow resistance value of 0.0, while a flow resistance value of 1.0 represents an extremely viscous fluid (Mørtzell 1996). To calculate the flow resistance ratio, an apparatus called FlowCyl is used. The FlowCyl test is a modification of the Marsh Cone test, and consists of a vertical cylindrical steel tube with a narrow nozzle at the bottom (Mørtzell, Maage & Smepllass 1996). After closing the outlet nozzle, the tube is filled with cement paste up to the level of 15 mm below the top. The paste flows through the nozzle and is directly weighed in a balance, which is connected to a computer recording the accumulated mass as a function of time. The weight increase is recorded every two seconds with a time interval 15 sec until 35 sec after opening the outlet (Mørtzell 1996). The dimensions of the FlowCyl and the Marsh Cone are illustrated in Fig.1.



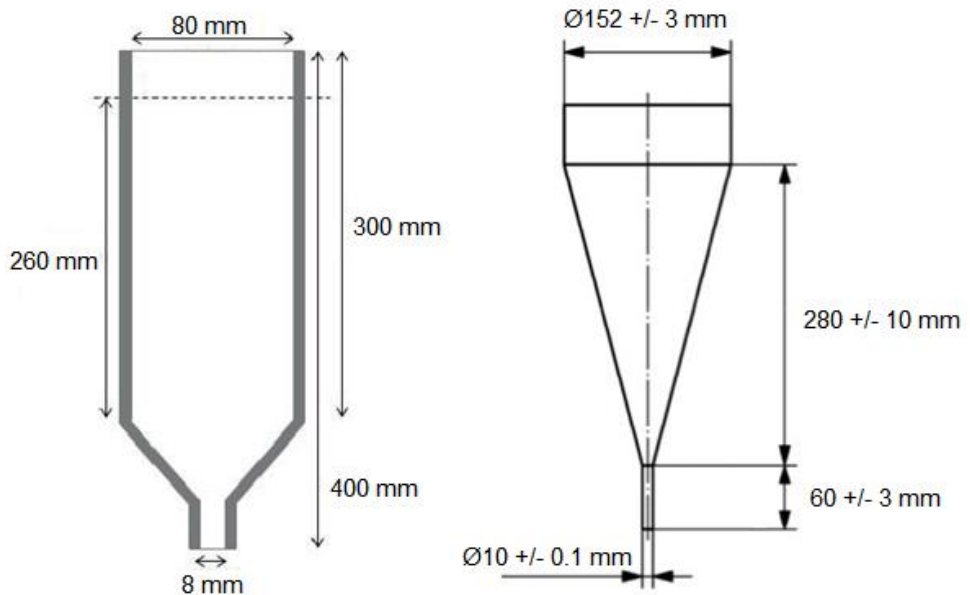


**Fig. 1** Dimensions of the FlowCyl (left) and the Marsh Cone (right). (Cepuritis & Smeplass 2016, BFT International).

Several previous studies show that the flow resistance ratio correlates well to the plastic viscosity of the tested material (Cepuritis & al. 2017), and the FlowCyl method has been successfully used to predict the workability of both conventional concrete and lightweight aggregate concrete mixes (Mørtzell 1996, Smeplass 2000). However, when applying to self-compacting concrete mixes, and mixes with high amounts of crushed sand, the FlowCyl has shown to have some limitations (Cepuritis, Jacobsen & Spangenberg 2017, Smeplass & Mørtzell 2001, Hammer & Wallevik 2005, Cepuritis & al. 2017). We think that its ability to measure effects of yield stress may be an important limiting factor. It has been shown (Cepuritis & al. 2017) that some of the limitations for the applicability of the FlowCyl could arise from the fact that the resulting parameter (flow resistance ratio) is mainly only dependant on the viscosity of the tested cementitious matrices, while these materials are known to be two parameter fluids (i.e. yield stress and viscosity).

This paper presents results from a computational fluid dynamics model, which analyses how different geometries of the FlowCyl affect the flow of the cement paste during the experiment. The objective is to investigate how the magnitude of shear rates in the FlowCyl can be reduced, in order to make the flow resistance ratio more dependent of the yield stress of the cement paste.

## 2. Numerical model

The CFD model that simulates the flow of the cement paste in the FlowCyl was developed in the commercial software, Flow3D, which previously has been used to simulate flow of cementitious materials (Roussel & al 2016). The software finds the primary unknowns (i.e. pressure and velocity fields) by solving the mass- and momentum conservation equations with the generalized minimal residual method. The free surface of the cement paste is computed by a precise interface tracking

method called the volume-of-fluid method (Hirt & Nichols 1981, Comminal, Spangenberg & Hattel 2015), and the walls of the FlowCyl are modelled with a no-slip boundary. The cement paste is modelled by a Bingham material model with a yield stress of 4.85 Pa and a plastic viscosity of 0.38 Pas, which corresponds to one of the cement pastes that was analysed in (Cepuritis & al. 2017). Additional information on the CFD model and its validation is presented in (Cepuritis & al. 2018, Cepuritis & al. 2017). Fig. 2 shows the model.



Fig. 2 Initial condition for FlowCyl model (Cepuritis & al. 2017).

### 3. Results and discussion

Fig. 3 illustrates how the shear rates in the FlowCyl are affected by the height of the cement paste inside the FlowCyl, i.e. the effect of the change in hydrostatic head. The shear rates are investigated 2 sec, 15 sec, 25 sec and 35 sec after the cement paste starts flowing through the nozzle. The lowest height is resulting in a reduction of the maximum shear rate by approximately 60 % from the original geometry. The maximum shear rates are of course always observed at the wall.

The diameter of the FlowCyl is also found to affect the magnitude of the shear rates. Fig. 4 illustrates how an increase in the diameter from 80 mm (standard) to 160 mm, results in an increase in maximum shear rate by approximately 60 %. Hence the flow conditions are clearly not a simple function of the hydrostatic head since there is such a big influence of the diameter of the FlowCyl and hence of the volume of paste.

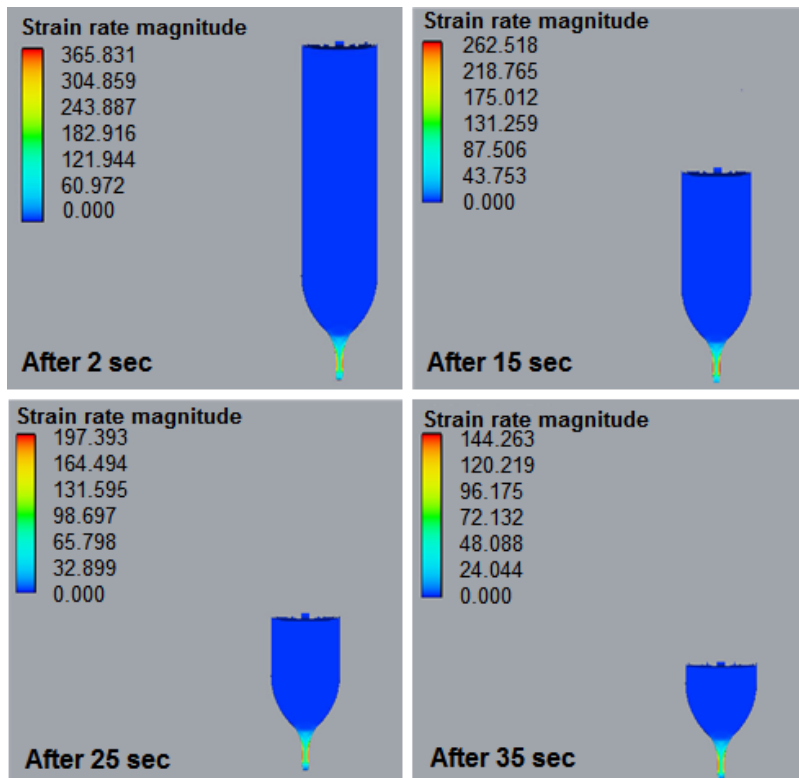


Fig. 3 Effect of hydrostatic head on the shear rates in the FlowCyl.

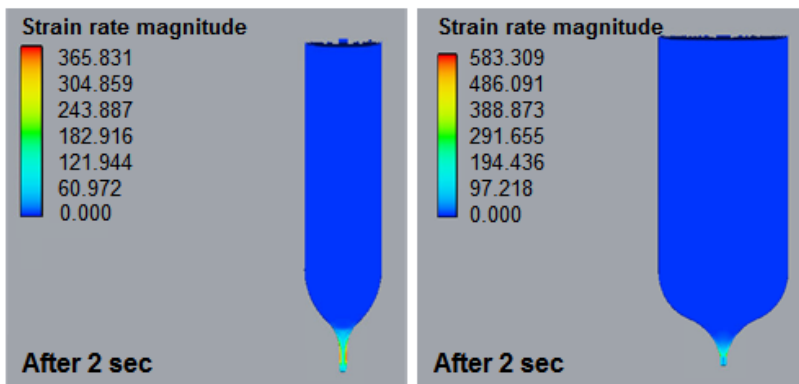


Fig. 4 The effect of increased FlowCyl diameter on the shear rates.

The effect of the outlet diameter on shear rates in the FlowCyl was also investigated. Two cases are simulated, with outlet diameters of 8 mm (standard) and 12 mm, shown in Fig. 5. The increase in outlet diameter leads to an increase in maximum shear rates by almost 30 %.

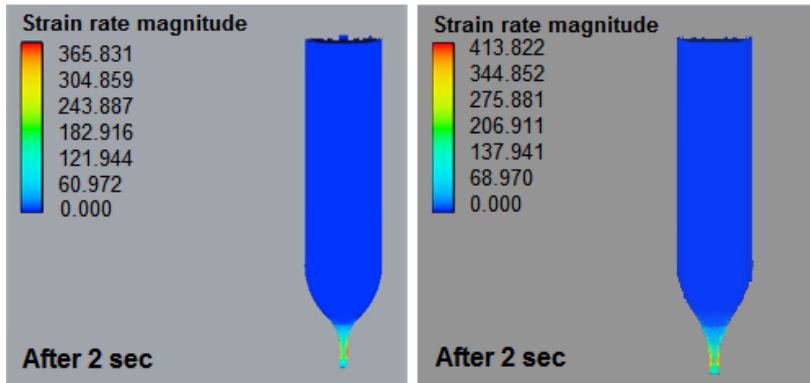


Fig. 5 Resulting shear rates for two different outlet diameters.

The difference in the occurring shear rates in the FlowCyl and in the Marsh Cone was also simulated, and the resulting shear rates after 2 sec are shown in Fig. 6. The lower shear rates in the Marsh Cone is assigned to a lower hydrostatic head, as seen in Fig. 1.

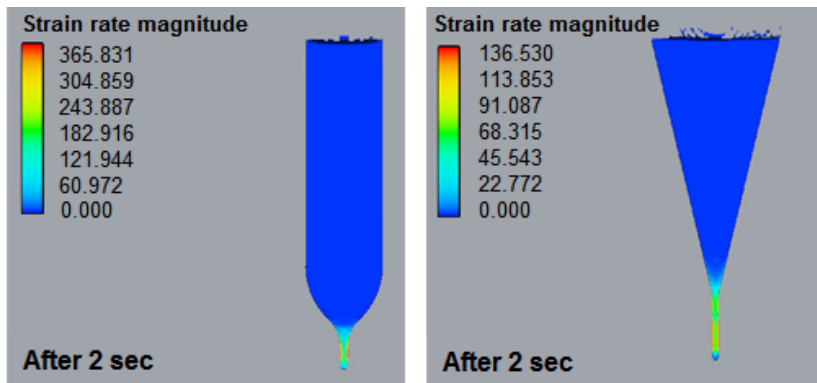


Fig. 6 Difference between the FlowCyl and the Marsh Cone.

The results are encouraging for the development of a simple one-point test based on FlowCyl that is more sensitive to both Bingham parameters. As a first experimental verification towards this goal FlowCyl experiments with materials with different combinations of Bingham parameters yield stress/plastic viscosity (low/low, low/high, high/low and high/high) should be conducted with low and high filling heights.

### 3. Conclusions

In this paper, the magnitude of shear rates for different modified geometries of the FlowCyl has been investigated with a computational fluid dynamics model. The research has aimed for a reduction of the shear rates at the outlet of the FlowCyl, in order to make the flow resistance ratio also dependent of the yield stress of the cement paste. The simulations found that the magnitude of shear rates decreases with decreasing hydrostatic head. In addition, the maximum shear rates was found to decrease both with decreasing FlowCyl diameter and outlet diameter. When comparing the FlowCyl and the Marsh Cone, the occurring shear rates are lowest for the Marsh Cone. This result is also assigned to the lower hydrostatic head seen in the Marsh Cone. In the future, laboratory experiments will be carried out in order to measure the flow resistance ratio for the same matrix with different filling heights of the FlowCyl.

### Acknowledgements

This work is based on work performed within the MiKS project – Mikroproporsjonering med Knust Sand (Norwegian for Micro-proportioning with Crushed Sand), which is a KPN project (Competence Project for the Industry) funded by the Research Council of Norway (RCN), contract No. 247619 and industrial partners. The authors would like to thank the RCN and the industrial partners (Norcem AS, Skanska Norge AS and Feiring Bruk AS) for their financial support and for facilitating the interaction between research and industry.

### References

- BFT International*. (2014, 10). Retrieved 03 20, 2018, from [http://www.bft-international.com/en/artikkel/bft\\_Compability\\_of\\_superplasticizers\\_with\\_cementitious\\_materials\\_2165293.html#](http://www.bft-international.com/en/artikkel/bft_Compability_of_superplasticizers_with_cementitious_materials_2165293.html#)
- Cepuritis, R., & Smepllass, S. (2016). Chapter 4 - Fresh concrete - proportioning. In *TKT 4215 concrete Technology I*. Trondheim.
- Cepuritis, R., Jacobsen, S., & Spangenberg, J. (2017). The Particle-Matrix model: limitations and further improvements needed. *Nordic Concrete Federation No 23 Paper 13, 23*.
- Cepuritis, R., Ramenskiy, E., Mørtzell, E., Smepllass, S., Kjos-Hanssen, H., Li, S., . . . Spangenberg, J. (2017). FlowCyl: one-parameter characterisation of matrix rheology. *Proceedings of the Second Concrete Innovation Conference*. Tromsø.
- Cepuritis, R., Skare E.L., Ramenskiy, E., Mørtzell, E., Smepllass, S., Li, S., Jacobsen, S. Spangenberg, J. (2018) Filler modified cement paste flow in the one-point FlowCyl test. 22p. *Unpublished manuscript NTNU/DTU*.
- Comminal, R., Spangenberg, J., & Hattel, J. H. (2015). Cellwise conservative unsplit advection for the volume of fluid method. *Journal of Computational Physics*, 283(C), 582-608.
- Hammer, T., & Wallevik, J. (2005). On the correlation between rheology of paste, mortar and concrete. *Proceedings of the Second North American Conference on the design and Use of Self-Consolidating Concrete (SCC) and the Fourth International RILEM Symposium on Self-Compacting Concrete*. Chicago.
- Hirt, C. W., & Nichols, B. D. (1981). Volume of Fluid (VOF) Method for the Dynamics of Free Boundaries. *Journal of Computational Physics*, 39, 201-225.
- Mørtzell, E. (1996). *Modelling the effect of concrete part materials on concrete consistency*. PhD. Norwegian University of Science and Technology.

- Mørtzell, E., Maage, M., & Smeplass, S. (1996). Production Methods and Workability of Concrete. *International Rilem Conference* (pp. 430-437). Paisley: E & FN Spon.
- Roussel, N., Gram, A., Cremonesi, L. K., Ferrara, V., Mechtcherine, S., Shychko, J., . . . Vasilic, K. (2016). Numerical simulations of concrete flow: A benchmark comparison. *Cement and Concrete Research*, 79, 265-271.
- Smeplass, S. (2000). *BE96-3942/R12 Applicability of the particle-matrix model to LWAC*. Brussel: EuroLightCon.
- Smeplass, S., & Mørtzell, E. (2001). The applicability of the particle matrix model to self compacting concrete. *Nordic Concrete Research*, 26



## Paper VIII

### **Investigating the flow curve of the FlowCyl test as a measure of yield stress**

Skare EL, Jacobsen S, Spangenberg J.

Manuscript submitted to *The International Federation for Structural Concrete 6th International FIB Congress* (2022).

This paper is awaiting publication and is not included in NTNU Open





# Paper IX

## **FlowFunnel for measuring yield stress and plastic viscosity of cement paste**

Skare EL, Jacobsen S, Spangenberg J.

Manuscript submitted to *Cement and Concrete Research*.

This paper is awaiting publication and is not included in NTNU Open

